Defence Research and Development Canada | Recherche et développement pour la défense Canada

DEFENCE R&D DÉFENSE

Lidar Polarization discrimination of pollens

Xiaoying Cao
Robert Bernier

Prepared by:
Les instruments optiques du Saint-Laurent inc.
17500 Montée Gascon
Mirabel, (Québec)
J7J 2C5

Project Manager: Robert Bernier 514-944-2526
Contract Number: W7701-071506
Contract Scientific Authority: Gilles Roy, 418-844-4000 (4335)

Defence R&D Canada – Valcartier

Contract Report
DRDC Valcartier CR 2011-237
March 2011

Canada

Lidar Polarization discrimination of pollens

Xiaoying Cao

Robert Bernier

Prepared by:
Les instruments optiques du Saint-Laurent inc.
17500 Montée Gascon
Mirabel, (Québec)
J7J 2C5

Project Manager: Robert Bernier 514-944-2526

Contract Number: W7701-071506

Contract Scientific Authority: Gilles Roy, 418-844-4000 (4335)

Defence R&D Canada – Valcartier

Contract Report
DRDC Valcartier CR 2011-237
March 2011

Original signed by Xiaoying Cao

Xiaoying Cao

Original signed by Robert Bernier

Robert Bernier

President - Les instruments optiques du Saint-Laurent inc.

Approved for release by

Original signed by Gilles Roy

Gilles Roy

Defence scientist

Work performed under: ARP 16ql: BioSense

Abstract

Aerosols or solid targets may have an effect on the polarization of the light scattered by them. The depolarization, by such particles or objects, of the light transmitted by a lidar system may be used as a signature by which these objects can be identified and discriminated against. This report is about the application of the RDDC-Valcartier polarization lidar system to the problem of discriminating between various bioaerosols, here namely pollens. For the first time to our knowledge, this technique has been applied to a great number of different bioaerosols, here 27. The development and application to the experimental data of the statistical tool named Mahalanobis distance has allowed to demonstrate that the polarization lidar technique renders possible the discrimination between bioaerosols (pollens). The work reported herein also addresses the question of whether the use of only one kind of polarization (be it circular or linear) is sufficient or if both polarizations are required for a complete discrimination among randomly distributed particles. This report concludes that only one polarization is sufficient.

Résumé

Des aérosols ou des cibles solides peuvent exercer un effet sur la polarisation de la lumière diffusée par eux. La dépolarisation, par ces particules ou objets, de la lumière transmise par un système lidar peut être utilisée à titre de signature permettant l'identification et la discrimination de ces objets. Ce rapport concerne l'application du système lidar à polarisation de RDDC-Valcartier au problème d'obtenir une discrimination parmi plusieurs bioaérosols, ici des pollens. Pour la première fois à notre connaissance, cette technique est appliquée à un nombre très grand de bioaérosols différents, ici 27. Le développement et l'application aux données expérimentales de l'outil statistique dit des distances de Mahalanobis a permis de discriminer entre les bioaérosols étudiés ici. Ce rapport s'adresse aussi à la question de savoir si l'utilisation d'une seule polarisation (circulaire ou linéaire) est suffisante ou si les deux polarisations sont requises aux fins d'une discrimination complète entre des particules distribuées aléatoirement. Ce rapport conclut qu'une seule polarisation est suffisante.

This page intentionally left blank.

Executive summary

Lidar Polarization discrimination of pollens

Cao, X.; Bernier, R.; DRDC Valcartier CR 2011-237; Defence R&D Canada – Valcartier; March 2011.

Introduction or background:

In the years 2007-2008, the RDDC-Valcartier polarization lidar system has been used in order to verify experimentally a theoretical prediction about the depolarization of light by spherical water droplets. This theoretical tool would be useful for a calibration method for space-based lidars. At the same time, the system was used to show that there was a relation between the information carried by linear and/or circular polarizations. The work reported here covers experimental and theoretical studies in the same domain carried at RDDC-Valcartier through the years 2008-2011. There were two objectives to the work reported here: first, apply the polarization lidar system to the new problem of discriminating between bioaerosols and, second, to verify whether the relation between linear and circular polarizations can be extended to non-spherical particles.

Results:

The lidar system has been applied to the study of 25 bioaerosols and 2 dusts. It is quantitatively the most important experimental work ever reported on the subject. The use of polarization at multiple wavelengths, associated with an appropriate statistical treatment of the data, have made possible to a good extent the discrimination between the aerosols. Also, the relation between circular and linear polarizations is shown to hold in the case of non-spherical particles as long as they are randomly oriented within the measurement volume.

Significance:

The results reported herein show that it would be possible to identify bioaerosols from a distance with a polarization lidar working at at most three wavelengths. If an appropriate data bank was assembled, such a system could be used as a remote sensor in view of detecting from far-off distances the presence of bioaerosols and assigning them a threat or non-threat qualifier. Also, the results reported here show that the use of only one polarization is sufficient for the case of randomly distributed particles, allowing for a simplification of the lidar system technical requirements.

Future plans:

More research is still to be done in view of asserting the relation between linear and circular polarizations and extend it to other types of targets.

Sommaire

Lidar Polarization discrimination of pollens

Cao, X.; Bernier, R.; DRDC Valcartier CR 2011-237; R & D pour la défense Canada – Valcartier; Mars 2011.

Introduction ou contexte:

Durant les années 2007-2008, le lidar à polarisation de RDDC-Valcartier a servi à vérifier expérimentalement une prédiction théorique concernant la dépolarisation de la lumière causée par des gouttelettes d'eau sphériques. Cet outil théorique pouvait être mis à contribution dans le cadre d'une méthode de calibration pour des lidars spatiaux. Dans le même temps, le système servait à montrer qu'il existe une relation entre l'information portée par les polarisations circulaire et linéaire. Le présent rapport concerne des travaux théoriques et expérimentaux dans le même domaine d'investigation menés à RDDC-Valcartier durant les années 2008-2011. Il y avait deux objectifs à ces travaux: premièrement, appliquer la technologie du lidar à polarisation à un nouveau problème, soit celui de discriminer entre différentes sortes de bioaérosols, et, deuxièmement, vérifier si la relation entre polarisations circulaire et linéaire peut être étendue au cas des particules non-sphériques.

Résultats:

Le système lidar a été appliqué à 25 bioaérosols et à 2 poussières. C'est, d'un point de vue quantitatif, le travail expérimental le plus important jamais rapporté dans ce champ d'application. L'utilisation de la polarisation à plusieurs longueurs d'ondes, associée à un traitement statistique approprié des données, ont rendu possible en bonne partie la discrimination entre les bioaérosols. Aussi, il a été montré que la relation entre les polarisations circulaire et linéaire continue de tenir pour des particules non-sphériques dans le cas où celles-ci sont orientées de façon aléatoire dans le volume où s'effectue la mesure.

Importance:

Les résultats rapportés ici montrent qu'il serait possible d'identifier des bioaérosols à distance au moyen d'un lidar à polarisation fonctionnant à tout au plus trois longueurs d'ondes. Si une banque de données appropriée était construite, un tel système pourrait être utilisé aux fins de la détection à distance de la présence de bioaérosols avec, à la clé, leur qualification en terme de dangerosité. De plus, les résultats rapportés ici montrent qu'une seule polarisation est suffisante pour les fins de discrimination entre particules distribuées de façon aléatoire, simplifiant d'autant les spécifications techniques requises pour le système lidar.

Perspectives:

De plus amples recherches sont prévues en vue de confirmer la relation entre les polarisations circulaire et linéaire et de l'étendre à d'autres types de matériaux.

Table of contents

List of figures

List of tables

Acknowledgements

We wish to thank Sylvie Buteau, Grégoire Tremblay, Christian Laflamme, Pierre Lahaie, Jean-Robert Simard and Sylvain Cantin for their assistance in this work.

1 INTRODUCTION

In the recent years, much work has been done at RDDC-Valcartier to investigate the possibilities of the technology of multiple wavelengths polarimetric lidars.

In 2007-2008, the polarimetric lidar system has been applied to make depolarization measurements on water droplets, fog oil and dust aerosols. One of the objectives of these works was to provide experimental validation of an empirical relationship existing between the layer integrated backscattered light and the layer accumulated depolarization ratio for linear depolarization for the case of water droplets clouds. This is a powerful relation allowing the calibration of space-based lidars and correction of the lidar signal for multiple scattering effects. Another objective of these works was to show that other such empirical relations also exist for submicrometer particles and nonspherical particles.

Those works have been reported in the Technical Report IOSL TR 2009-001 entitled 'Depolarization of light scattered by spherical and non-spherical particles' [1]. In a paper published about the results of these works, Cao et al. [2] showed that the empirical relationship proposed by Hu et al. [3] was verified experimentally. They also verified experimentally a modified relationship, that last one being based on a relation between the circular and linear depolarization ratios under multiple-scattering conditions that had been first established by Roy and Roy [4].

The polarimetric lidar may be a powerful tool for the remote sensing of aerosols or solid targets. One of the interesting applications would be to detect and warn against toxic bioaerosols. Another one would be as a ground probing system for terrain mapping applications. During the years 2008-2011, the RDDC-Valcartier multiple wavelengths polarimetric lidar has been applied to both of these tasks.

In this report, the works that have been done for the discrimination of bioaerosols are described. In the present work, the polarization signature at various wavelengths has been obtained for 25 different pollens as well as for 2 aerosol dusts. A statistical analysis based on the calculation of Mahalanobis distances has shown that a good though not complete discrimination between the 27 aerosols could be obtained with at most 3 different wavelengths.

Also, building on previous works wherein circular polarization was studied in its relation to linear polarization, the works presented in this report show that the use of only one of the polarization states (circular or linear) is sufficient for obtaining a complete polarization signature on all randomly oriented particles.

Hence, it can be said that the works reported herein had two objectives: first, to investigate whether the polarimetric lidar could be used to discriminate between bioaerosols; second, to verify whether one polarization state would be sufficient for a complete characterization of at least some types of materials.

The structure of this report reflects the fact that there were some points that were common to those two objectives, while some other points differed.

The section 2 will describe the experimental setup, which was common to both investigations.

The section 3 will introduce the theoretical relations that explain how the lidar signal was processed in view of obtaining the polarization signature of the aerosols. In that section, the equations are given for the calculation of the various depolarization ratios, circular or linear, and the relations between them. The depolarization parameter *d* introduced by Gimmestad [5] is also introduced and discussed in its relation to the other definitions of depolarization ratios.

The section 4 will discuss the specific details of the measurements and calculations done for the discrimination of the bioaerosols. The results of this part of the work will be given and discussed. In this section, also, are presented the results of some preliminary works on the time evolution of the polarization signature in conditions of high humidity.

The section 5 will do the same for the calculations that were done in view of finding out whether one polarization only would be sufficient. The results of this part of the work will be given and discussed.

Finally, the section 6 will summarize the works and results and discuss further research work to be done in this field.

The results of these works have been published in two different peer reviewed papers which constitute references [12] and [13].

2 DESCRIPTION OF THE EXPERIMENTAL SETUP

For the works that are going to be described, two different experimental setups were actually used at different times.

The first setup was used in the year 2008 and was a Multiple Field of View polarimetric lidar. It will be called the Imaging MFOV Dual-Polarization Lidar setup. It was equipped with an Intensified Charge Coupled Detector (ICCD) area camera. For retrieving the energy collected within a specific Field of View (FOV), integration of the energy over the many pixels comprising the FOV had to be performed.

The second setup was used for the years 2009-2011 because the first setup had ceased to be available. It will be called the Non-Imaging Dual-Polarization Lidar setup. In this setup, for any experiment, only one FOV is available. However, through the use of an appropriately set iris, the extent of the FOV may be varied at will for any series of experiments. In the case of this setup, the integration of the energy within the selected FOV is made directly at the surface of the detector.

It must be noted that, except for the method to be used for integrating the energy over one FOV, all data are processed and treated in the same way whether they originate from the Imaging MFOV Dual-Polarization Lidar or from the Non-Imaging Dual-Polarization Lidar.

In what follows, we briefly describe both setups.

2.1 The Imaging MFOV Dual-Polarization Lidar

Figure 1 is a schematic of the Imaging MFOV Dual-Polarization Lidar optical setup.

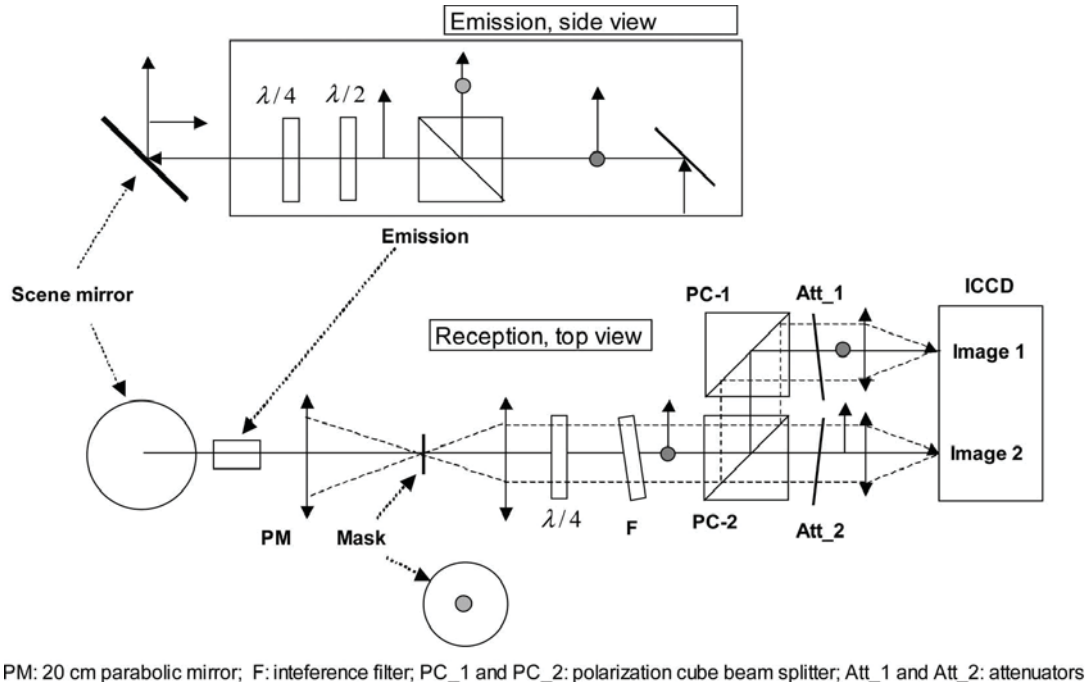

Figure 1: Imaging MFOV Dual-Polarization Lidar optical setup

The status of polarized light transmitted by the lidar is controlled by adjusting the quarter and half wave plates in the emission arm of the instrument. By rotating the half-wave plate by 45° in one or the other direction, the linear polarization of the laser light can be oriented either horizontally or vertically. By rotating the quarter-wave plate by ±45°, this linear polarization state can be made into a left or right circular polarization state.

In the reception arm of the instrument, the use of the quarter-wave plate is important. Circularly polarized incoming light will be reconverted to linearly polarized by the appropriate rotation by ±45° of the quarter-wave plate. If light is already linearly polarized the quarter-wave plate will be left in a 0° position. Passed the quarter-wave plate, the polarizing cube beam splitters will direct the vertically and horizontally polarized fractions of the incoming light to the right (Image 1) or left (Image 2) half of the ICCD sensor area.

The choices of the settings of the various waveplates in both arms of the instrument will thus allow any state of light polarization to be selected for the measurements. Details of wave plates settings can be found in ref 4.

Selection among different sets of attenuators will allow the signal to be recorded with the highest possible voltage resolution without ever saturating the camera.

The total energy for each and any of the variously defined FOV's will be obtained by adding the energy contained in each of the pixels in the camera image that are included in a circle whose radius is calculated from the numerical value of the angular FOV selected and whose center is located on the optical axis of the receiver. The details of these calculations can be found in ref 1.

For the year 2008, that is when the Imaging MFOV Dual-Polarization Lidar just described was used, two different laser sources were used, one at 532 nm, the other at 1.57 µm. This would allow for a first polarization signature of pollens to be obtained, which would be upgraded later at other wavelengths with the Non-Imaging Dual-Polarization Lidar.

2.2 The Non-Imaging Dual-Polarization Lidar

Figure 2 is a schematic of the Non-Imaging Dual-Polarization Lidar optical setup.

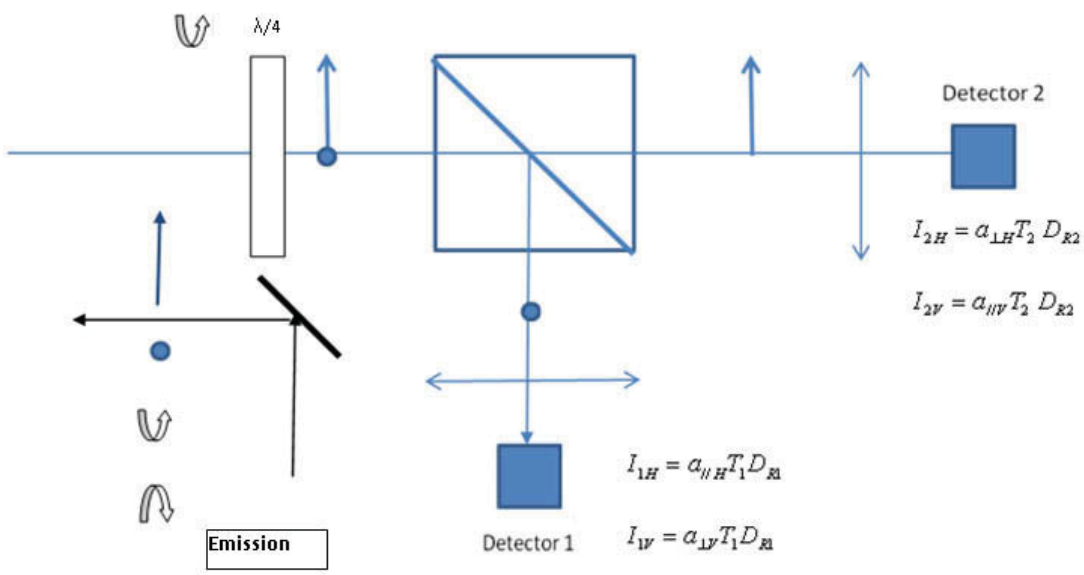

Figure 2: Non-Imaging Dual-Polarization Lidar optical setup

The emission arm of the instrument is not described in the Figure 2 but it is identical to the one in Figure 1 and will not be discussed here.

The reception arm of the instrument has been changed greatly since the ICCD area camera is no longer available. The two polarization states are now recorded at two different detectors. The integration of the energy is automatically and instantaneously done at the surface of the detectors themselves. Hence, no calculation needs to be done for retrieving the total energy in each polarization.

The settings of the various waveplates are chosen in the Non-Imaging Dual-Polarization Lidar along the same method as they are done for the Imaging MFOV Dual-Polarization Lidar and will not be discussed again.

The light used for these experiments came in four different wavelengths. A first laser source consists of a 100 Hz repetition rate Nd-YAG laser (Solar 629). This laser provides three wavelengths: 355 nm (40 mJ), 532 nm (80mJ) and 1064 nm (200 mJ). The other wavelength of 1570 nm (25 mJ) is obtained from an OPO (Optical Parametric Oscillator) resonator. Beam expanders were used to obtain outgoing laser beams with a 2 cm diameter and a 0.5 mrad divergence (80 % total energy).

Here again, because of the close range to the targets, attenuators with transmission of 0.01 or 0.001 are used depending on the detectors used.

In addition to the primary optics, the lidar system is equipped with a 20 cm diameter scanner. This allows to steer the lidar in any direction but it has an effect on the polarization of the light at emission.

The scanner mirrors orientation and its effect on the polarization state of the light emitted by the instrument is illustrated in figure 3.

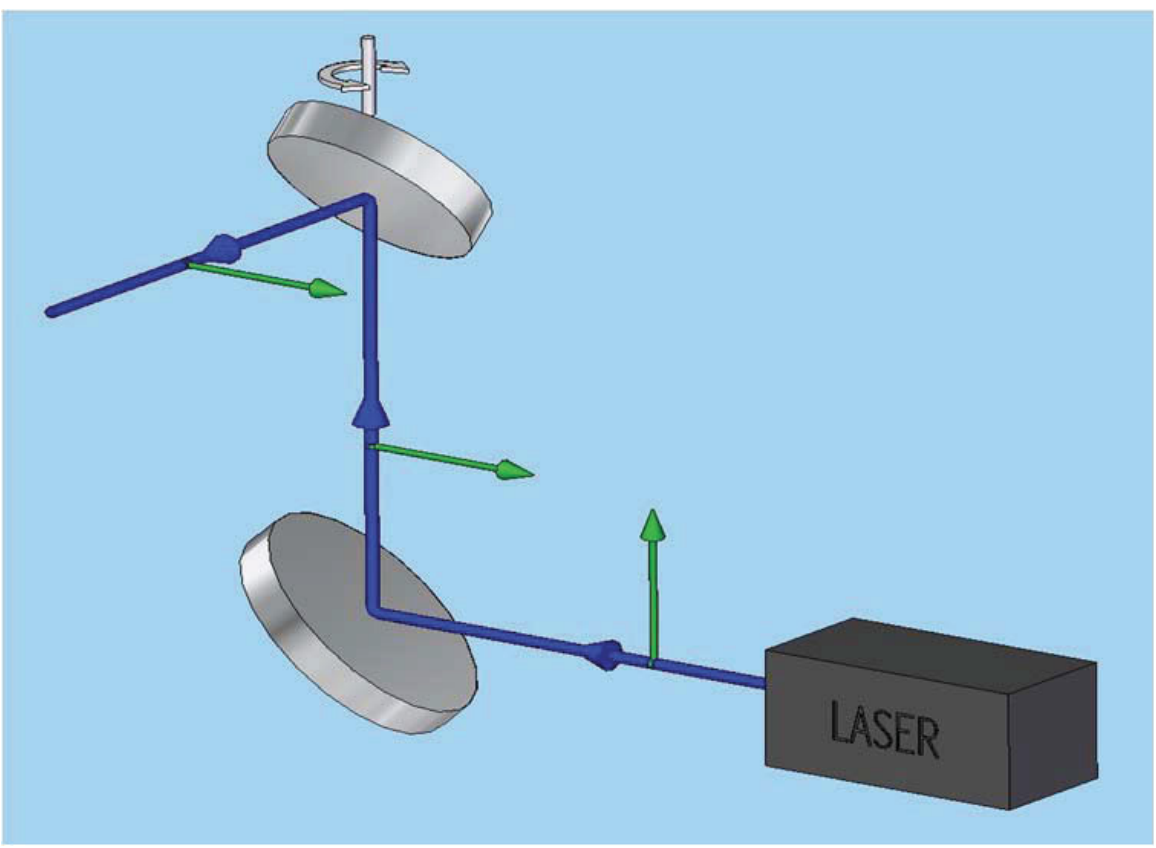

Figure 3: Effect of the scanner mirrors on the polarization state of the light at emission

Mirror reflectivity is not the same for parallel and perpendicular incident light polarizations. The mirrors are mounted in such a way that the parallel and perpendicular mirrors compensate each other to some extent (parallel incident light is perpendicular on the second mirror and vice versa). Gold coated mirrors have been used for the 1064 and 1570nm while protected aluminum coating has been used for the 355nm and 532 nm. Although it would have been possible to perform measurements at more than one wavelength simultaneously using dichroic optics, single wavelength measurements were performed to avoid polarization effects caused by such optics.

3 THE THEORETICAL FRAMEWORK

In this work, the polarization signature of bioaerosols is to be obtained. The effect the particles have on the polarization state of the incoming light, that is the depolarization effect they have on it, is what constitutes their polarization signature.

Two approaches were used to examine the target depolarization: what Gimmestad [ref 5] calls the legacy approach that examines the depolarization ratio (δ) and a novel approach defined by examining the depolarization parameter d which was introduced by Flynn et al [6] and has been redefined by Gimmestad [ref 5] as a measure of the propensity of the scattering medium to depolarize the incident polarization. The depolarization parameter d is used here because it conforms to standard radiative transfer theory, particle scattering theory and polarization measurement principles as noted in ref 5.

If linearly polarized light is emitted by the lidar and probed thereafter by its reception arm, then the linear depolarization ratio δ_L is to be defined and measured. The same will apply in the case where circularly polarized light is being used and circular depolarization ratio δ_C is being measured.

In the case where the particles that are being probed are randomly oriented in the measurement volume, specific relations obtain between the depolarization ratios δ_L and δ_C as well as between these and the parameter *d*.

In what follows, those various parameters will be defined and the algorithms for calculating them will be discussed.

3.1 The linear depolarization ratio δ_L

Since a founding paper by Schotland et al. [7] in the field of polarization lidar, the linear depolarization ratio δ_L has been defined as:

$$\delta_L = \frac{P_\perp}{P_{//}} \qquad \text{(eq. 1)}$$

where $P_\perp$ is the power received in the detection channel with polarization perpendicular to the polarization state of the light that was emitted and $P_{//}$ is the power received in the detection channel with polarization parallel to the polarization state of the light that was emitted.

For instance, if the emitted light was horizontally polarized, the lidar equations for the parallel and perpendicular received powers would be written:

$$P_{H//}(z) = P_{0H} F(z) \frac{c\tau}{2} \frac{A}{z^2} \alpha_s(z) p_{H//}(r, z, \beta = \pi) \exp\left[-2 \int_0^{z_c} \alpha(z') dz' \right] \quad \text{(eq. 2)}$$

and

$$P_{H\perp}(z) = P_{0H} F(z) \frac{c\tau}{2} \frac{A}{z^2} \alpha_s(z) p_{H\perp}(r, z, \beta = \pi) \exp\left[-2 \int_0^{z_c} \alpha(z') dz' \right] \quad \text{(eq. 3)}$$

Where, as usually, P_{0H} is the laser pulse power for horizontal polarization emission, c the speed of light, τ the pulse duration, A the area of the collecting optics, z the sounding distance, $F(z)$ the overlap function, α and α_s respectively the extinction and the scattering extinction coefficients and $p_{//}(r, z, \beta = \pi)$ and $p_{\perp}(r, z, \beta = \pi)$ the values of the phase functions parallel and perpendicular to the incident light for backscattering (β of 180°), while r is the particle size radius.

The depolarization ratio is given by the ratio of the perpendicular to the parallel phase functions and is a measure specific to a given aerosol that is independent of the measurement instrument. So it is the ratio of the perpendicular to the parallel phase functions we are truly interested to measure.

$$\delta_H(z) \equiv \frac{p_{H\perp}(r, z, \beta = \pi)}{p_{H\|}(r, z, \beta = \pi)} = \frac{P_{H\perp}(z)}{P_{H//}(z)} \quad (4)$$

Although simple in principle, it is difficult in practice to obtain a system independent measurement. The lidar signals measured $P_{D1,H//}(z)$ and $P_{D2,H\perp}(z)$ are affected by the detectors responsivities D_{R1} and D_{R2}, the optical transmissions T_1 and T_2 and the polarization effects caused by the various mirrors that could be used: $\Re_{H\perp}$ and $\Re_{H//}$. The same considerations would apply if a verically polarized light was emitted.

In what follows, it will be shown that there is a simple means by which the system dependent parameters just discussed can be compensated for. The procedure implies that a measurement be made in each of the two orthogonal linear polarization states: horizontal and vertical.

Set:

$$B(z) = P_{0H} F(z) \frac{c\tau}{2} A \alpha_s(z) \exp\left[-2 \int_0^z \alpha(z') dz' \right] \quad \text{(eq. 5)}$$

And it will be obtained:

$$P_{D1,H//}(z) = \frac{B(z) p_{H//}(r, z, \beta_b)}{z^2} T_1 D_{R1} \Re_{H//} \quad \text{(eq. 6)}$$

and

$$P_{D2,H\perp}(z) = \frac{B(z) p_{H\perp}(r, z, \beta_b)}{z^2} T_2 D_{R2} \Re_{H\perp} \quad \text{(eq. 7)}$$

The linear depolarization ratio for the horizontally polarized light is thus:

$$\delta_H(z) = \frac{(z^2 P_{D_2,H\perp})}{(z^2 P_{D_1,H//})} \frac{T_1 D_{R1} \Re_{H//}}{T_2 D_{R2} \Re_{H\perp}} \quad \text{(eq. 8)}$$

The same type of equation can easily be derived for vertical (*V*) illumination.

$$P_{D2,V//}(z) = \frac{B(z) p_{V//}(r, z, \beta_b)}{z^2} T_2 D_{R2} \Re_{V//} \quad \text{(eq. 9)}$$

$$P_{D1,V\perp}(z) = \frac{B(z) p_{V\perp}(r, z, \beta_b)}{z^2} T_1 D_{R1} \Re_{V\perp} \quad \text{(eq. 10)}$$

From which the linear depolarization ratio for the vertically polarized light is calculated to be:

$$\delta_V(z) = \frac{(P_{D1,V\perp} z^2)}{(P_{D2,V//} z^2)} \frac{T_2 D_{R2} \Re_{V//}}{T_1 D_{R1} \Re_{V\perp}} \quad \text{(eq. 11)}$$

As aerosols are randomly oriented in the atmosphere and have thus no preferred orientation, consequently the depolarization ratio is expected to be the same for vertical and horizontal illumination, i.e., $\delta_H(z) = \delta_V(z) = \delta_L(z)$, where the subscript '*L*' stands

for linear polarization. Multiplying Eq. 8 by Eq. 11, we obtain a value for the geometric mean of the linear depolarization ratio:

$$\delta_L(z) = \sqrt{\frac{(P_{D1,V\perp}z^2)}{(P_{D2,V//}z^2)}\frac{(P_{D2,H\perp}z^2)}{(P_{D1,H//}z^2)}\frac{\Re_{H//}}{\Re_{H\perp}}\frac{\Re_{V//}}{\Re_{V\perp}}} \qquad \text{(eq. 12)}$$

Equation 12 thus provides the depolarization ratio independently of the detectors responses. Also, in absence of mirrors or for perfectly compensating arrangements of mirrors, the depolarization ratio is directly obtained from the measured signal intensities and is thus shown to be independent of the instrument characteristics:

$$\delta_L(z) = \sqrt{\left(\frac{(P_{D1,\perp}z^2)}{(P_{D2,//}z^2)}\right)_V\left(\frac{(P_{D2,\perp}z^2)}{(P_{D1,//}z^2)}\right)_H} \qquad \text{(eq. 13)}$$

Which can be rewritten in the more compact way:

$$\delta_L(z) = \sqrt{\delta_H\delta_V} \qquad \text{(eq. 14)}$$

Figure 3 in section 2.2 illustrates the fact that the arrangement of mirrors in the Dual-Polarization lidars used in this work, the MFOV included, corresponds to the conditions which allow to use equations 13 and 14. It is thus expected that the data processing along the line of the equations 13 and 14 will yield system independent results.

3.2 The circular depolarization ratio δ_C

In the same way as were defined two orthogonal states of linearly polarized light (H and V), two orthogonal states of circularly polarized light may be defined: Right (R) and Left (L) rotating polarizations.

If the H and V indices that appear in the equations 2 to 14 above are everywhere replaced respectively by R and L, then the definition that is arrived at for the circular depolarization ratio δ_C is:

$$\delta_C = \sqrt{\delta_R\delta_L} \qquad \text{(eq. 15)}$$

The same discussion applies here as for the case of linear polarization and it is expected that the data processing along the line that leads to equation 15 will yield system independent results.

3.3 Relations between δ_L and δ_C

It has been established first by Mishchenko and Hovenier [8] that, for randomly oriented nonspherical particles, there exists a specific relation between the two depolarization ratios defined above. The relation was stated as:

$$\delta_C = \frac{2\delta_L}{1-\delta_L} \qquad \text{(eq. 16)}$$

On theoretical bases, the relation had been shown to hold for randomly oriented nonspherical particles at the backscattering angle (180°) with the condition that only single scattering occurred. Interestingly, Mishchenko and Hovenier note that the theoretical background that leads to eq. 16 puts no restriction on the aspect ratio of the particles, as long as they have circular symmetry around one axis (Chebyshev particles). They tested it for aspect ratios as large as 3. However, they show numerical simulation results to conclude that 'δ_L and δ_C cannot be considered a universal measure of the departure of particle shape from that of a sphere'.

In their paper, Roy and Roy [ref. 4] extended the relation (eq. 16) between the two depolarization ratios to the case of multiple-scattering and to all scattering angles. Their work included both a theoretical approach and an experimental validation.

The fact that this relation may hold true for all nonspherical particles at all angles, with seemingly any aspect ratio, as long as they are randomly oriented, has an important implication on design considerations for polarization lidars. The implication is that a complete polarization signature can be obtained for all such particles with only one sort of polarization, be it circular or linear. This fact somehow eases the technical requirements for polarimetric lidars.

Part of the research reported here is to investigate this possibility experimentally.

3.4 The depolarization parameter *d*

The parameter d is used here because it conforms to standard radiative transfer theory, particle scattering theory and polarization measurement principles as noted in ref 5. This was the reason for Gimmestad to introduce it in 2008. It departs from the traditional way of defining the depolarization ratios that had been dominating in the field of polarimetric lidars since 1971.

From first principles, Gimmestad established the following two equations for the depolarization parameters d_C and d_L which are calculated respectively in case of circular polarization or linear polarization. The equations are:

$$d_C = \frac{I_\perp}{I_\perp + I_{//}} \qquad \text{(eq. 17)}$$

and

$$d_L = \frac{2I_\perp}{I_\perp + I_{//}} \qquad \text{(eq. 18)}$$

The parameter *d* can also be calculated from the other two depolarization ratios. In the case of randomly oriented particles, the parameter *d* should actually be the same, be it measured with linear polarization or circular polarization light. Hence, below, is given only one equation relating the depolarization parameter *d* to either one of the two depolarization ratios introduced above:

$$d = \frac{2\delta_L}{1+\delta_L} = \frac{\delta_C}{1+\delta_C} \qquad \text{(eq. 19)}$$

That it would be calculated using equation 17, 18 or 19 should make no difference in the case of the randomly oriented particles on which the measurements have been done in this work. The parameter *d* should be the same in all cases within the condition of random orientation.

Actually, that the results would differ whether one or the other equation is used could indeed be seen as an indication that the particles are not randomly oriented or that the optical system itself induces some not accounted for intrinsic depolarization. In an application like the one here where it is attempted to discriminate between bioaerosols for instance, or in another one where it is the discrimination between solid targets that is aimed at, this information may be of importance. And the same would be true if, instead of trying to calculate the parameter *d* from two types of polarization, we were trying to calculate δ_C from δ_L or vice versa.

4 DISCRIMINATION OF BIOAEROSOLS (POLLENS)

In this section, the specific details for the measurements on bioaerosols (pollens) will first be given. Then, the procedure for data processing will be outlined. This will be followed by the presentation of the results. Finally, the significance of the results will be discussed.

4.1 Experimental setup and measurement protocol

4.1.1 Measurements with the Imaging MFOV Dual-Polarization Lidar

As stated in section 2, there were two different series of measurements. A first one occurred in 2008 with the Imaging MFOV Dual-Polarization Lidar described in section 2.1. Measurements at 532 nm and 1.57 µm were performed. The detectors, one for each polarization, were the two halves of the same ICCD area camera.

Pollens were burst out into a chamber which was 105 m away from the lidar housing trailer. The aerosol chamber is 22 m long by 2.4m x 2.4m. Both ends can be closed with flexible doors that are simply hang-up to close and drop-down to open within 0.5 s upon request. A typical measurement sequence is as follows: the chamber doors are closed and the dissemination of 2 g of the selected pollen is done within a few seconds with a pneumatic nozzle. Mixing fans are operated, during and after the dissemination, for 10 s in order to ensure a good homogeneity inside the chamber. The front door is then opened and lidar measurements are performed. After completion of the lidar data acquisition, the back door is opened and the chamber aerosol evacuated within a few minutes.

For 532 nm lidar, three gated widths (40 ns, 80 ns and 120 ns) were pre-set up in the gated ICCD camera. Thus, three measurements were performed for each polarization state.

Before the pollens were released, there already were some background aerosols in the air. The signals that will be acquired are thus actually compound results of pollens released and background aerosols. When the measurement was finished, the back-end door was opened to allow the pollen particles to move out of the chamber or deposit to the floor. Then, a measurement of the lidar signal from the background aerosols alone was performed. The background signals need to be subtracted from the first step measurements in order to get pure pollen signals.

The lidar sequence of measurements comprise four illumination polarizations (linear horizontal, linear vertical, circular right and circular left) performed serially. For each polarization, 200 laser shots were acquired. Typically the four polarization measurements are performed within 15 seconds. For each illumination, there were two detection schemes: detection parallel followed by detection perpendicular to the illumination polarization.

The depolarization signature of the various pollens can be contaminated by the fact that the instrument itself may induce a depolarization of the light being detected. This could occur due to depolarization by optical components or due to a transmissivity difference between the two

polarization channels. These effects need to be compensated for. Two different methods were applied.

For the measurements at the 532 nm wavelength, the calibration procedure introduced by Roy and Roy [ref. 4] was used. For the measurements at the 1.57 µm wavelength, the instrument effect was removed by using the geometric mean of the two orthogonal depolarization ratios as explained in section 3.1, equations 14 and 15.

The pollens examined are listed in Table 1. The mass released for most of those pollens was 2 g, with a few exceptions when the 532 nm lidar was used, as marked in the table.

Table 1: Pollens and corresponding mass examined

Category	Serial #	Material	Category	Serial #	Material
Arizon dust	1	Arizon dust	Cultivated Plants	15	Mustard
Trees and shrubs	2	Aspen		*16	Red Clover
	3	White Oak		17	Alfalfa
	4	White Polar	Dust	18	Barley Grain
	5	Maple Sugar		19	Wheat Grain
	6	paper Mulberry	Smuts	*20	Wheat
	*7	White Birch		21	Oat
	8	Virginia Pine		22	Corn
Weeds	9	Rag Weed	Fungi	23	Penicillium Chrysogenum
	10	Common Mugwart		24	Neurospora Intermedia
	**11	English Plantain	Insects	25	Mosquito
	12	Common Sagebrush		26	Moth
Flowers	13	Ox-Eye Daisy	Grasses	**27	Timothy
	14	Sunflower		28	Perennial Rye

*means 1 g and ** means 1.5 g pollens were released.

Pollens' electronic microscopic images are shown in Annex A for those pollens for which they were available. The dimensions of those pollens are also given in Annex A.

4.1.2 Measurements with the Non-Imaging Dual-Polarization Lidar

In the years 2009-2011, all other measurements were made with the Non-Imaging Dual-Polarization Lidar described in section 2.2. The measurements were done at four different wavelengths as described in section 2.2: 355 nm (40 mJ), 532 nm (80mJ), 1064 nm (200 mJ) and 1570 nm (25 mJ).

The same pollens as described earlier in Table 1 were measured. In this series of measurements, however, 2 g of each pollen were always released.

In this series of measurements, the calibration procedure was always the one involving equations 13 and 14 of section 3.1 (geometric mean of the depolarization ratio).

The measurement protocol is the same as described in section 4.1.1.

A typical lidar signal, as recorded by the PMT detectors, is shown in the figure 4 below. Figure 4 shows range corrected lidar signals of one type of pollen studied. It is clear that the cloud ranges mainly from 103 to 107 m from the lidar.

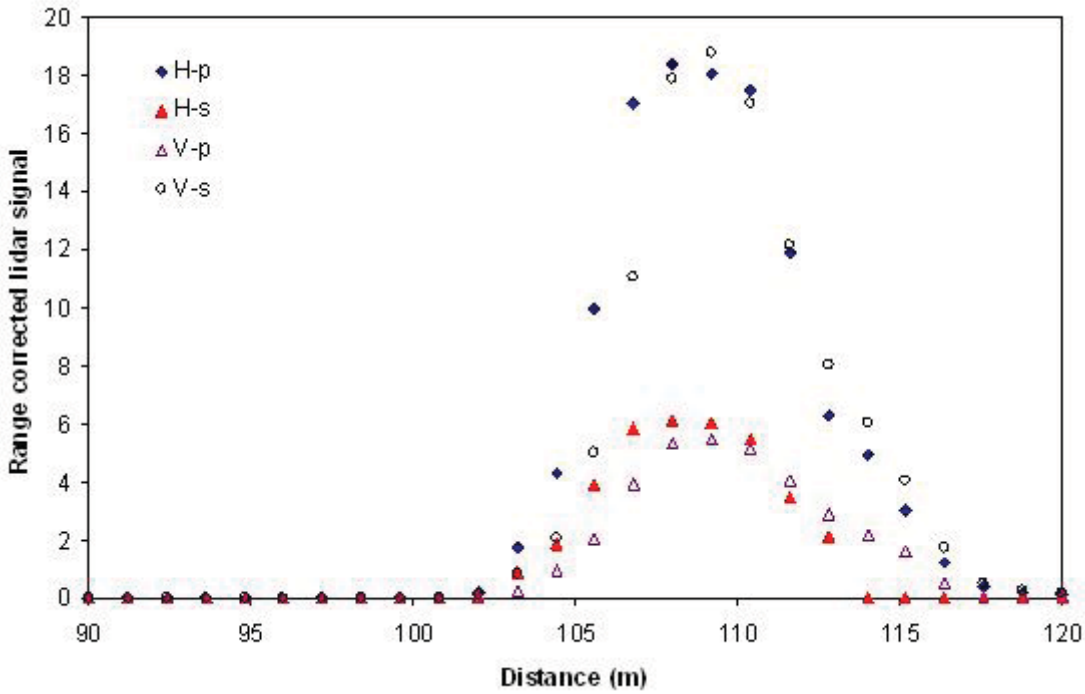

Figure 4: Range corrected lidar signal of pollen vs. distance. H and V represent Linear Horizontal and Vertical, and p and s represent detectors 1 and 2 signals

4.2 Data processing

One difference has already been noted between the data processing for the 2008 measurements and the one for the later years data. It is the fact that, in 2008, the calibration procedure used for the 532 nm wavelength (from ref 4) was different from the one used for the 1.57 µm wavelength (eq. 14 and 15). Now, the method used for the 1.57 µm wavelength (eq. 14 and 15) in 2008 is the same as the one that has been used for all the data at all wavelengths for the years 2009-2011.

Another difference between the data processing between 2008 and later years has to do with the fact that two completely recording systems have been in use: one in the Imaging MFOV Dual-Polarization Lidar, the other one in the Non-Imaging Dual-Polarization Lidar. The first was an

ICCD area camera, the other were PMT single cell detectors. Hence, a second difference in data processing is that, for the Imaging MFOV Dual-Polarization Lidar, the energy within a specific FOV needs to be integrated over many pixels in the camera image. The complete procedure for doing this has been discussed more fully in ref [1]. In the case of the Non-Imaging Dual-Polarization Lidar, this integration process is done automatically and instantaneously at the PMT surface.

Those two differences will not be discussed any further in this report.

For those two different instruments, once the calibration is done and once the energy is appropriately integrated in an FOV, the polarization signature for pollens is obtained along the same procedure. The statistical analysis of the results in order to answer the question as to whether or not discrimination between bioaerosols can be achieved is done along the same lines as well. This is this common data processing that is discussed in this section.

Figure 4 showed typical single laser shot lidar returns for horizontal and vertical polarization illuminations.

The average depolarization ratio can be calculated point by point, meaning one calculation per digitization bin. However, the synchronization of 2 acquisition channels is not perfect: there is often one digitization bin difference between the two channels. This causes larger variance into the depolarization ratio data. To overcome that problem, it is the ratio of the integrated signal that is calculated, that is the sum of the signal energy for the distances of approximately 103 to 107 m from the lidar. Also, in order to improve the specificity of each bioaerosol depolarization signature, the background aerosol signals $P_{ib\perp}$ and $P_{ib//}$ were subtracted from the pollen signals as already stated. For the ith pollen, the depolarization is then calculated as follows:

$$\delta' = \frac{\sum (P_{i\perp} - P_{ib\perp}) z_i^2}{\sum (P_{i//} - P_{ib//}) z_i^2} \qquad \text{(eq. 20)}$$

Based on eqs. 13 and 14, the pollen linear depolarization ratios are:

$$\delta_L = \sqrt{\delta'_H \delta'_V} \qquad \text{(eq. 21)}$$

The depolarization ratios, circular and linear, of the various pollens have been calculated and the results are presented in the following section.

The discrimination between pollens by their polarization signature, which is one objective of this work, is achieved when the polarization signature clearly separates each of them from all the others in some feature space related to their polarization behavior. As will be shown in the next section by looking at the data, this is no easy task.

4.2.1 Discrimination in 2-D feature space

For instance, if a representation of the data is done by locating each pollen polarization signature in a 2-D feature space where one axis is the depolarization ratio in one wavelength and the other axis is the same depolarization ratio in another wavelength, it must be concluded that a complete discrimination is not obtained. The figure 5 shows the case for the linear depolarization ratio of all pollens, and for all the possible combinations of two wavelengths. The size of the symbols is representative of the smallest 3 standard deviations (99.7%) of the data from the two wavelengths. Some pollens are clearly separated from others, while some others superimpose. Visualization of data for dimensions higher than 2 being difficult and subjective, it will not be attempted here.

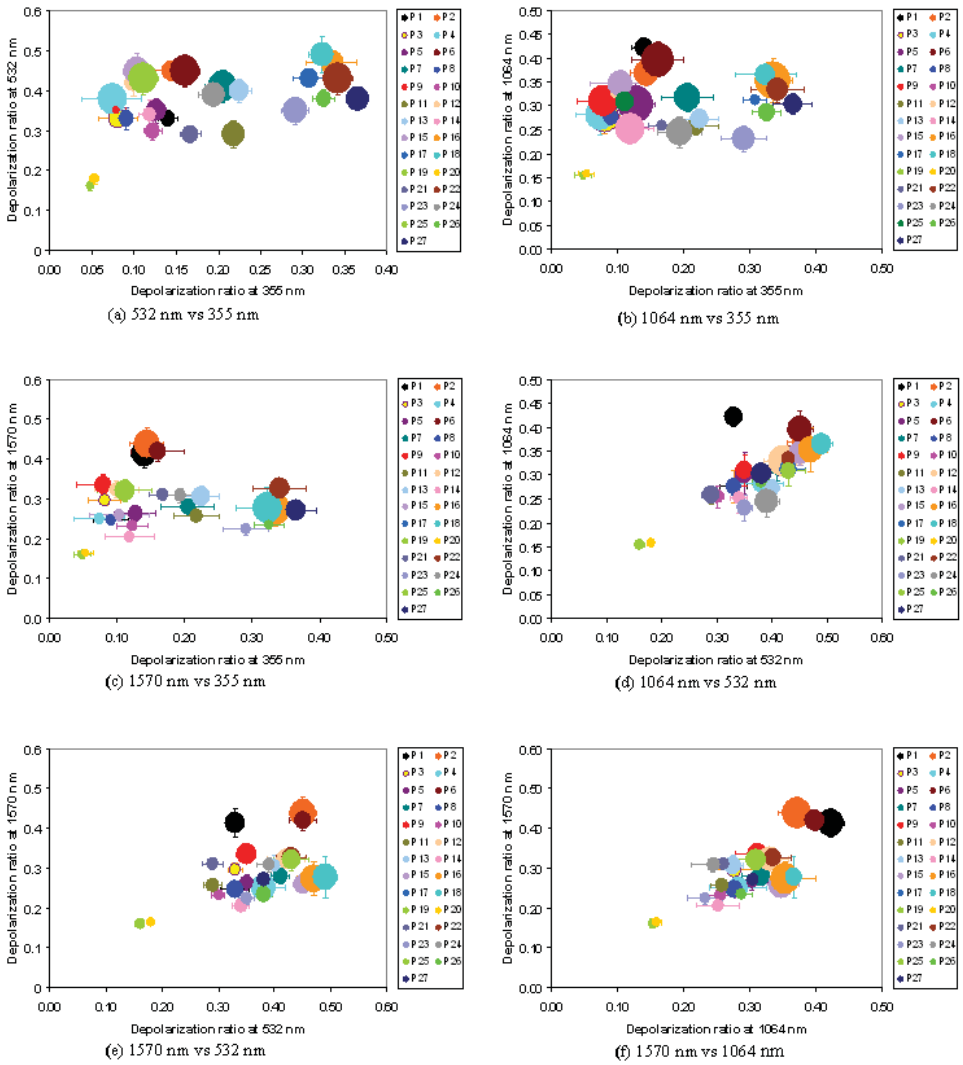

Figure 5: Graphical illustration of pollens discrimination using 2-wavelengths depolarization. (a) 355-532 nm; (b) 355-1064 nm; (c) 355-1570 nm; (d) 532-1064 nm, (e) 532-1570 nm; (f) 1064-1570 nm.

4.2.2 Discrimination by Cumulative Distribution

From the data that were presented in the previous section, it was noticed that some categories of pollens would show larger standard deviations within their depolarization ratio values at some wavelengths than some other categories. It was thought that another type of feature space could be helpful in the task of discriminating between pollens. That representation would show the cumulative distribution of the depolarization ratio of each pollen as is illustrated in the figure 6.

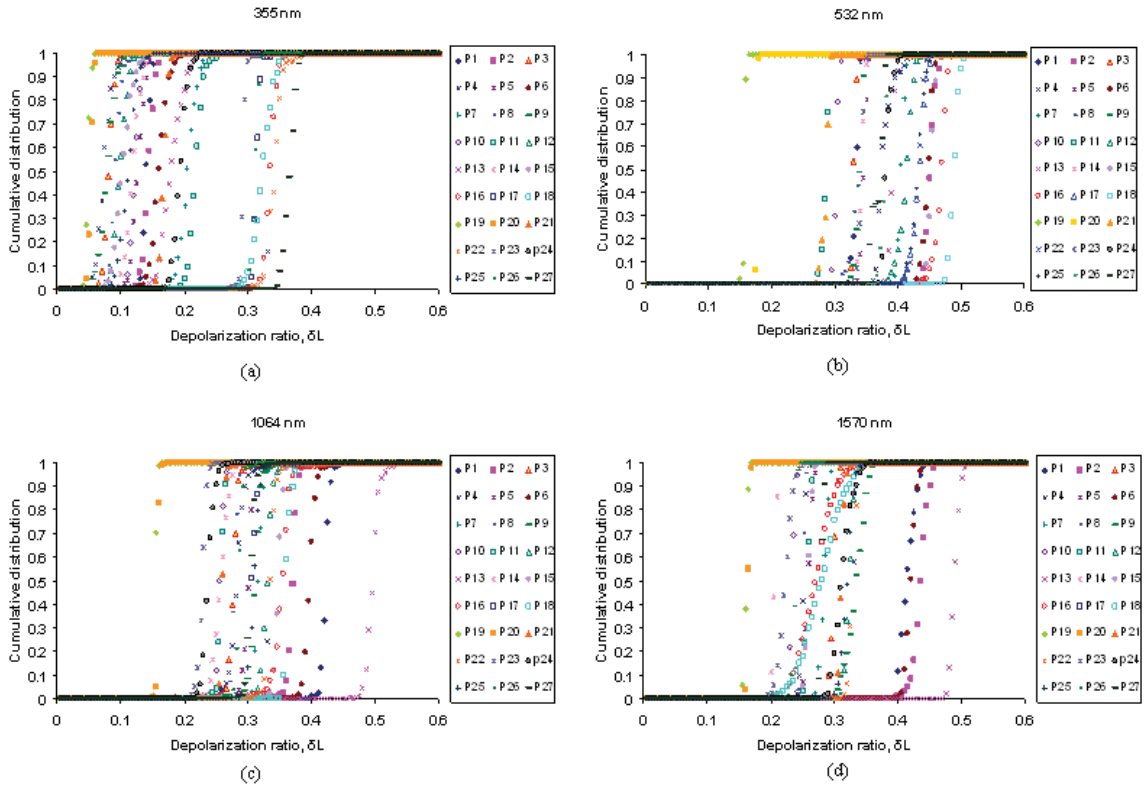

Figure 6: Cumulative distribution of pollen linear depolarization ratio at wavelength (a) 355 nm; (b) 532 nm; (c) 1064 nm and (d) 1570 nm

All the distributions are narrow and, though we can see the grouping of some pollens separated from others, many superimpose onto each other.

4.2.3 Discrimination by Mahalanobis distances

A statistical analysis tool is required to quantify the difference between each distribution. To do so, for a given pollen 'j', a vector is formed from each of the depolarization ratios obtained at the various wavelengths. Depending on how many wavelengths are considered, the vectors $\vec{p}_j$ will

be of different dimensions. All the different wavelengths combinations were considered. This leads to the following vectors definitions:

Single wavelengths: $\vec{p}_j(\delta_i)$: $\vec{p}_j(\delta_{355})$, $\vec{p}_j(\delta_{532})$, $\vec{p}_j(\delta_{1064})$, $\vec{p}_j(\delta_{1570})$;

Two wavelengths: $\vec{p}_j(\delta_i,\delta_k)$: $\vec{p}_j(\delta_{355},\delta_{532})$, $\vec{p}_j(\delta_{355},\delta_{1064})$, $\vec{p}_j(\delta_{355},\delta_{1570})$, $\vec{p}_j(\delta_{532},\delta_{1064})$, $\vec{p}_j(\delta_{532},\delta_{1570})$, $\vec{p}_j(\delta_{1064},\delta_{1570})$;

Three wavelengths: $\vec{p}_j(\delta_i,\delta_k,\delta_n)$: $\vec{p}_j(\delta_{355},\delta_{532},\delta_{1064})$, $\vec{p}_j(\delta_{355},\delta_{532},\delta_{1570})$, $\vec{p}_j(\delta_{355},\delta_{1064},\delta_{1570})$, $\vec{p}_j(\delta_{532},\delta_{1064},\delta_{1570})$;

Four wavelengths: $\vec{p}_j(\delta_i,\delta_k,\delta_m,\delta_n)$: $\vec{p}_j(\delta_{355},\delta_{532},\delta_{1064},\delta_{1570})$.

The correlation of the different vectors can be calculated as follows: $d_{Eucledian\_j,k} = (\vec{p}_j - \vec{p}_k)'(\vec{p}_j - \vec{p}_k)$.

However, when doing so, the variance of each measurement is not accounted for, and this could lead to false conclusions regarding whether or not two pollens have been discriminated against each other. For example, the distance based on the mean depolarization ratios between two pollens could be very large but, if the variance is large also, the two measurements could well be indistinguishable. Also, the distance based on the mean depolarization ratios between two pollens could be very small but, if the variance is small as well, the two measurements could well be distinguishable. In calculating the distance between two pollens, the variance of the measurements can be taken into account by using the following definition of the Mahalanobis distance:

$$d_{j,k} = (\vec{p}_j - \vec{p}_k)' M^{-1} (\vec{p}_j - \vec{p}_k) \qquad \text{(eq. 22)}$$

where M is the covariance matrix. The measurements of the different pollens at the different wavelengths being statistically independent, the covariance matrix is diagonal. What is interesting with the Mahalanobis distance is that it weighs the difference between two measurements with the inverse of the variance of the measurements. Consequently, the difference between two vectors could be very small but, if their variance is small also, they will show a large Mahalanobis distance, and vice versa.

Figures 7a and 7b show, for pollens P1 and P8 respectively, their calculated Mahalanobis distances (M-Ds) to all other pollens.

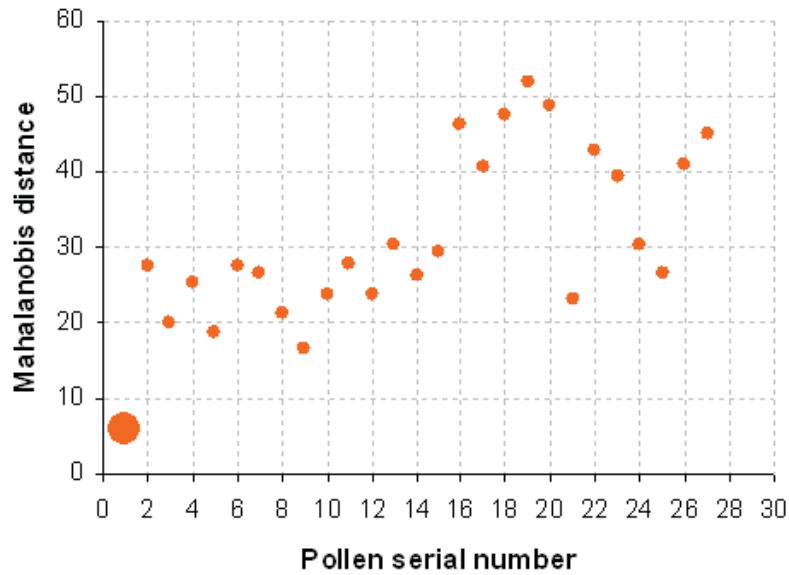

(a): P_1

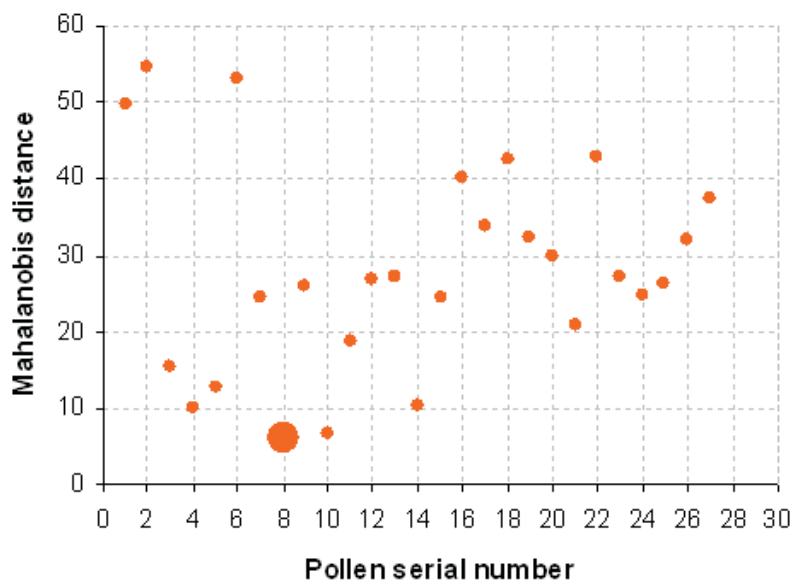

(b): P_8

Figure 7: Mahalanobis distances for pollens (a) P1 and (b) P8. The distance of each pollen to itself is shown with a double size symbol.

The M-D for the pollen with itself is naturally zero. Doing so, unless two pollens superimpose perfectly it seems it will always be possible to distinguish pollens from each other. But, in reality,

when we calculate the distances of each pollen with itself, we must account for the variance of the measurements. A natural way to do this is to resample a given pollen 'j' with bootstrap techniques for a given number of acquisitions and calculate the mean and variance and calculate the M-Ds. In a simplified manner, we can also calculate the M-Ds of the pollens with themselves at ± 3σ for instance (σ is the standard deviation) as follows:

$$d_{j\pm 3\sigma.j} = (\vec{p}_{j\pm 3\sigma} - \vec{p}_j)' M^{-1} (\vec{p}_{j\pm 3\sigma} - \vec{p}_j) \qquad \text{(eq. 23)}$$

And in a similar manner we calculate the M-Ds with the other pollens as follows:

$$d_{j\pm 3\sigma,k} = (\vec{p}_{j\pm 3\sigma} - \vec{p}_k)' M^{-1} (\vec{p}_{j\pm 3\sigma} - \vec{p}_k) \qquad \text{(eq. 24)}$$

The equation 24 has been used to calculate the M-Ds of all pollens between each other and will be the basis for estimating the efficiency of discrimination by polarization signature.

4.3 Results of discrimination with Mahalanobis distances

The data are presented in the Annex B. The Tables 4, 5, 6 and 7 in the Annex B present the calculated depolarization ratios for all pollens for the wavelengths 355 nm, 532 nm, 1064 nm and 1570 nm respectively. The figures 12, 13, 14 and 15 in Annex B do graphically represent the various depolarization ratios for each pollen for the wavelengths 355 nm, 532 nm, 1064 nm and 1570 nm respectively.

The values for δ_L and δ_C have been calculated with the equations 14 and 15 respectively. The values d_L and d_C represent the values of the parameter *d* when calculated by using the equations 18 and 17 respectively.

A look at any of the graphs presented in the figures 12, 13, 14 and 15 in Annex B will show that it will prove very difficult to obtain good discrimination by using only one of the depolarization ratios at only one wavelength. For instance, looking at the graph in the upper left corner of figure 12 (linear depolarization ratio δ_L at 355 nm), if a class of depolarization ratio between 0 and 0.1 was created, that class would have to include the pollens 2, 4, 6-7, 9-13, 15, 17, 21-23 and 27. The vertical error bars, which represent the 3σ deviations, need to be taken into account when deciding whether or not a pollen enters a specific class. The same difficulty for discrimination can be seen in any of the graphs presented in the figures 12, 13, 14 and 15 in Annex B. Of course, the discrimination task becomes the more difficult whenever we increase the extent of the uncertainty zone around each pollen. Taking 3σ deviations instead of 1σ deviations, makes the discrimination a more demanding task. This will be discussed later in this section.

Not much more can be concluded from the figures 12 to 15 except that the pollens 18-20 (barley grain, corn grain and wheat grain dusts) always seem to show large deviations, and this at all wavelengths. The figure 16 in Annex B shows an expanded view of the figure 6. Figure 6 shows the cumulative distributions of linear depolarization ratios for all pollens at all wavelengths. If some pollens, like the grain dusts 18-20, show peculiarities in the fluctuation of their signal, figure 16 shows that this behavior could hardly be used to achieve a better discrimination.

This consideration led to the use of an objective statistical analysis tool for discriminating between the pollen polarization signatures. This tool is the Mahalanobis distance described in section 4.2.3 and equations 23 and 24.

The M-Ds were calculated with equations 23 and 24 for all the possible combinations of wavelengths. They were calculated for the case of the linear depolarization ratio only. The M-Ds for the 4-wavelengths case are represented graphically in the figure 17 a to d in Annex B. The M-Ds are shown distributedly over the 4 figures 17a to 17d in order to reduce confusion. No claim of similarity between the polarization signatures should be sought for behind the choice of the members of any group of pollens shown in the figures. The M-Ds of the pollens (+3σ) to themselves in the 4-wavelengths case, calculated with Eq. 23, equal 6 and are indicated with symbols twice the size. So any pollen 'k' with $d_{j\pm3\sigma,k}$ smaller than or equal to $d_{j\pm3\sigma,j}$ (here = 6) cannot be distinguished from the pollen 'j'.

It is the goal of this work to quantify the strength of the discrimination of the different pollens and we make it through the use of the Mahalanobis distances. To do so, histogram distributions $f(d_{j\pm3\sigma,k})$ of Mahalanobis distances have been constructed from our data set for vectors of dimension 1, 2, 3 and 4. The aim is to quantify, for each set dimensionality, the percentage of M-Ds that are located above the discrimination level, which is calculated in terms of the pollens self-distances.

The histograms are built with 30 classes defined as follows:

$$\Delta_l = Log(d_{\min}) + (l/L)(Log(d_{\max}) - Log(d_{\min}))\text{ ; } l=0 \text{ to } L\ (L=29). \qquad \text{(eq. 25)}$$

The different classes are: $x_l = 10^{\Delta_l}$; the x_l are the upper limits for each class. The total number of possible distances (1458) has been normalized to 100%. For each plot, $f(d_{j\pm3\sigma,j})$ is built with $d_{j\pm3\sigma,j}$ being obtained from the autocorrelations of $\vec{p}_j$ with $\vec{p}_{j,+3\sigma}$ and $\vec{p}_{j,-3\sigma}$. The value of $f(d_{j\pm3\sigma,j})$ always represents 3.7% of all the distances and its position on the scale of all M-Ds is shown in dark on the graphics.

Figures 8a to 8d below show the 1-wavelength vectors results while figures 9a to 9f show the histograms for the 2-wavelengths vectors data set made out of the six vectors $\vec{p}_j(\delta_i, \delta_k)$. Figures 10a to 10d show the histograms for the 3-wavelengths vectors data set made out of the four

vectors $\vec{p}_j(\delta_i, \delta_k, \delta_m)$. Finally figure 11 shows the histogram for the 4-wavelengths data set $\vec{p}_j(\delta_{355}, \delta_{532}, \delta_{1064}, \delta_{1570})$.

For all the graphics, the extent of the region of the distribution $f(d_{j\pm 3\sigma,k})$ with M-Ds larger than the value of $f(d_{j\pm 3\sigma,j})$, which we remember to be the value of the self-distances, is taken to be a measure of the discrimination power of the method.

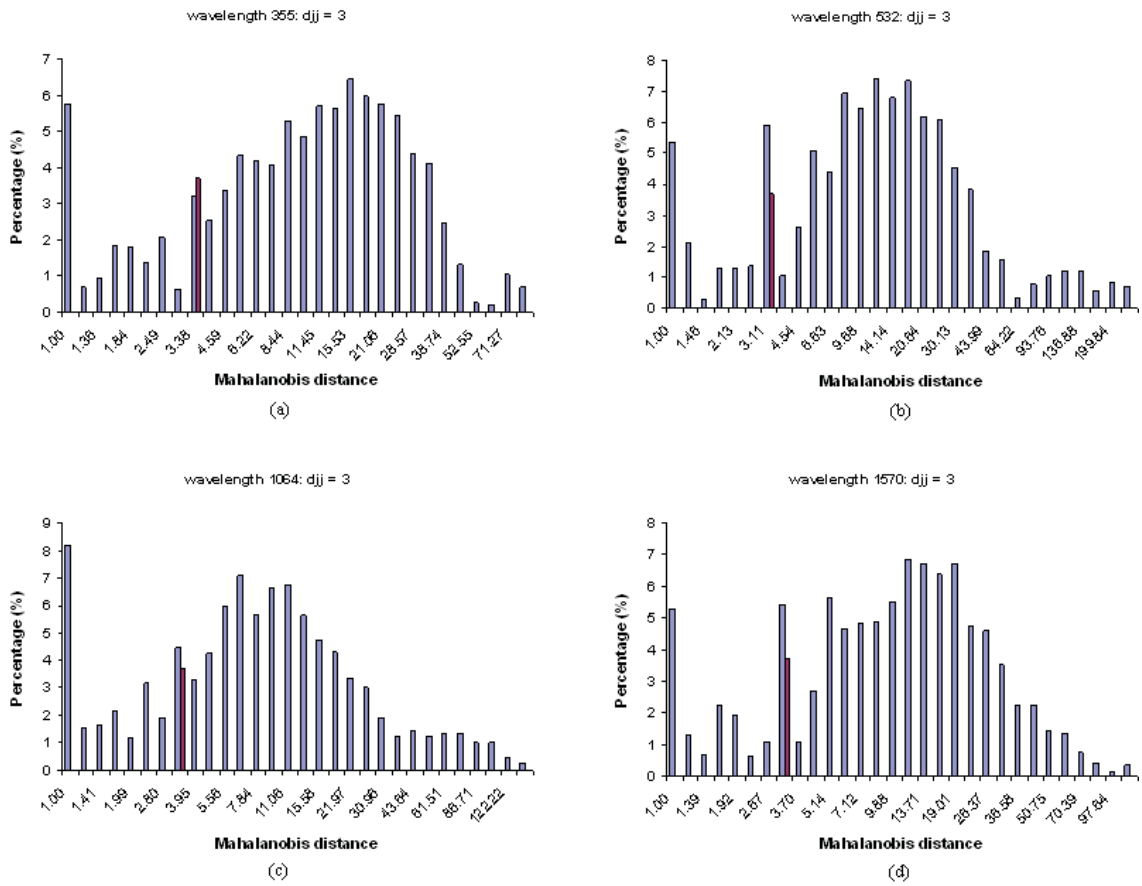

Figure 8: Histograms of pollen discrimination based on Mahalanobis distance using one wavelength (a) 355 nm, (b) 532 nm, (c) 1064 nm and (d) 1570 nm.

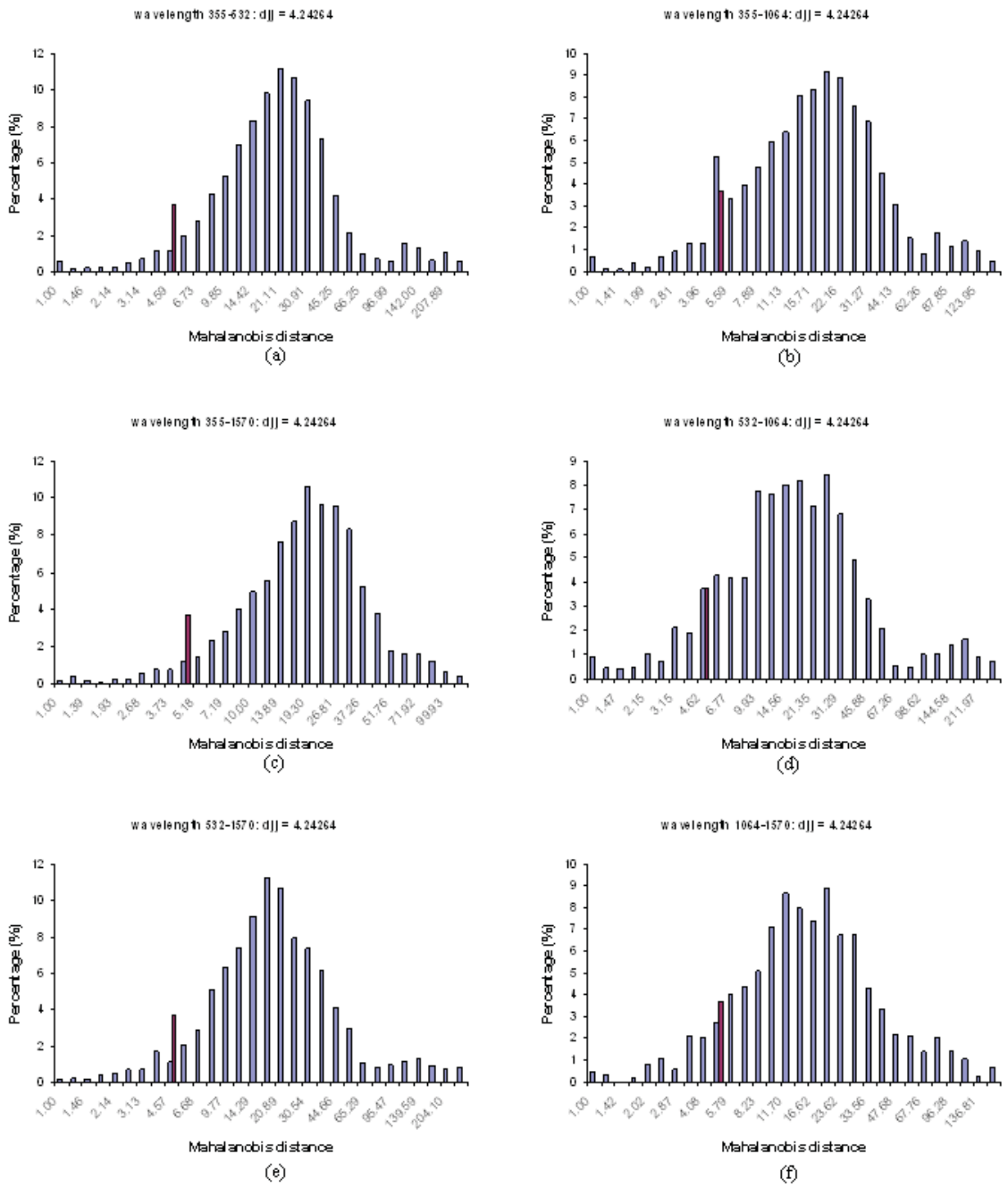

Figure 9: Histograms of pollen discrimination based on Mahalanobis distance using two wavelengths (a) 355-532 nm; (b) 355-1064 nm; (c) 355-1570 nm; (d) 532-1064 nm; (e) 532-1570 nm; (f) 1064-1570 nm.

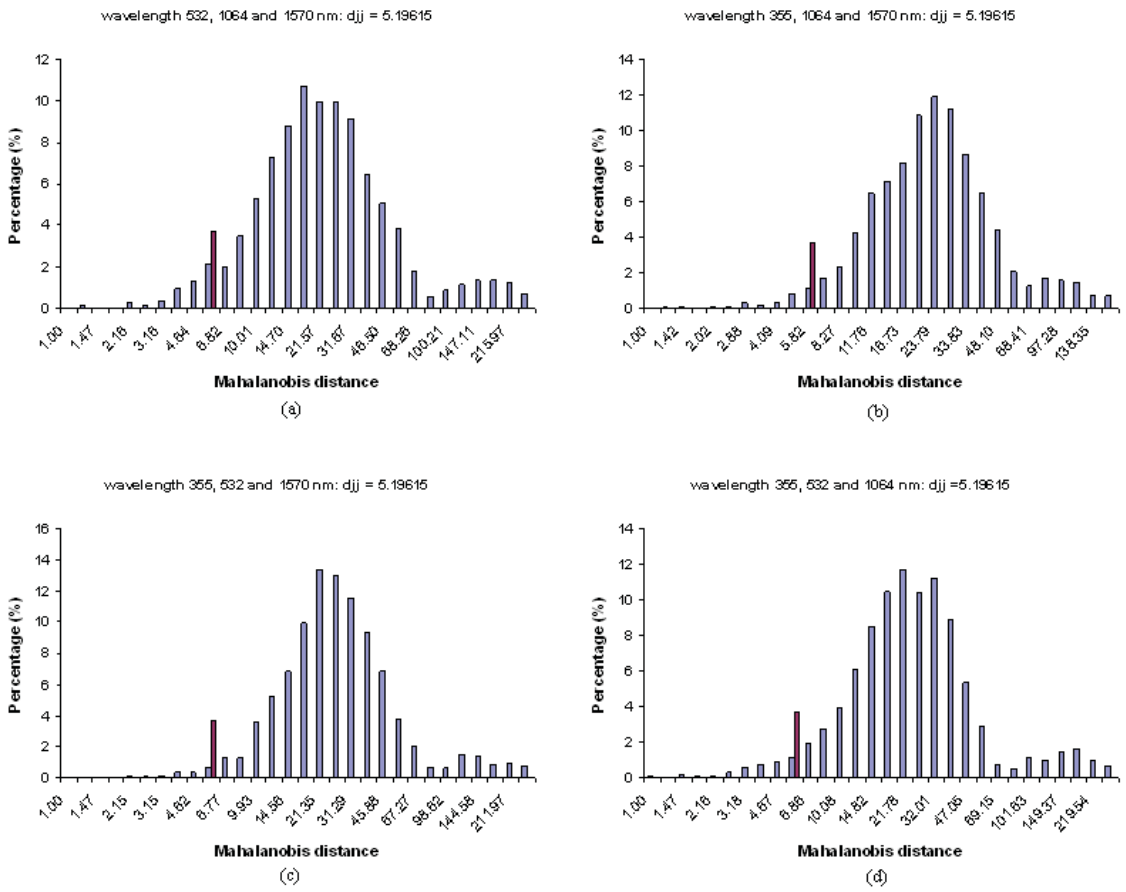

Figure 10: Histograms of pollen discrimination based on Mahalanobis distance using three wavelengths (a) 532-1064-1570 nm; (b) 355-1064-1570 nm; (c) 355-532-1570 nm; (d) 355-532-1064 nm.

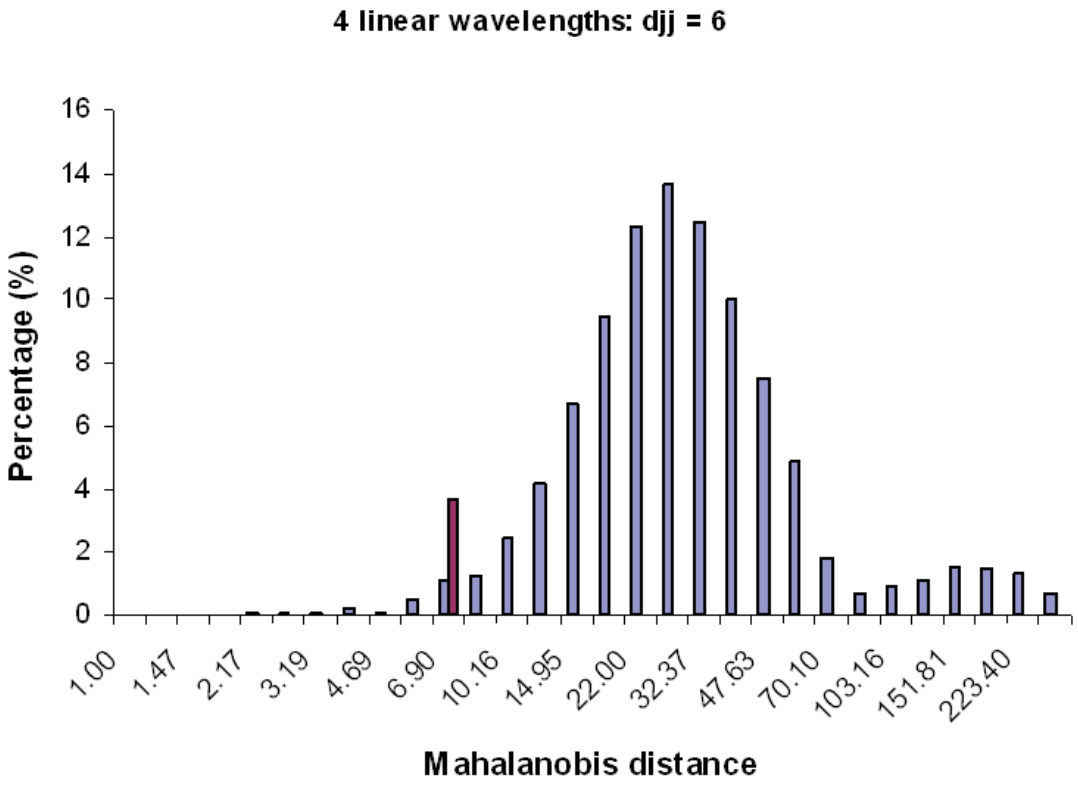

Figure 11: Histogram of pollen discrimination based on Mahalanobis distance using four wavelengths (355-532-1064-1570 nm).

The Table 2 below summarizes the results of the figures 8 to 11. In short, for a single wavelength system, non-discrimination rate is between 17% and 24%. The non-discrimination rate goes down to values ranging from 4% to 10% for the 2-wavelengths measurements. For the 3-wavelengths measurements, it is between 1% and 4% and, for the combination of 4 wavelengths, non-discrimination goes down to a level of 1%.

Table 2: Statistics of non-discrimination of pollens using different numbers of wavelengths

Number of wavelength	wavelengths (nm)	Non-discrimination (%)
4	355, 532, 1064 and 1570	1
3	532, 1064 and 1570	4
	355, 1064 and 1570	3
	355, 532 and 1570	1
	355, 532 and 1064	4
2	355 and 532	5
	355 and 1064	6
	355 and 1570	4
	532 and 1064	10
	532 and 1570	5
	1064 and 1570	8
1	355	17
	532	17
	1064	24
	1570	18

Generally, the more wavelengths are used, the higher the discrimination rate is expected to be. However, the same discrimination is obtained here with a 3-wavelengths combination (355, 532 and 1570 nm), whose non-discriminate rate is only 1%, as the one obtained with the 4-wavelengths combination (with discrimination rate also 1%). If the system is limited to 2 wavelengths, the best result is obtained with 355 and 1570 nm. For single wavelength systems, the best choice would appear to be 355 or 532 nm.

It must be recalled here that the M-Ds have been calculated and analyzed in the case of the linear depolarization ratio only.

The results above must be interpreted in the following way: among all the 1458 possible combinations of pollens MDs calculations, a few percents only (1 to 4 for the 4 and 3 wavelengths cases respectively) showed MDs under the value of the self MDs. Now, these few percents may correspond to real and non negligible absolute values. In order to be more factual about the capability of the polarimetric lidar to discriminate between different bioaerosols, it is necessary to peer more in depth into the calculated results. This is done by comparing, for each possible combination of pollen *j* with pollen *k*, the value of the MD self-distance (equation 23) to the value of the *j*-*k* MD (equation 24). When this is done, it is found that the efficiency to discriminate between bioaerosols will greatly depend on the extent of the uncertainty zone traced around each particle. If it is asked that all particles be defined by a 3σ deviation zone, then it is found that, even in the case of 4 wavelengths, only 74% of the bioaerosols will be truly discriminated against the others. If the uncertainty zone is reduced by steps from 3σ to 1σ, then it is found that a 100% discrimination rate is achieved in the case of 4

wavelengths and a 98% discrimination rate is achieved in the case of 3 wavelengths (355, 1064 and 1570 nm). These results are presented in the Table 3 below.

This is not surprising since there exist physical similarities between many of those various pollens. As a consequence, demanding too large an uncertainty zone around each pollen will have closely related pollens fall into each other's uncertainty zone.

Table 3: Absolute results of non-discrimination of individual pollens using different numbers of wavelengths and different uncertainty zones

		Wrong discrimination rate			
Nb of wavelengths	**wavelength**	**1σ**	**1.5σ**	**2σ**	**3σ**
1	355 nm	81.48%	83.33%	90.74%	92.59%
	532 nm	68.52%	83.33%	83.33%	85.19%
	1064 nm	75.93%	87.04%	90.74%	92.59%
	1570 nm	74.07%	81.48%	85.19%	90.74%
2	355+ 532	12.96%	29.63%	46.30%	64.81%
	355+1064	18.52%	38.89%	50.00%	62.96%
	355+1570	20.37%	38.89%	50.00%	62.96%
	532+1064	35.19%	51.85%	57.41%	68.52%
	532+1570	16.67%	31.48%	42.59%	61.11%
	1064+1570	29.63%	38.89%	50.00%	66.67%
3	532+1064+1570	9.26%	16.67%	27.78%	50.00%
	355+1064+1570	1.85%	11.11%	24.07%	44.44%
	355+532+1570	3.70%	7.41%	20.37%	29.63%
	355+532+1064	3.70%	16.67%	35.19%	51.85%
4	355+532+1064+1570	0.00%	1.85%	5.56%	25.93%

The results displayed in the Table 3 show that the previous assessment of the capability of a polarimetric lidar to discriminate between bioaerosols still holds.

4.4 Discussion of the results

It has been shown that pollens have specific signatures in terms of lidar linear depolarization ratios. The measurements were performed under a semi-controlled environment in this sense that the aerosols (2g) were disseminated as a dry powder in an aerosol chamber. The measurements were performed at 4 wavelengths: 355 nm, 532 nm, 1064 nm and 1570 nm.

Validation of the repeatability of depolarization measurements has been performed on 4 materials using the exact same experimental procedure. The depolarization ratios agree from one measurement to another within a few percents and the variance is practically identical. The good agreement between independent measurements is attributed to the way the depolarization ratios

are measured; it is practically free from calibration or system drift as explained in section 3. Naturally, the agreement would not be as good if the time between horizontal and vertical illumination was long, allowing temperature change in the sensor and electronics. The major difference in the values of the depolarization ratios from one lidar system to another will most likely come from depolarization caused by the collecting optics. For instance, the use of protected aluminum coating instead of gold coating for the scanning platform mirrors can lead to an increase of the linear depolarization by as much as 20% at 1570 nm as an example.

However, the reported values are not exempt of specificities regarding the experiments as they were conducted. For example, the dissemination device used has an influence on the amount of agglomeration of the particles [9] and that certainly could affect the depolarization ratios. The effect of relative humidity on the depolarization signature of natural aerosols has been observed. The observed effects are mainly attributed to the solubility of aerosols [10, 11]. Hence, as long as the bioaerosols are not soluble, change in the depolarization signature should not be important when dry aerosols are being dispersed, and this has been the case here. However, bioaerosols dispersed from water slurry will show depolarization ratios that will increase with time because of the evaporation of the water surrounding the bioaerosol. The rate of evaporation of the droplet is a function of relative humidity and temperature. The section 4.5 that immediately follows reports the results of some preliminary works that have been done on the subject of the influence of humidity and temperature on the time evolution of the polarization signature of bioaerosols.

Another source of specificities of our results comes from the lidar systems themselves, be it the Imaging MFOV or the Non-Imaging one. The use of horizontal and vertical polarization illuminations to measure the depolarization ratio allows, to a good extent, system free measurements but not completely. A system using scanning mirrors will show some varying depolarization effects caused by the mirrors. Also, a multi-wavelengths system will most likely use dichroic mirrors to separate the various wavelengths prior to do the polarization separation. Here again, mirrors induced polarization effects will be difficult to avoid.

There remains still that the lidar depolarization ratios measurements show specificities that allow discrimination to a good extent. Our main observations are as follows:

i. the depolarization ratios are wavelength dependent;
ii. for single wavelength measurements, higher discrimination is obtained at shorter wavelengths;
iii. the discrimination efficiency increases significantly with the number of wavelengths used;
iv. the depolarization ratios are usually system dependent.

In the next section, the question as to whether or not two polarizations (linear and circular) or only one (linear or circular) are required for bioaerosols discrimination will be investigated.

4.5 Preliminary results on the time evolution of the polarization signature due to humidity and temperature

In order to start gaining some experience with this subject of the time evolution of the polarization signature which could be caused by the evaporation of the water attached to bioaerosols, some preliminary works have been done with some dusts.

The materials that have been tested are: Arizona dust (ARD), Afghanistan dust (AFD), some glass microbeads (GLS) and some graphite particles (GRA). For each material, 2 grams of it was mixed with 200 ml of unpurified water and the same pneumatic nozzle dissemination system and procedure as described in section 4.1 was used. For each material, 10 to 12 consecutive measurements were performed, each consisting of 200 to 1000 acquisition shots, depending on the duration of the time evolution of the polarization effects.

The figures 18a to 18d show the results of time evolution of the depolarization ratio for the ARD. These data are very representative of all the others, which are presented in the Annex C. Each figure gives the result for one specific wavelength.

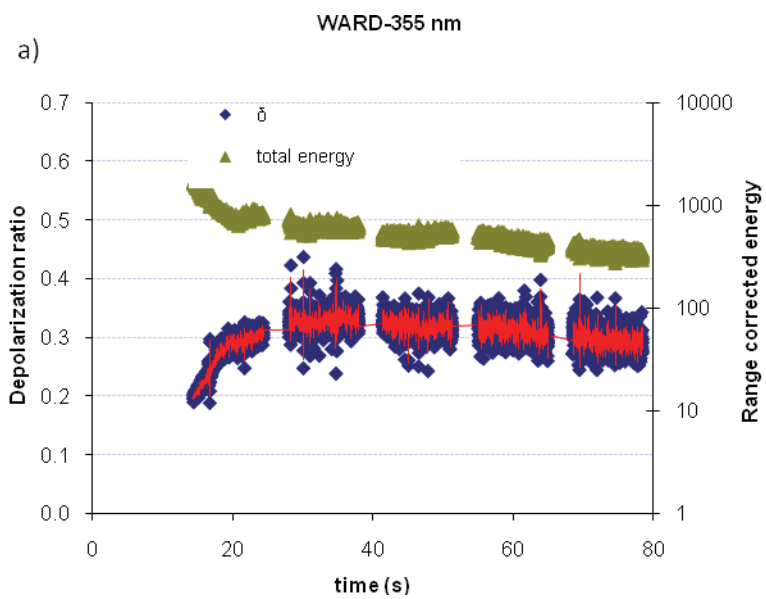

b)

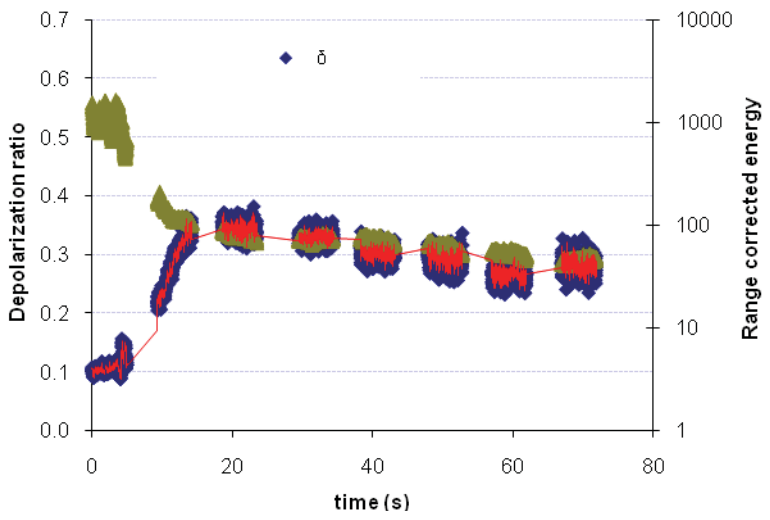
WARD-532 nm
δ
Depolarization ratio
Range corrected energy
time (s)
0.0
0.1
0.2
0.3
0.4
0.5
0.6
0.7
1
10
100
1000
10000
0
20
40
60
80

c)

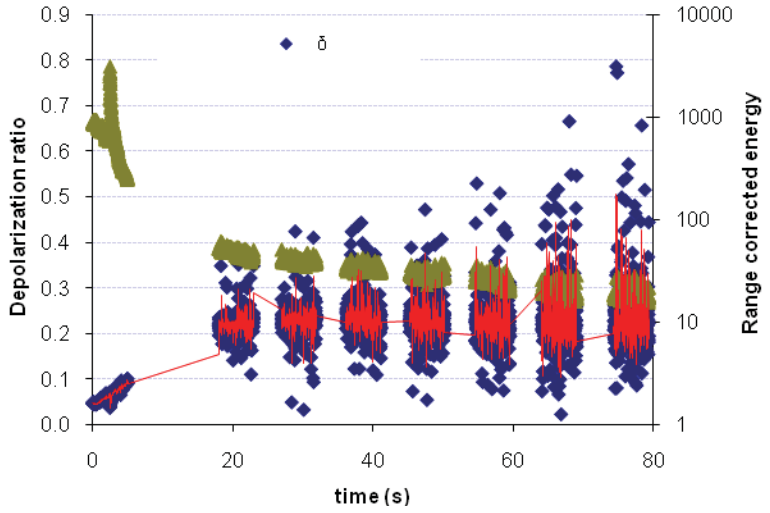
WARD-1064 nm
δ
Depolarization ratio
Range corrected energy
time (s)
0.0
0.1
0.2
0.3
0.4
0.5
0.6
0.7
0.8
0.9
1
10
100
1000
10000
0
20
40
60
80

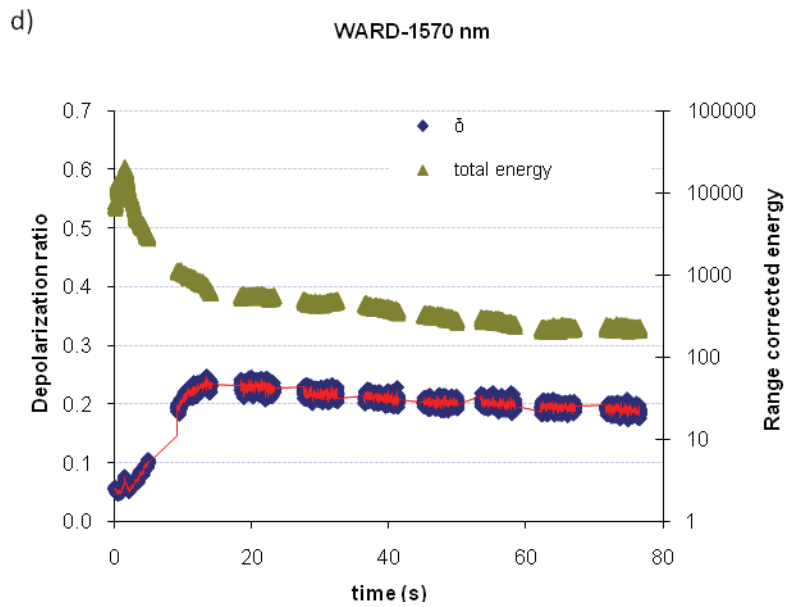

Figure 18: Time evolution of the polarization signature of wet Arizona dusts at a) 355 nm, b) 532 nm, c) 1064 nm and d) 1570 nm.

For the measurements taken at any specific wavelength, the values of the temperature T and Relative Humidity RH were the same for all the specimen, including those whose results are only displayed in Annex C. The values of those parameters are given in the Table 8.

Table 8: Temperature and Humidity conditions for measurements on wet dusts

Wavelength (nm)	Temperature (^{o}C)	Relative Humidity (%)
355	12	50
532	Not recorded	Not recorded
1064	17	31
1570	27	22

What is observed in all these figures is that, as the water content of the particulate cloud evaporates as time goes on, the depolarization ratio increases until it reaches a stable level, which is representative of the dry dust polarization signature. An example of the depolarization ratio of a dry ARD specimen at 355 nm is shown in the figure 19. The depolarization ratio is very stable at 0.30, very close to the stabilization level reached after 40 s in figure 18a.

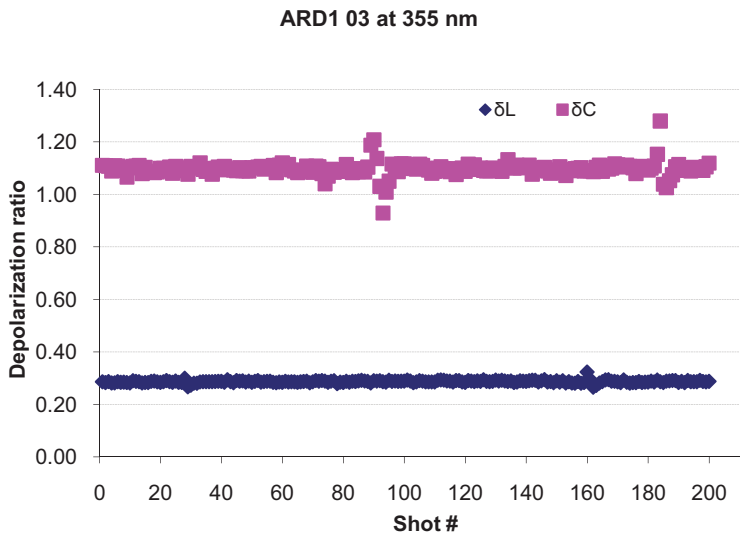

Figure 19: Depolarization ratio of dry ARD at 355 nm

The water which was used for all these tests was not purified water. Hence, it could itself include dusts or some other contaminant materials. The figures 20a to 20d show, for water specimen of the type used for the mixes described above, the same time evolution graphs as were displayed in figures 18a to 18d for ARD.

a)

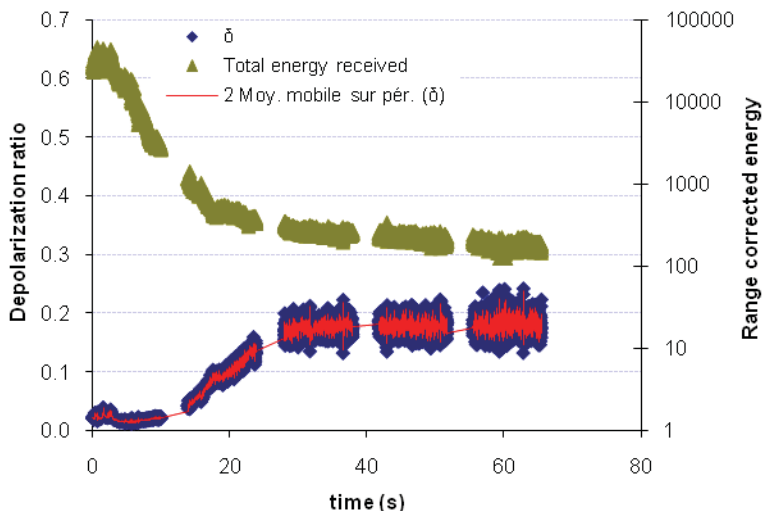
water-355 nm
δ
Total energy received
2 Moy. mobile sur pér. (δ)
Depolarization ratio
Range corrected energy
time (s)
0.7
0.6
0.5
0.4
0.3
0.2
0.1
0.0
100000
10000
1000
100
10
1
0
20
40
60
80

b)

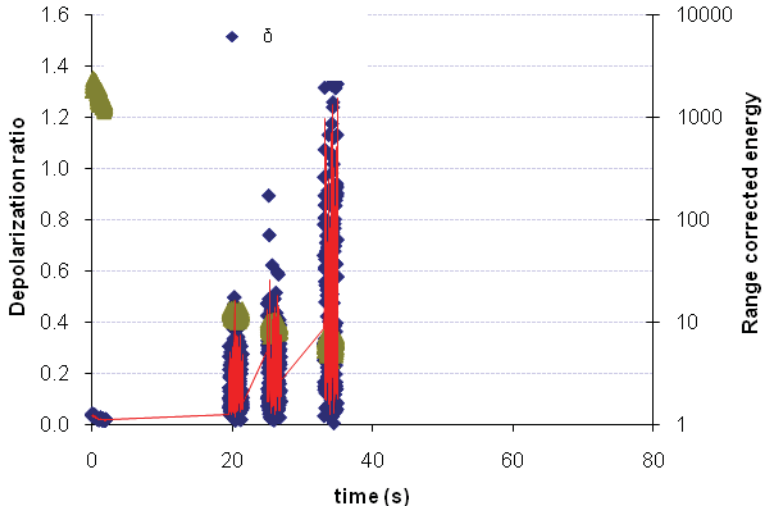
water-532 nm
δ
Depolarization ratio
Range corrected energy
time (s)
1.6
1.4
1.2
1.0
0.8
0.6
0.4
0.2
0.0
10000
1000
100
10
1
0
20
40
60
80

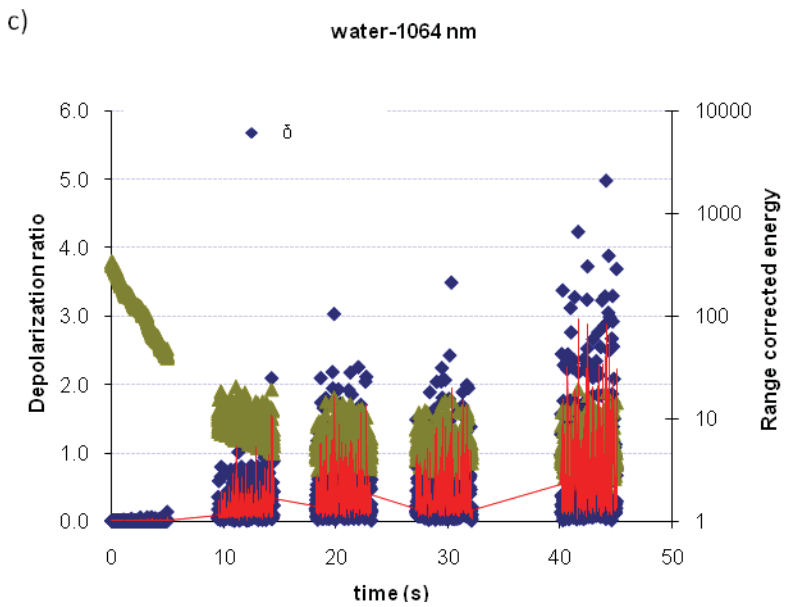

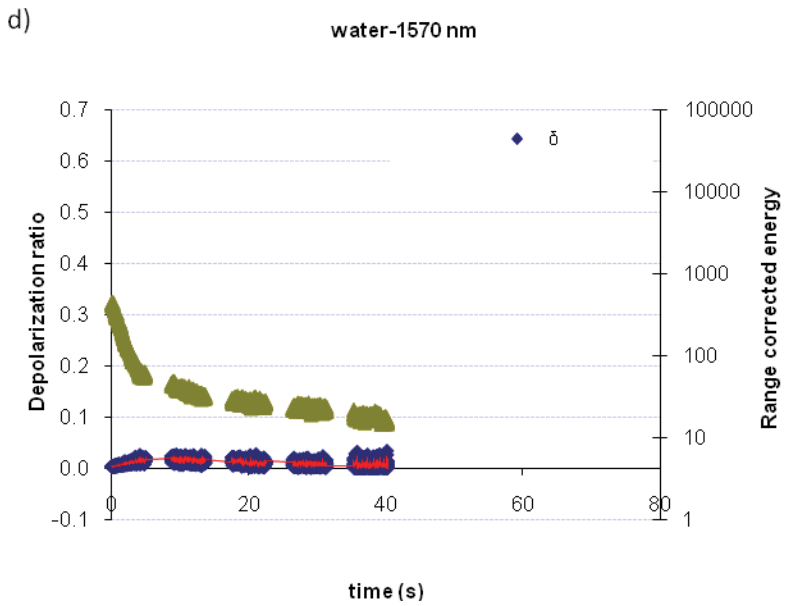

Figure 20: Time evolution of the polarization signature of non purified water specimen at a) 355 nm, b) 532 nm, c) 1064 nm and d) 1570 nm.

The type of time evolution of the depolarization ratio seen in the figures 20a to 20d is comparable to that observed for ARD in figures 18a to 18d. This suggests that there were contaminants in the water specimen and that, as soon as water itself evaporates away, it is the dry state depolarization ratio of those contaminants which is measured.

The preliminary results obtained here are consistent with those presented in references 10 and 11 briefly discussed in the section 4.4 above.

Further works remain to be done in this area. The results for AFD, GLS and GRA are given in the Annex C. They show the same general trend and will not be discussed further here.

5 ABOUT THE INFORMATION CONTENT OF LINEAR AND CIRCULAR POLARIZATIONS FOR POLLENS

In reference [5], Gimmestad has established that the depolarization by a random distribution of particles should be representable by a one parameter only scattering matrix. The parameter *d* is deemed to include all pertinent information concerning the effect of those particles on incident polarized light.

Indeed, according to the theory, the linear depolarization and circular depolarization ratios are physically as well as algebraically related to each other for randomly oriented aerosols. Therefore, in theory, the linear depolarization ratio can be obtained from the circular depolarization one and vice-versa. Moreover, the use of the depolarization parameter, *d*, leads to a Mueller scattering matrix having a single free parameter, in occurrence *'d'*. Indeed the general form of the Mueller matrix that describes a partially depolarizing backward scattering process is:

$$M_{atm} = p(180^o)\begin{pmatrix} 1 & 0 & 0 & 0 \\ 0 & 1-d & 0 & 0 \\ 0 & 0 & d-1 & 0 \\ 0 & 0 & 0 & 2d-1 \end{pmatrix} \qquad \text{(eq. 26)}$$

The relation between the linear depolarization ratio, the circular depolarization ratio and the parameter *d* was already given in equation 19 above but we recall it here:

$$d = \frac{2\delta_L}{1+\delta_L} = \frac{\delta_C}{1+\delta_C} \qquad \text{(eq. 19)}$$

If equations 26 and 19 are supported by the experimental data, this has a major impact on the considerations that must be gone through while designing a polarimetric lidar for the atmospheric or space-based lidar studies of randomly distributed particles. Indeed, if only one polarization state contains all pertinent information about those particles, then the technical specifications of such lidars are considerably relaxed.

It is the specific aim of the works reported in this section to investigate further into the phenomenological validity of these two equations. For achieving this goal, the data in the Tables 4, 5, 6 and 7 have been used. In those tables, the linear depolarization ratio δ_L has been calculated from the experimental data with equation 14. Then, equation 19 was used in order to calculate the linear depolarisation parameter d_L. In the same tables, the circular depolarization ratio δ_C has been calculated from the experimental data with equation 15. Then, equation 19 was used in order to calculate the circular depolarization parameter d_C. If equations 26 and 19 are right, we should expect to find $d_L = d_C$ and a graph of d_L with respect to d_C to yield a right line of slope 1.

First, equation 19 has been manipulated in order to rewrite δ_C in terms of δ_L :

$$\delta_C = \frac{2\delta_L}{1-\delta_L} \qquad \text{(eq. 27)}$$

If the data obey equation 27, it will mean that the circular depolarization ratio can be obtained from the linear one and vice versa. It would then follow that the measurement of only one polarization is sufficient to cover all the information content pertinent to randomly distributed particles.

However, the data need first to be corrected for the effects of intrinsic system depolarization due to the scanning mirrors.

In order to characterize the inherent system depolarization, measurements on fog-oil droplet cloud have been performed (an ideal system will measure a depolarization of zero because backscattering from spherical particles does not depolarize the light). Figures 21 and 22 reproduce some lidar signals from fog-oil droplets clouds at the wavelength of 532 nm. Figure 21 is for linear polarization (Horizontal and Vertical), while figure 22 is for circular polarization (Right and Left). Due to the very small secondary polarization signals, a log scale has been used.

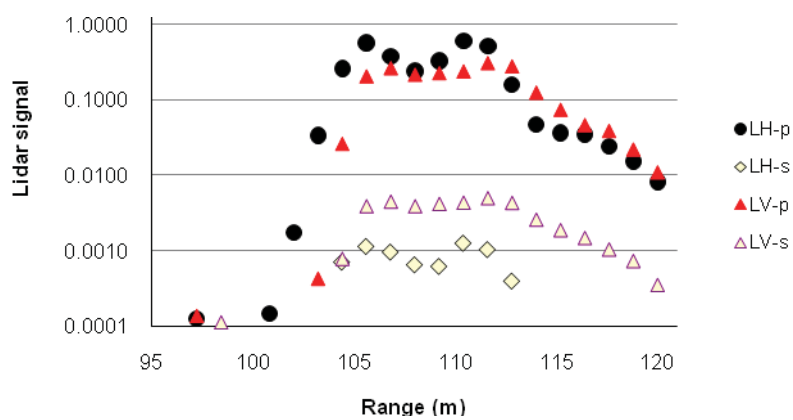

Figure 21: Range corrected lidar signal returns of a fog oil vs. distance. H and V represent linear horizontal and vertical illumination, and p and s represent principal and secondary polarization signals

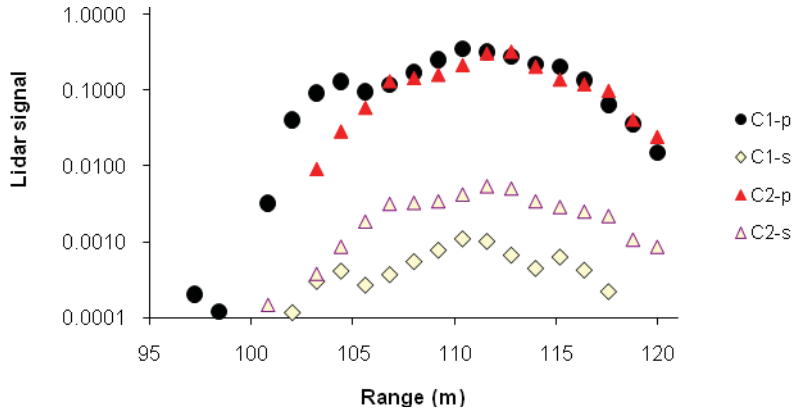

Figure 22: Range corrected lidar signal returns of a fog oil vs. distance. C1 and C2 represent circular right and circular left, and p and s represent principal and secondary polarization signals

Table 9 shows the inherent system depolarization for linear and circular polarization for the 4 wavelengths.

Table 9: Measured inherent depolarization of the lidar system at different wavelengths and for different mirrors coatings

	δL	δC
355 (Protected Aluminum)	0.01	0.04
532 (Protected Aluminum)	0.01	0.26
532 (Silver)	0.01	0.02
1064 (Protected Aluminum)	0.02	0.04
1064(Gold)	0.02	0.02
1570(Gold)	0.01	0.01

The inherent depolarization ratios are usually fairly low: a few percents except for the circular polarization at 532 nm with a protected aluminum coating. At 355, 532 and 1064 nm protected aluminum mirrors have been used. At 355 nm and 1064 nm, the inherent depolarization is quite acceptable while at 532 nm the effect is very important. Use of a silver coating at 532 nm changed the situation. This is the problem with protective optics and great care must be given in the selection of mirror coatings for polarimetric lidars. Additional tests were performed at 532 nm using bare silver coating on the scanning platform to verify that indeed the depolarization was caused by the mirror coating.

We thus recalculated δ_L as per the equation 28 to account for the intrinsic depolarization:

$$\delta_L = \sqrt{\delta'_H \delta'_V} - \delta_{LS} \qquad \text{(eq. 28)}$$

We also recalculated new values for δ_C as a function of equation 29:

$$\delta_C = \sqrt{\delta'_R \delta'_L} - \delta_{CS} \qquad \text{(eq. 29)}$$

Figure 23 shows the corrected circular depolarization ratio as a function of the corrected linear depolarization ratio for the 4 wavelengths. Also shown on the plots, the theoretical relationship provided by Eq. 27. The measured depolarization ratios follow rather well the theoretical relationship. It seems there are small positive biases on the circular polarization measurement and there are a few measurements that appear off the general tendency.

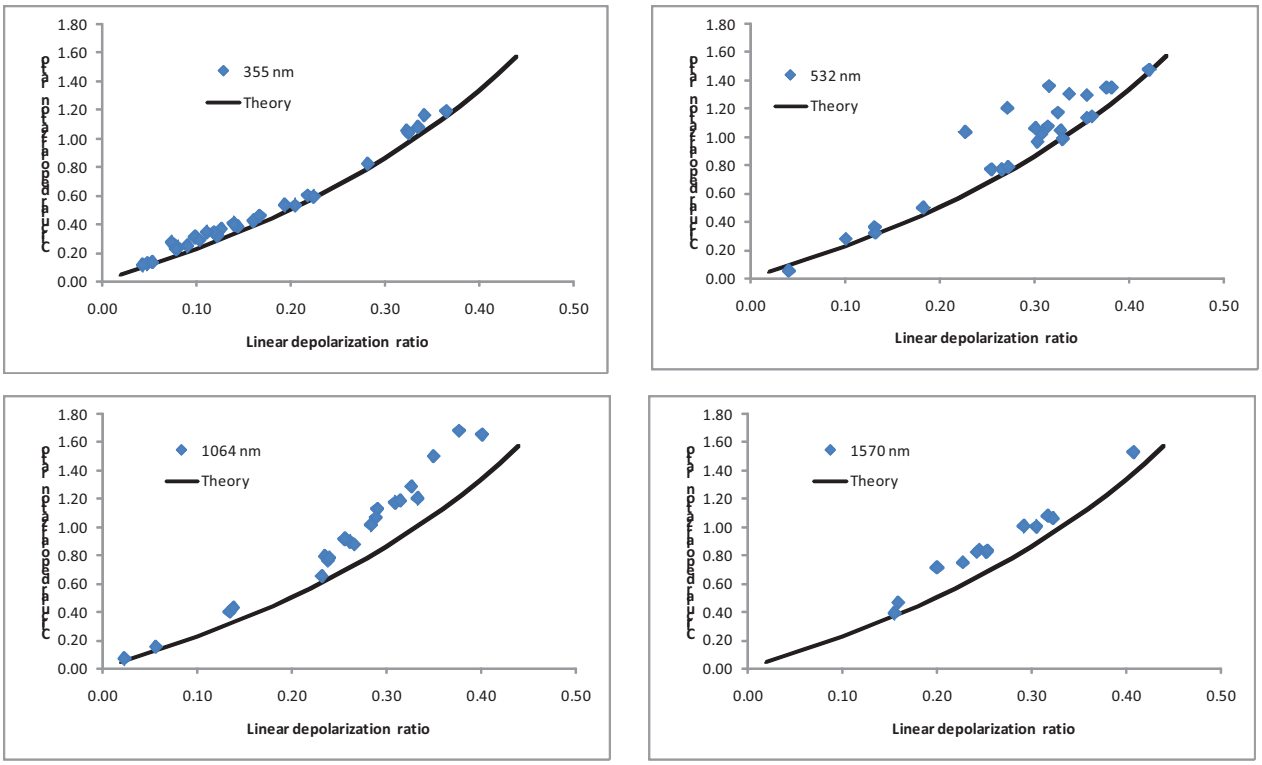

Figure 23: Circular depolarization ratio as a function of the corrected linear depolarization ratio for the 4 wavelengths: 355 nm; 532 nm; 1064 nm and 1570 nm.

In figure 20, the solid line represents the theoretical relationship of equation 27 which should be found between δ_C and δ_L. The equation 27 is very close to be perfectly obeyed except at the wavelength 532 nm. Also, from the graphs above, it is seen that the circular depolarization ratio δ_C is always higher than predicted by the equation 27. This fact points towards the presence of a systematic error. This error was found to lie in the intrinsic depolarization induced by the instrument itself and to vary from one wavelength to the next. This intrinsic instrumental

depolarization is related to the effect that the scanning mirrors have on the source light polarization.

Now we can address the main objective of this section: to show that the representation of the Mueller matrix for randomly oriented aerosols is achieved with a single parameter, namely the depolarization parameter, *d*. To do so, corrected depolarization parameters are calculated by subtracting the inherent depolarization ratio of the system from the depolarization measurement:

$$d_L = \frac{2(\delta_L - \delta_{LS})}{(1 + (\delta_L - \delta_{LS}))} \tag{30}$$

$$d_C = \frac{(\delta_C - \delta_{CS})}{(1 + (\delta_C - \delta_{CS}))} \tag{31}$$

Figures 24 to 27 show the corrected depolarization parameters for circular polarizations as a function of the polarization parameter obtained from linear polarizations. Also shown on the same figures the uncorrected polarization parameters. Results obtained with some spectralon specimen are also displayed with different symbols. Spectralon specimens seem an easy way to emulate systems of randomly distributed particles.

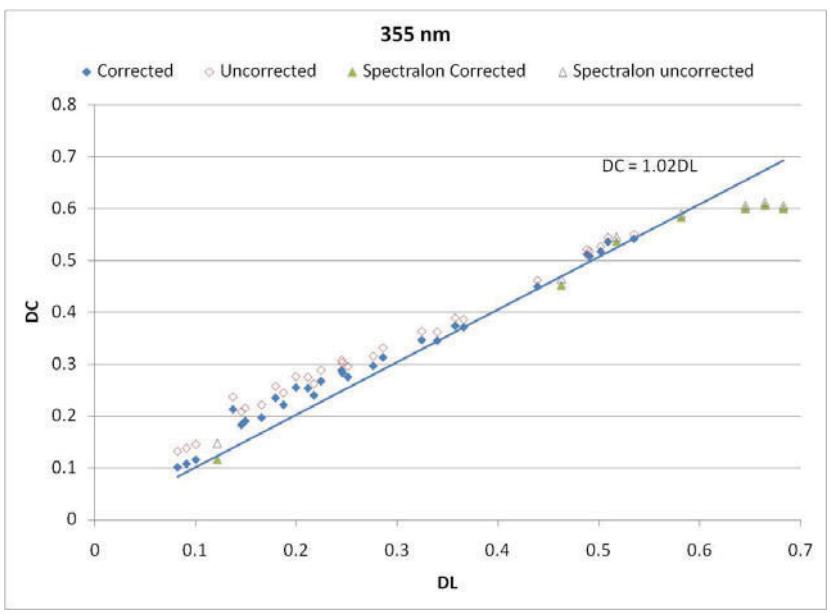

Figure 24: Depolarization parameters for circular polarization as a function of the depolarization parameter obtained for linear polarization. The measurements are performed at 355 nm.

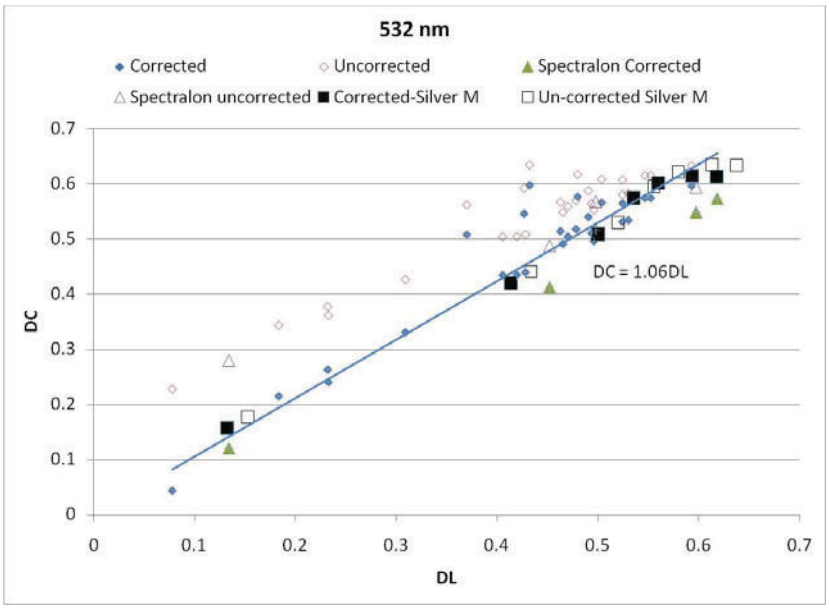

Figure 25: Depolarization parameters for circular polarization as a function of the depolarization parameter obtained for linear polarization. The measurements are performed at 532 nm.

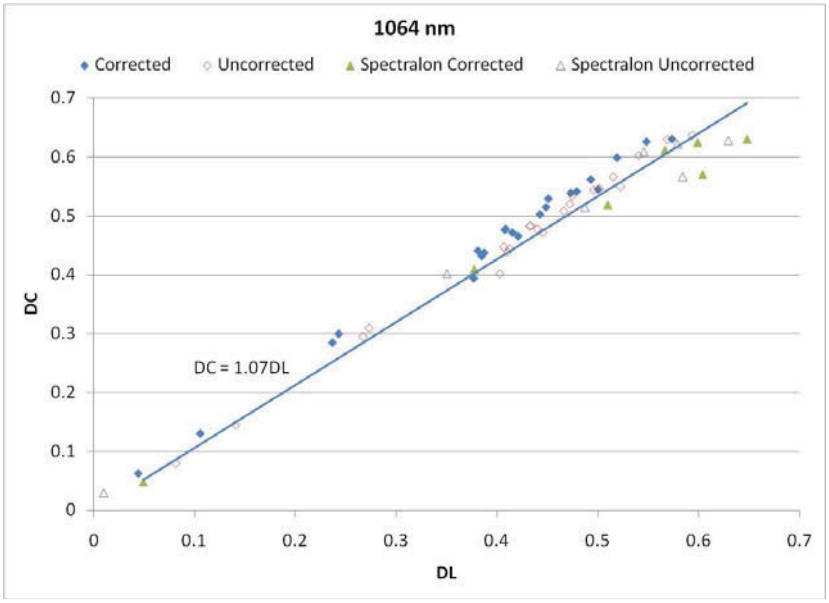

Figure 26: Depolarization parameters for circular polarization as a function of the depolarization parameter obtained for linear polarization. The measurements are performed at 1064 nm.

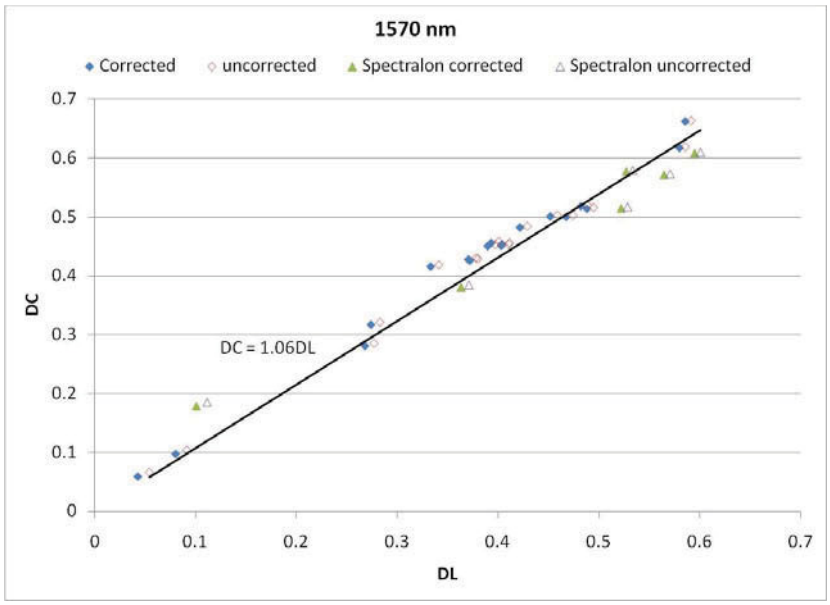

Figure 27: Depolarization parameters for circular polarization as a function of the depolarization parameter obtained for linear polarization. The measurements are performed at 1570 nm.

The relationship between d_L and d_C is practically one to one and of good enough quality to claim experimental validation of the theory for randomly oriented aerosols. However the fit is not perfect and there is still room for improvement. For all the figures, d_C shows a higher value than d_L. In theory, the combined measurement of the linear horizontal and vertical or circular left and circular right illumination should compensate instrumental influence. However, they do not compensate changes of depolarization caused by mirrors. This is why the inherent system depolarization must be taken into account via Eqs. 30 and 31. The effect is not very important except for the measurements at 532 nm displayed on Figure 25. The simple correction applied to the 532 nm results is important and does enhance significantly the quality of the fit. Also shown on the plots, results obtained on spectralons using bare silver coating mirrors that show a practically one to one relationship between d_L and d_C. These results clearly indicate that the protected aluminum coating did indeed induce a strong depolarization that could be corrected reasonably well by simple subtraction of the inherent system depolarization.

A system that will be free of mirrors will most likely provide results with the highest quality.

The results shown in figures 24 to 27 are summarized in the figure 28 below where the results from all 4 wavelengths are concatenated.

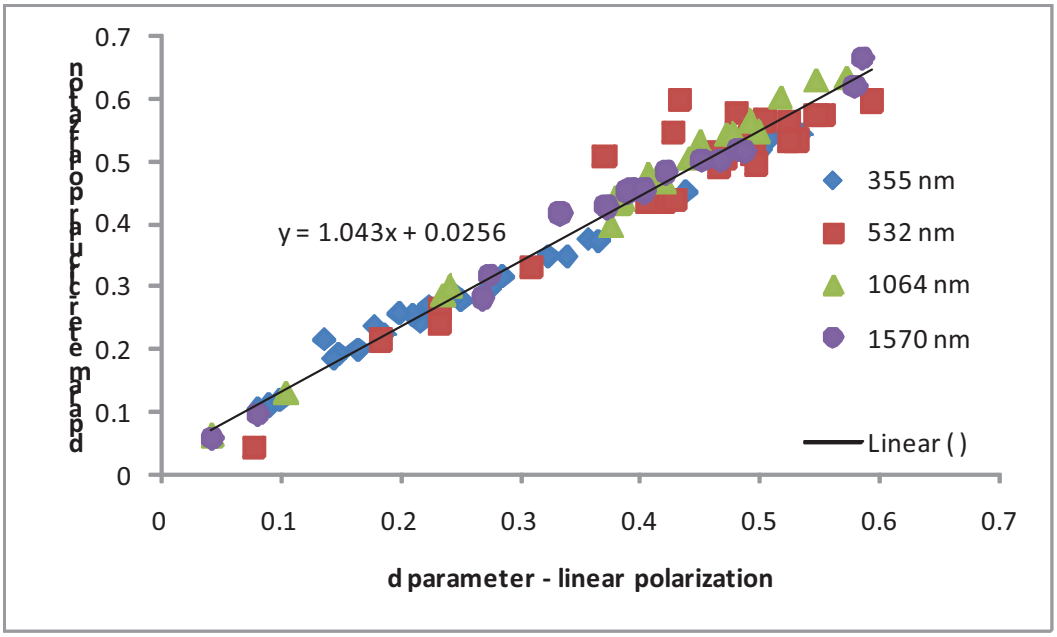

Figure 28: 'd' parameter obtained from circular polarization as a function of the 'd' parameter obtained from linear polarization.

5.1 Conclusion on the topic of the content of information in linear and circular polarizations

We have used linear and circular polarizations experimental data under controlled environment to validate the representation of the Mueller matrix for randomly oriented aerosols with a single parameter, namely the depolarization parameter *d*. Validation of the theory has a direct consequence on the design and future use of the polarimetric lidar. For randomly oriented aerosols, there is no added information when linear and circular polarizations are used: the simple use of either one will provide the exact same information. Other considerations not discussed here might guide in the choice of one or the other.

Throughout this work, we have tried to obtain depolarization signatures that are independent of the measurement instrument. From the demonstration made here of the relation between the two depolarization parameters, one can draw the important practical conclusion that, when measurements are performed using linear and circular polarizations, it is actually possible to verify the proper behaviour of the measurement system. This can be done by performing measurements of the depolarization parameters *'d_{lin}'* and *'d_{cir}'* on a randomly oriented materials: if $d_{lin} \neq d_{cir}$, then it is most likely because some optical components induce depolarization or the relative response of the detectors is incorrect, and corresponding calibration or correction will be required.

6 Future work

This work has been initiated in the context where we wanted to use the polarimetric signature of bioaerosols to discriminate them from the background aerosols and among themselves. The experimental work presented was performed under 'ideal conditions' in a controlled environment using an aerosol chamber and dry aerosols. The final aim is to create a bank of polarimetric signatures of aerosols/bioaerosols that is as much as possible independent from the instrument that performs the measurement. The use of the depolarization parameter and the cross validation of the measurements using linear and circular polarizations measurements increase the confidence in the reported values. As discussed in ref. [12] and [13] by Cao et al., the "identification" of an aerosol type in the field based on its polarimetric signature appears possible in principle for simple cases, for instance in cases of low concentration of a single type of dry aerosol. In order to be successful, attention should however be paid to the following questions:

-Develop clouds detection algorithms that take background fluctuations into account;

-Subtract background aerosol cloud from detected cloud;

-Study the time evolution of the cloud response: if the depolarization increases with time, it is most likely that the aerosol is contained inside water droplets that are evaporating;

-Verify that the polarimetric lidar system is free of stray depolarization effects.

Finally, there is no doubt that polarimetric measurements of aerosol/bioaerosol contain information on the nature of the scatterers. The demonstration made here is only to the effect that only one single parameter is of importance for those measurements. In a near future, we will explore the time evolution of wet aerosol polarimetric signatures and address the problem of field detection of low concentration clouds.

Annex A ELECTRONIC IMAGES OF POLLENS

Maple Sugar: 35-40 µm

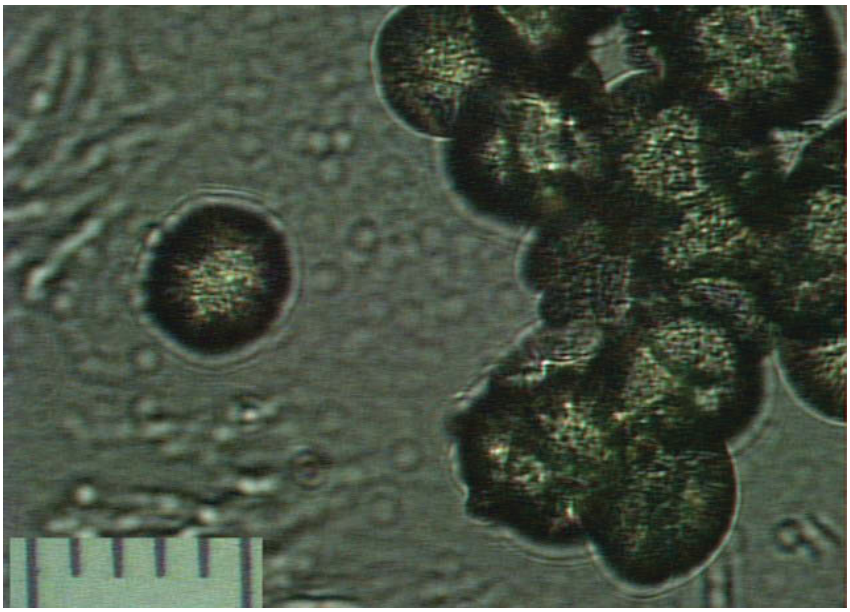

Pollen 1: Mulberry, paper: 8-10 µm

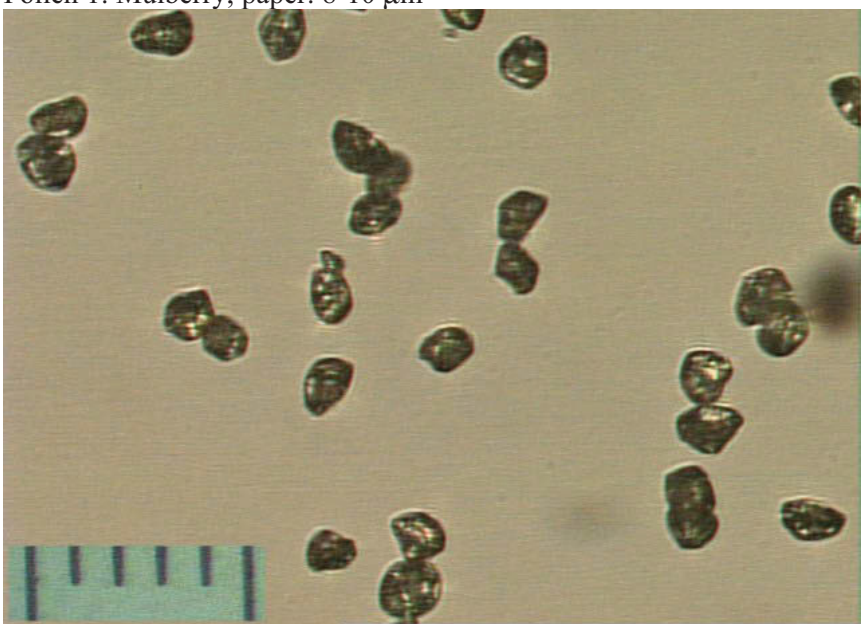

Pollen 2: Aspen: 25-30 µm

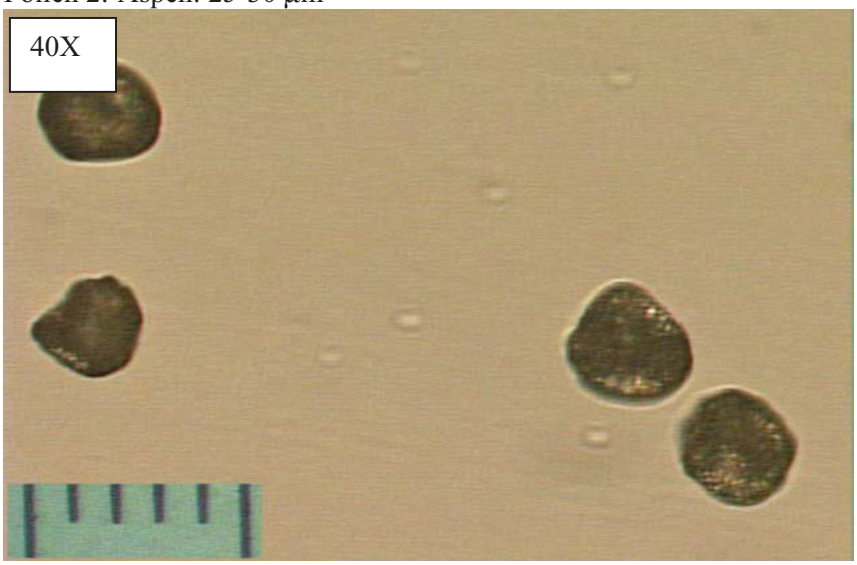

Pollen 3: Birch, White: 30-35 µm

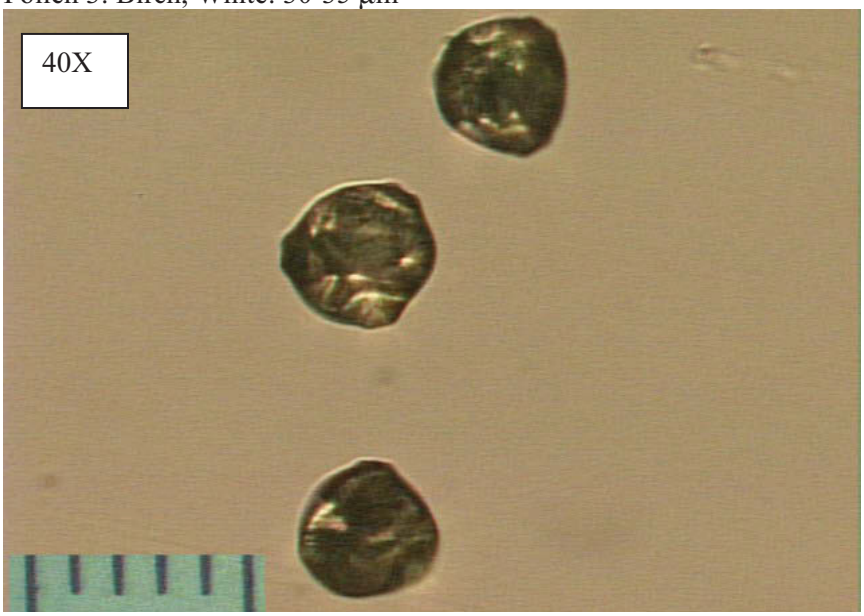

Pollen 4: Oak, white: 25-30 µm

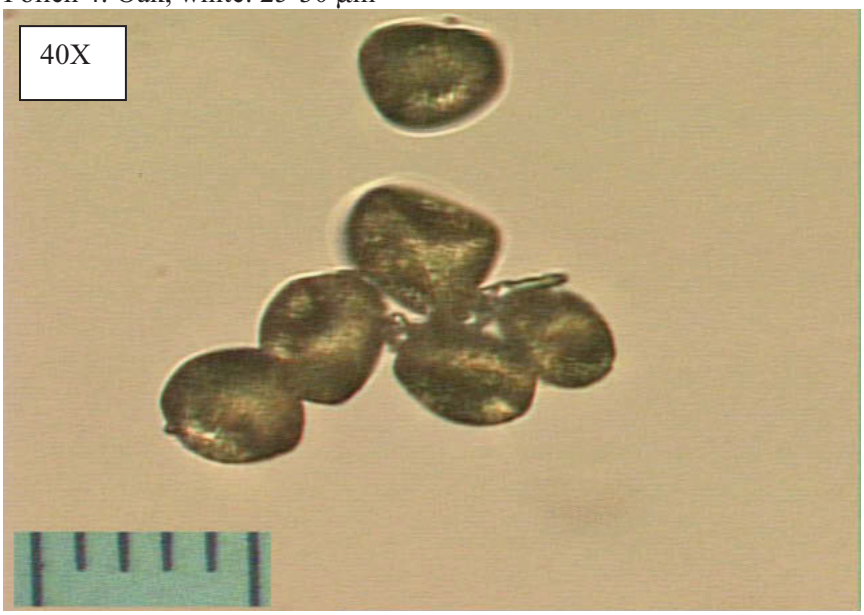

Pollen 5: Elm, American: 20-30 µm

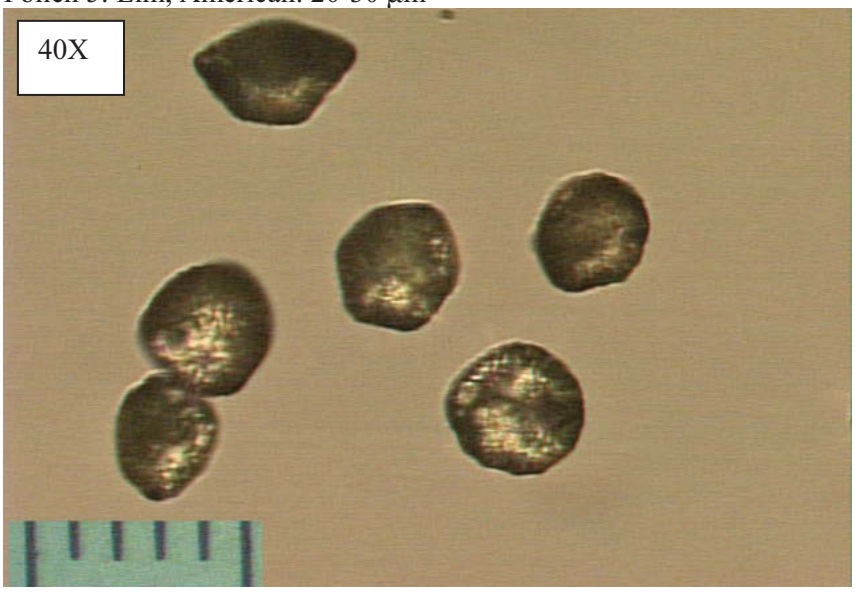

Pollen 6: Poplar, White: 20-30 µm

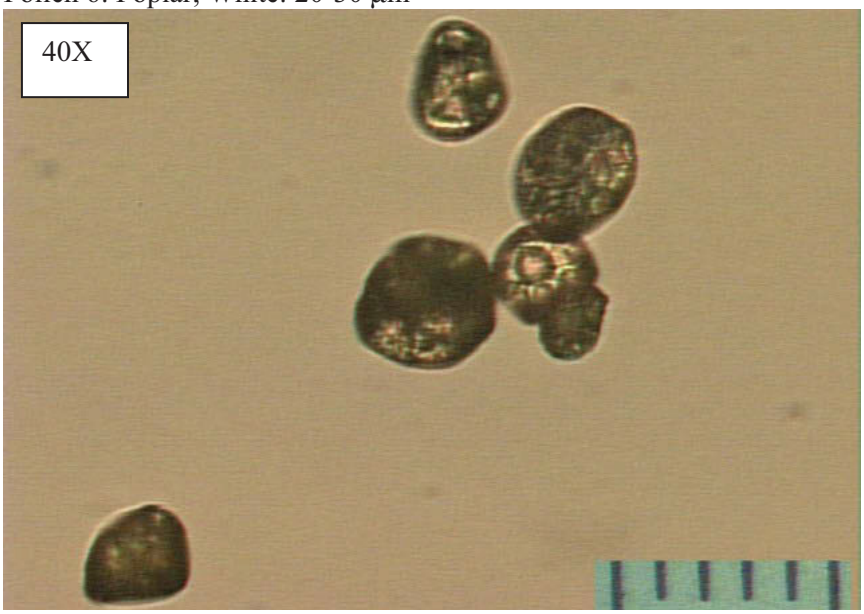

Pollen 8: Ragweed, short: 20 µm

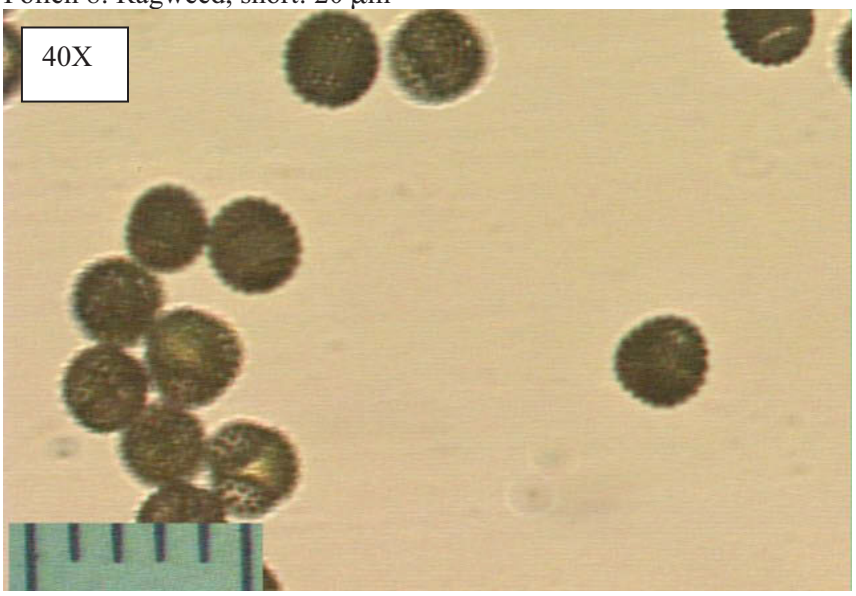

Pollen 9: Plantain: 20-25 µm

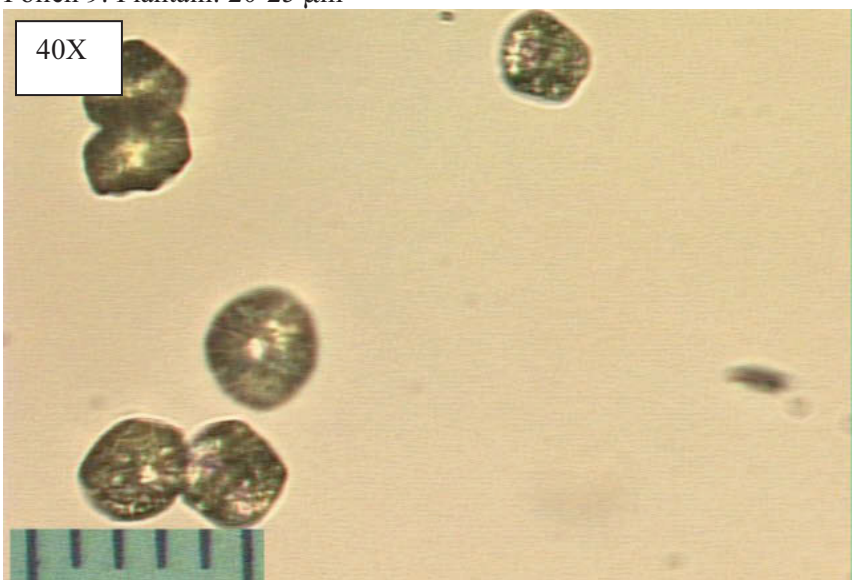

Pollen 11: Mugwort, common: 15-25 µm

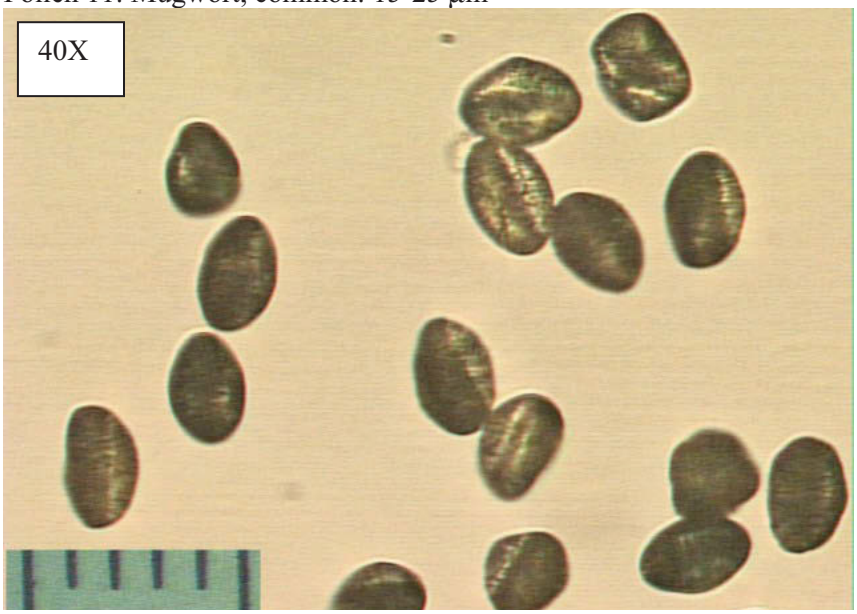

Pollen 13: Daisy, Ox-Eye: 24-30 µm

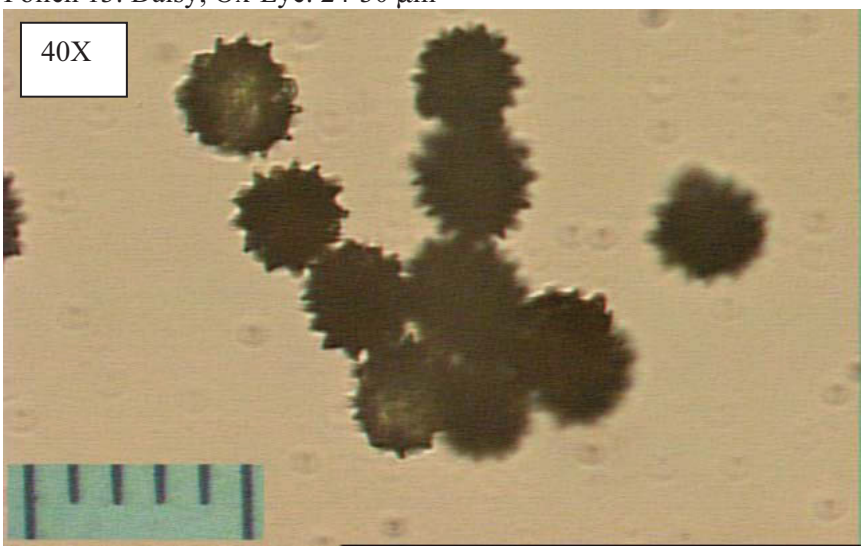

Pollen 14: Alfalfa: 25-40 µm

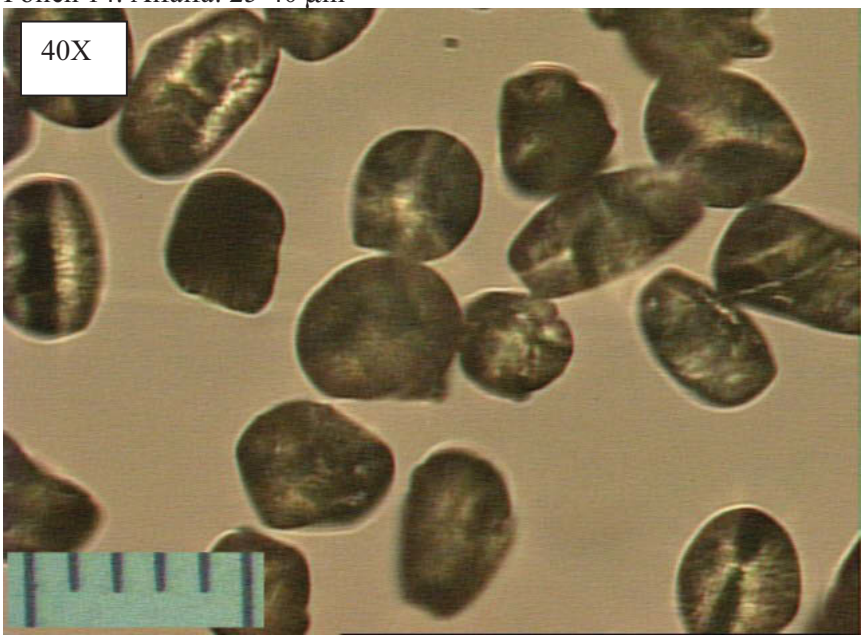

Clover, Red: 25-50 µm

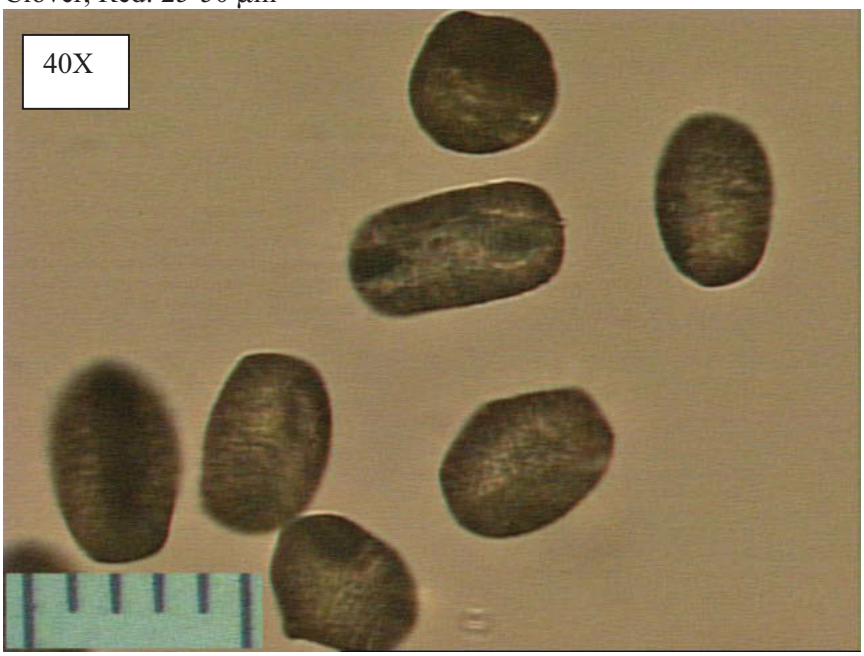

Pollen 16: Barley Grain Dust: 8-20 µm (notice the agglomeration)

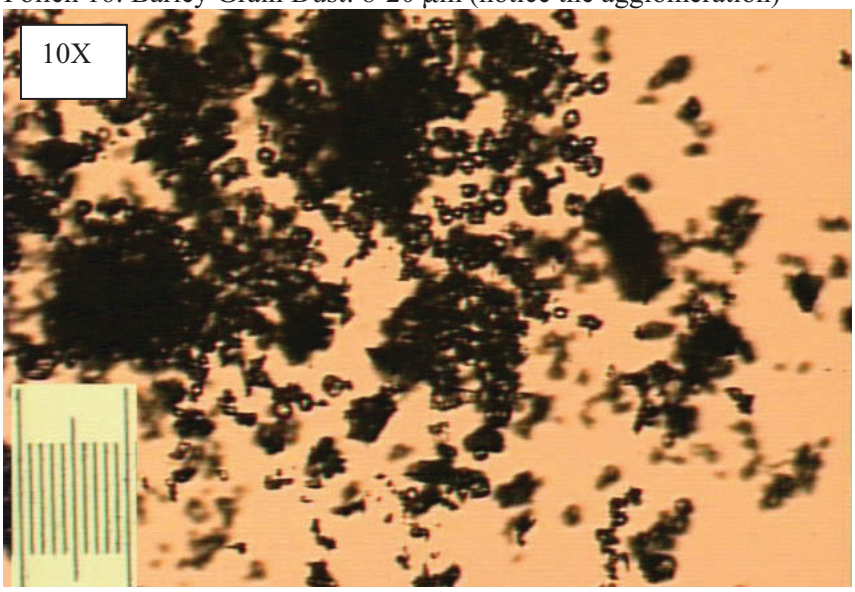

Pollen 16 (suite)

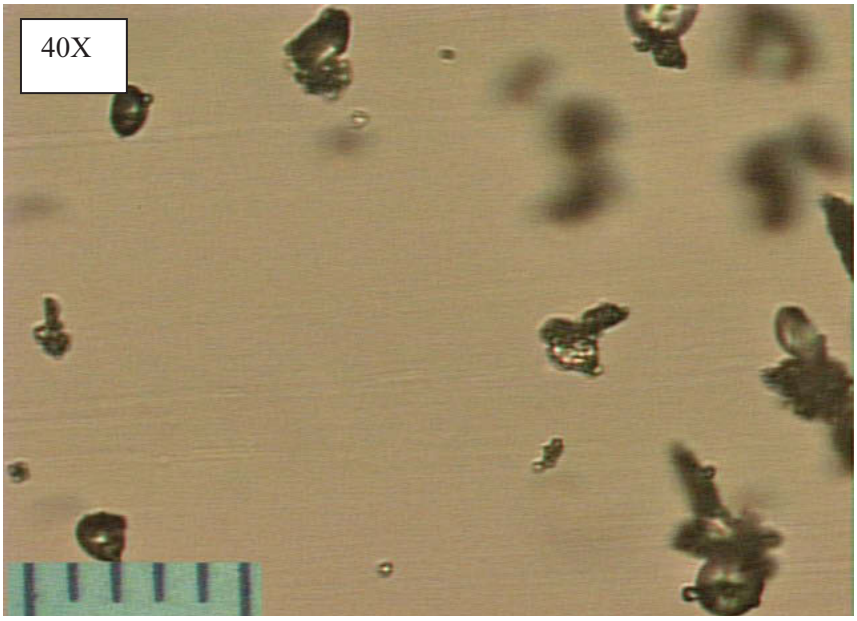

Pollen 17: Corn Grain Dust: 8-20 µm (notice the agglomeration)

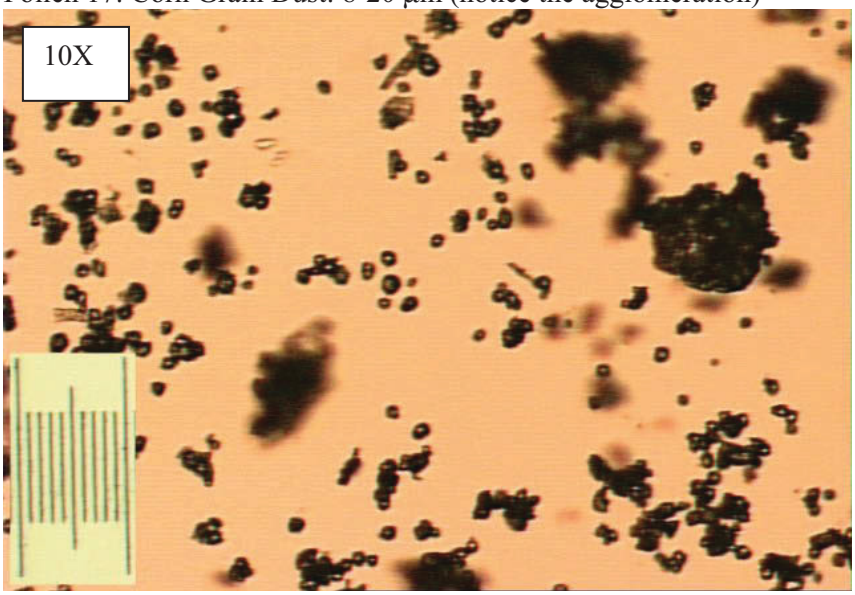

Pollen 17: (Suite)

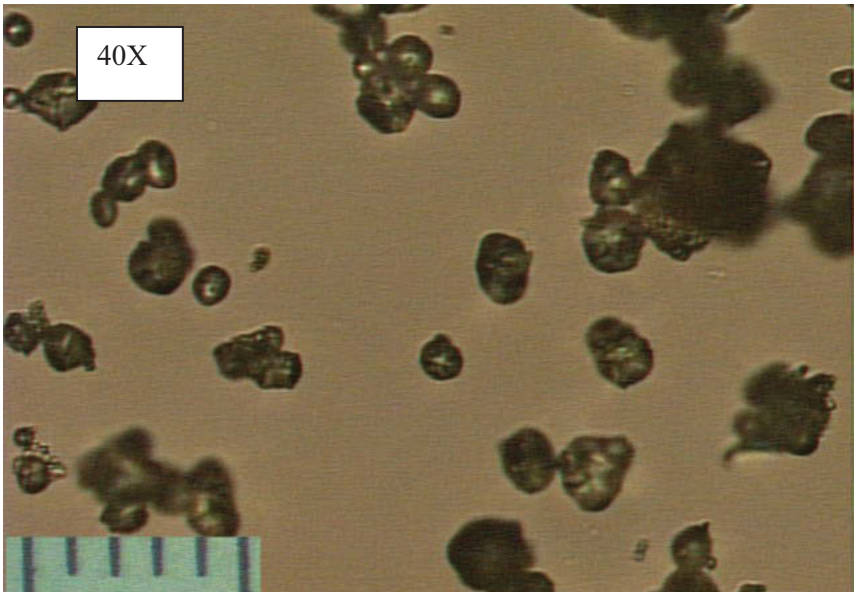

Pollen 18: Wheat Grain Dust: 8-25 µm (notice the agglomeration)

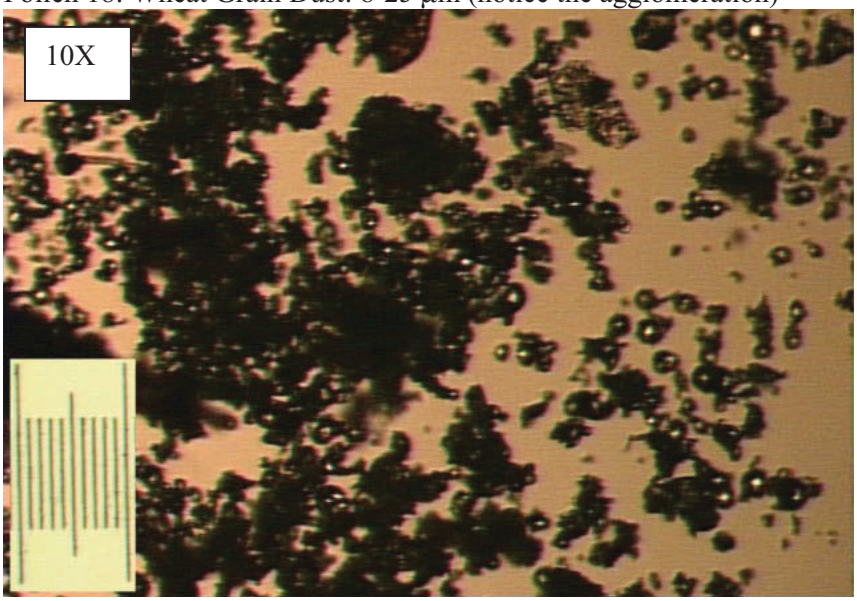

Pollen 18: (Suite)

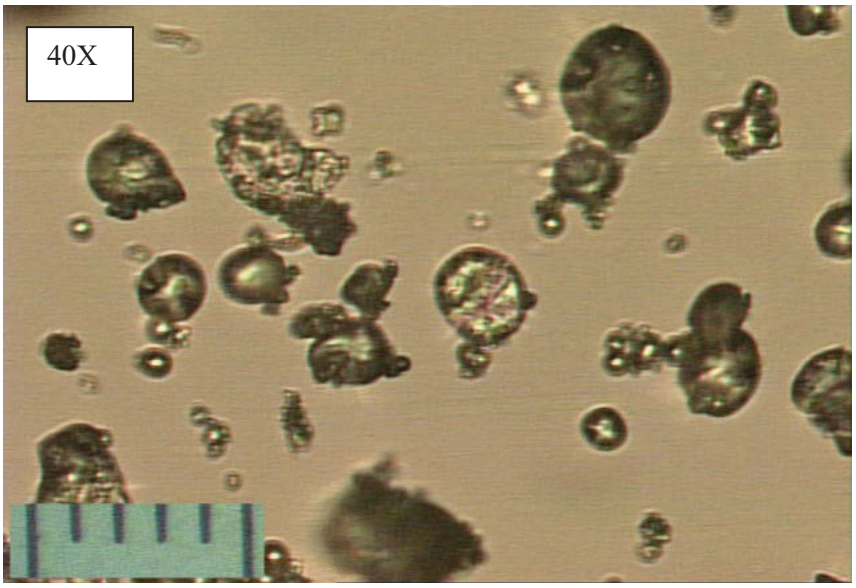

Pollen 19: Oat Smut: 5-7 µm

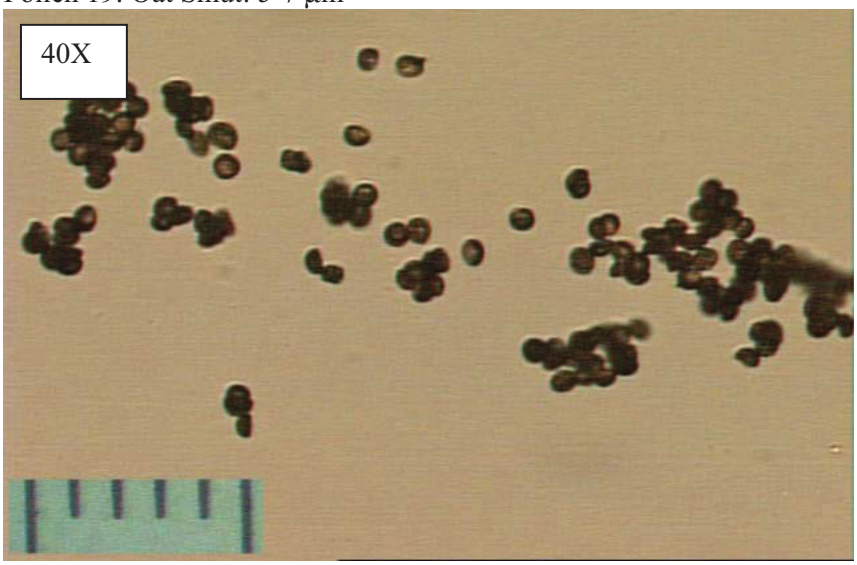

Pollen 20: Wheat Smut: 5-8 µm

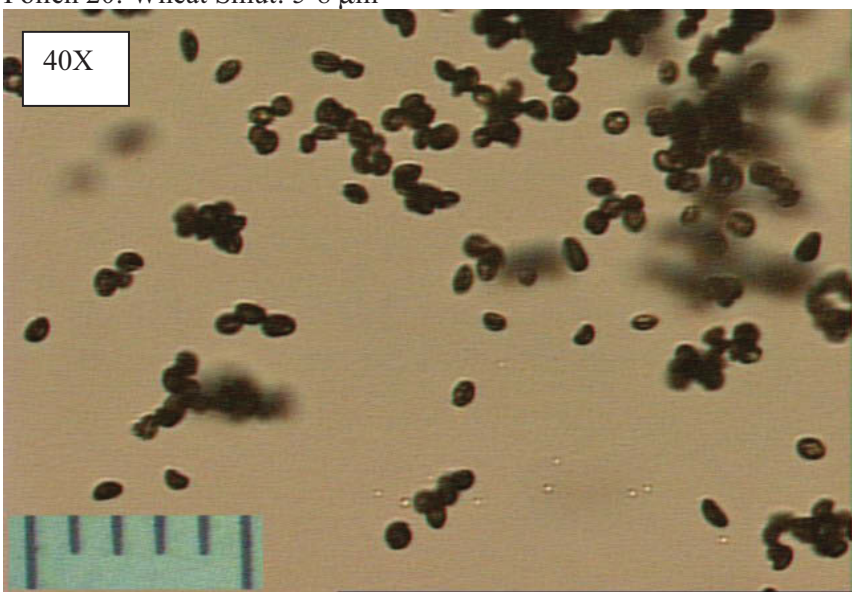

Pollen 24: Rye, Perennial: 20-30 µm

Pollen 25: Timothy: 35-40 µm

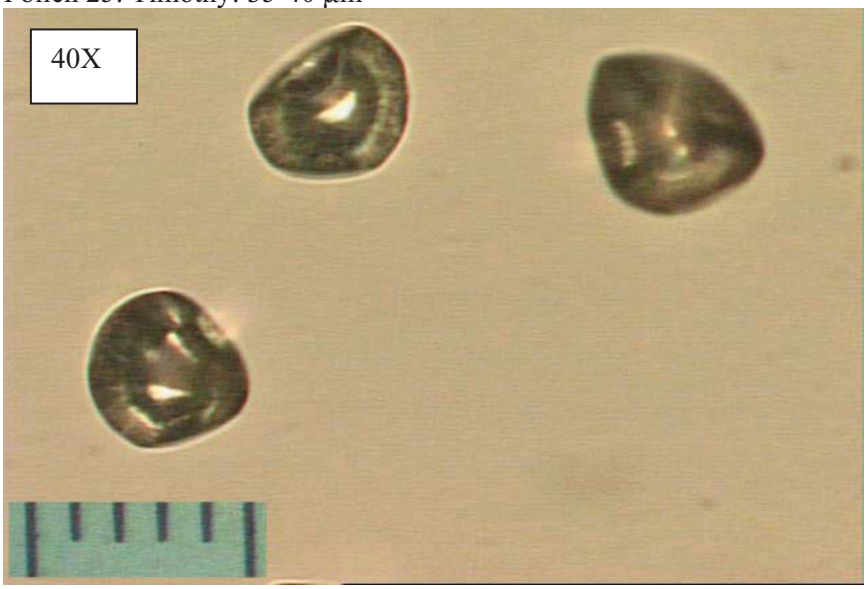

Annex B NUMERICAL AND GRAPHICAL RESULTS (2009 DATA)

Table 4: Depolarization ratios per pollen for 355 nm

	Wavelength	355 nm								
		Pollen#	**δL**	**3*std_dev**	**dL**	**3*std_dev**	**δC**	**3*std_dev**	**dC**	**3*std_dev**
trees and shrubs	Maple Sugar	1								
	Mulberry, paper	2	0,11	0,0114	0,20	0,0185	1,28	0,0769	0,56	0,0148
	Aspen	3	0,22	0,0234	0,36	0,0316	1,49	0,1337	0,60	0,0215
	Birch, White	4	0,09	0,0233	0,16	0,0394	1,35	0,1724	0,57	0,0308
	Oak, White	5	0,15	0,0350	0,26	0,0528	1,49	0,2033	0,60	0,0326
	Elm, American	6	0,08	0,0117	0,15	0,0202	1,40	0,1620	0,58	0,0280
	Poplar, White	7	0,09	0,0179	0,17	0,0299	1,50	0,1546	0,60	0,0245
	Pine, Virginia	8	0,18	0,0203	0,30	0,0293	1,48	0,1484	0,60	0,0240
Weeds	ragweed, short	9	0,04	0,0056	0,07	0,0105	1,24	0,0734	0,55	0,0146
	Plantain, English	10	0,04	0,0108	0,07	0,0200	1,40	0,2050	0,58	0,0359
	Sagebrush, common	11	0,07	0,0108	0,14	0,0187	1,33	0,0876	0,57	0,0162
	Mugwort, Common	12	0,08	0,0093	0,14	0,0161	1,30	0,0740	0,57	0,0140
Flowers	sunflower	13	0,05	0,0095	0,10	0,0172	1,46	0,1334	0,59	0,0221
	Daisy, Ox-Eye	14	0,17	0,0157	0,28	0,0231	1,49	0,1094	0,60	0,0176
Cultivated Plants	Alfalfa	15	0,04	0,0123	0,08	0,0226	1,38	0,2039	0,58	0,0361
	Clover, Red	16								
	Mustard	17	0,06	0,0156	0,11	0,0279	1,47	0,1725	0,59	0,0282
Dusts	Barley Grain Dust	18	0,31	0,0298	0,47	0,0345	1,87	0,1456	0,65	0,0175
	Corn Grain Dust	19	0,28	0,0192	0,44	0,0231	1,71	0,1416	0,63	0,0191
	Wheat Grain Dust	20	0,31	0,0154	0,48	0,0178	1,75	0,1757	0,64	0,0228
Smuts	Oat Smut	21	0,03	0,0040	0,06	0,0076	1,08	0,0674	0,52	0,0156
	Wheat Smut	22	0,03	0,0051	0,06	0,0097	1,08	0,0490	0,52	0,0113
	Corn Smut	23	0,11	0,0126	0,19	0,0205	1,32	0,0695	0,57	0,0129
Fungi	neurospora intermedia	24	0,33	0,0177	0,50	0,0199	1,82	0,0872	0,65	0,0110
	Penicillium chrysogenum	25	0,28	0,0155	0,44	0,0189	1,72	0,1305	0,63	0,0174
grasses	Rye, Perennial	26	0,17	0,0182	0,30	0,0263	1,51	0,0729	0,60	0,0116
	Timothy	27	0,10	0,0178	0,18	0,0293	1,59	0,1601	0,61	0,0238
	ARD	28	0,32	0,0132	0,49	0,0151	1,81	0,1089	0,64	0,0140
	AFD	29	0,34	0,0122	0,50	0,0137	1,85	0,0857	0,65	0,0106

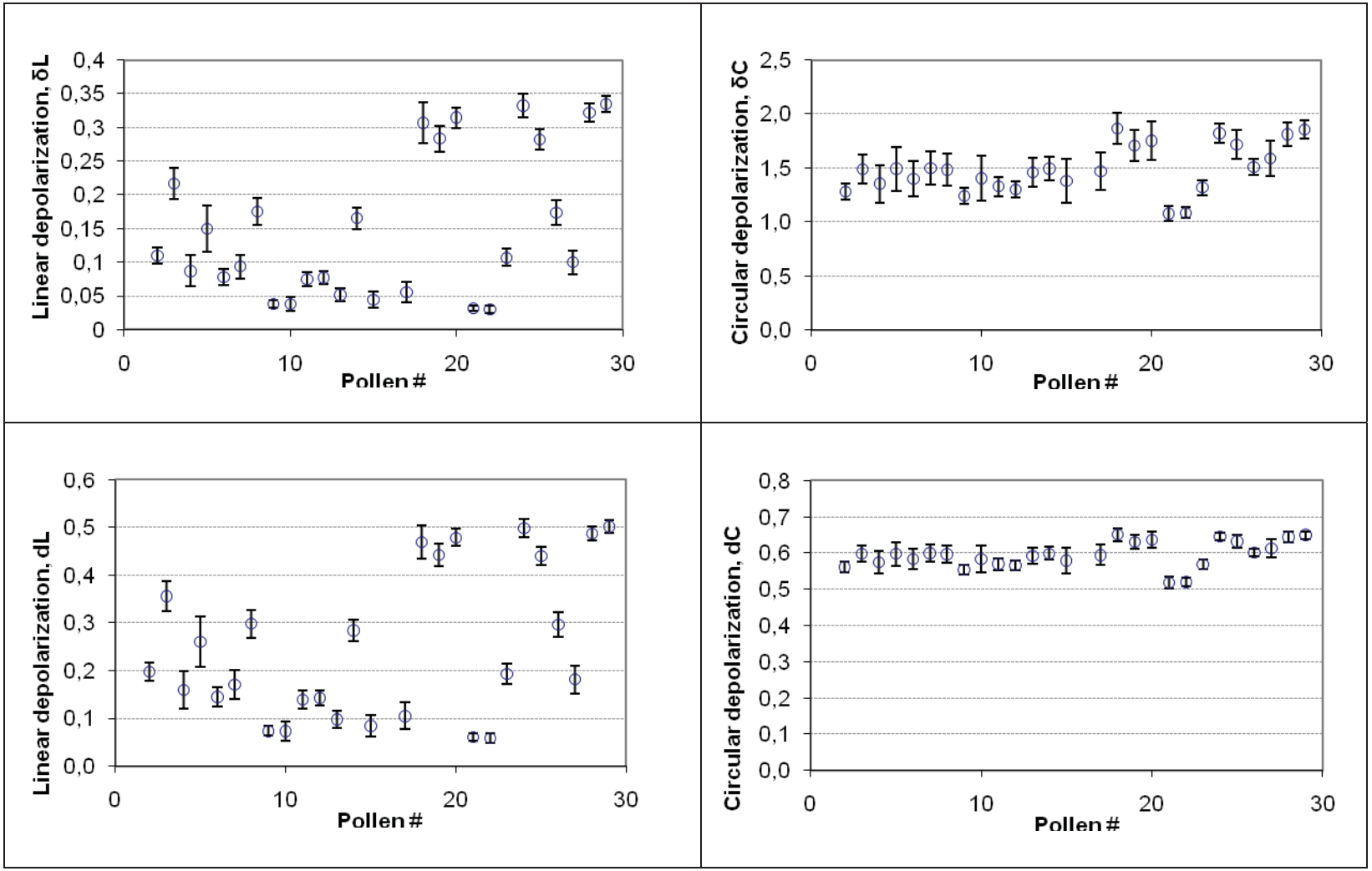

Figure 12: Graphs of depolarization ratios per pollen for 355 nm

Table 5: Depolarization ratios per pollen for 532 nm

	Wavelength	532 nm								
		Pollen#	**δL**	**3*std_dev**	**dL**	**3*std_dev**	**δC**	**3*std_dev**	**dC**	**3*std_dev**
trees and shrubs	Maple Sugar	1								
	Mulberry, paper	2	0,33	0,0152	0,50	0,0171	1,07	0,0729	0,52	0,0171
	Aspen	3	0,45	0,0239	0,62	0,0227	1,30	0,0360	0,57	0,0069
	Birch, White	4	0,34	0,0115	0,50	0,0130	1,04	0,0270	0,51	0,0066
	Oak, White	5	0,38	0,0393	0,55	0,0409	1,08	0,0330	0,52	0,0078
	Elm, American	6	0,35	0,0143	0,51	0,0158	0,96	0,0825	0,49	0,0216
	Poplar, White	7	0,45	0,0237	0,62	0,0227	1,40	0,0909	0,58	0,0159
	Pine, Virginia	8	0,41	0,0166	0,58	0,0168	1,45	0,0621	0,59	0,0102
Weeds	ragweed, short	9	0,33	0,0249	0,50	0,0283	1,10	0,0606	0,52	0,0138
	Plantain, English	10	0,34	0,0172	0,51	0,0192	1,06	0,1050	0,52	0,0252
	Sagebrush, common	11	0,30	0,0120	0,46	0,0142	0,96	0,0552	0,49	0,0144
	Mugwort, Common	12	0,29	0,0161	0,44	0,0195	0,92	0,0582	0,48	0,0159
Flowers	sunflower	13	0,41	0,0346	0,59	0,0349	1,27	0,1020	0,56	0,0237
	Daisy, Ox-Eye	14	0,39	0,0145	0,56	0,0150	1,45	0,1128	0,59	0,0192
Cultivated Plants	Alfalfa	15	0,34	0,0152	0,51	0,0169	0,98	0,0426	0,50	0,0108
	Clover, Red	16								
	Mustard	17	0,45	0,0165	0,62	0,0156	1,40	0,0561	0,58	0,0099
Dusts	Barley Grain Dust	18	0,47	0,0304	0,64	0,0284	1,41	0,1665	0,58	0,0297
	Corn Grain Dust	19	0,43	0,0314	0,60	0,0307	1,38	0,1179	0,58	0,0213
	Wheat Grain Dust	20	0,49	0,0209	0,66	0,0188	1,42	0,0969	0,59	0,0168
Smuts	Oat Smut	21	0,16	0,0077	0,27	0,0115	0,49	0,0159	0,33	0,0072
	Wheat Smut	22	0,18	0,0038	0,30	0,0055	0,54	0,0237	0,35	0,0099
	Corn Smut	23	0,29	0,0181	0,45	0,0219	0,83	0,0870	0,45	0,0267
Fungi	neurospora intermedia	24	0,43	0,0263	0,60	0,0258	1,43	0,0963	0,59	0,0165
	Penicillium chrysogenum	25	0,34	0,0133	0,51	0,0148	1,05	0,0429	0,51	0,0102
grasses	Rye, Perennial	26	0,38	0,0224	0,55	0,0233	1,11	0,0369	0,53	0,0084
	Timothy	27	0,43	0,0312	0,60	0,0305	1,22	0,1101	0,55	0,0228
	ARD	28	0,38	0,0152	0,55	0,0161	1,11	0,0354	0,53	0,0081
	AFD	29	0,37	0,0314	0,54	0,0337	1,28	0,0705	0,56	0,0138

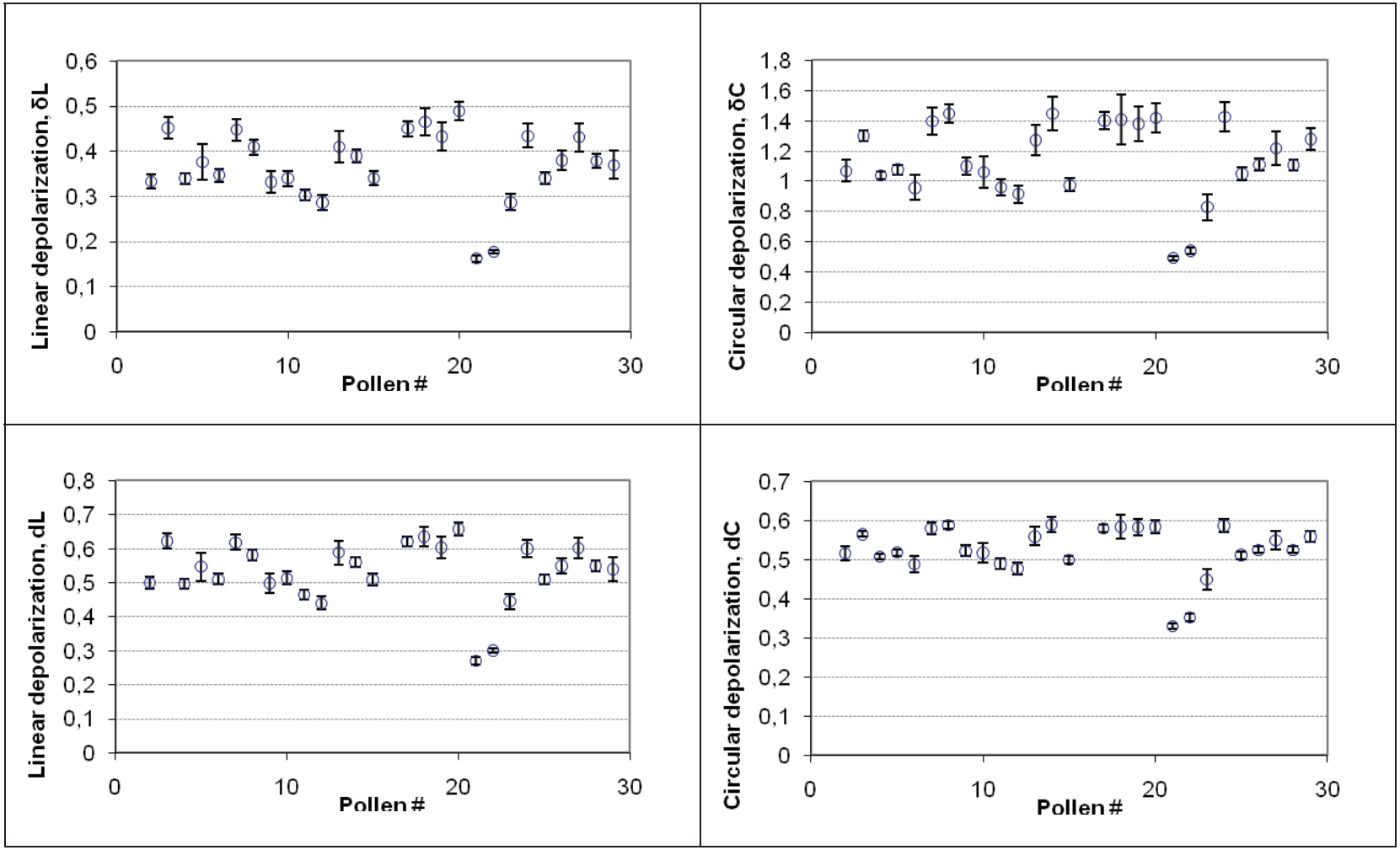

Figure 13: Graphs of depolarization ratios per pollen for 532 nm

Table 6: Depolarization ratios per pollen for 1064 nm

	Wavelength	1064 nm								
		Pollen#	**δL**	**3*std_dev**	**dL**	**3*std_dev**	**δC**	**3*std_dev**	**dC**	**3*std_dev**
trees and shrubs	Maple Sugar	1	0,29	0,0728	0,45	0,0856	1,09	0,2019	0,52	0,0466
	Mulberry, paper	2	0,38	0,0198	0,56	0,0207	1,66	0,0570	0,62	0,0081
	Aspen	3	0,29	0,0186	0,46	0,0222	1,10	0,0941	0,52	0,0214
	Birch, White	4	0,40	0,0245	0,57	0,0249	1,11	0,0752	0,53	0,0169
	Oak, White	5	0,30	0,0223	0,46	0,0266	1,05	0,0977	0,51	0,0235
	Elm, American	6	0,32	0,0208	0,48	0,0240	1,07	0,0484	0,52	0,0113
	Poplar, White	7	0,42	0,0269	0,60	0,0267	1,59	0,0892	0,61	0,0133
	Pine, Virginia	8	0,34	0,0218	0,50	0,0244	1,23	0,0849	0,55	0,0170
Weeds	ragweed, short	9	0,27	0,0179	0,42	0,0223	1,00	0,0392	0,50	0,0099
	Plantain, English	10	0,30	0,0147	0,46	0,0174	1,11	0,0524	0,53	0,0118
	Sagebrush, common	11	0,26	0,0104	0,42	0,0131	0,97	0,0491	0,49	0,0127
	Mugwort, Common	12	0,24	0,0087	0,39	0,0113	0,92	0,0393	0,48	0,0107
Flowers	sunflower	13	0,45	0,0436	0,62	0,0416	1,35	0,1180	0,57	0,0214
	Daisy, Ox-Eye	14	0,36	0,0258	0,53	0,0279	1,33	0,0814	0,57	0,0149
Cultivated Plants	Alfalfa	15	0,30	0,0344	0,46	0,0410	0,93	0,1296	0,48	0,0349
	Clover, Red	16								
	Mustard	17	0,44	0,0848	0,61	0,0815	1,31	0,2055	0,57	0,0387
Dusts	Barley Grain Dust	18	0,50	0,0803	0,66	0,0699	1,39	0,1575	0,58	0,0276
	Corn Grain Dust	19	0,41	0,0285	0,59	0,0285	1,77	0,1566	0,64	0,0205
	Wheat Grain Dust	20	0,48	0,0319	0,65	0,0293	1,60	0,0862	0,62	0,0127
Smuts	Oat Smut	21	0,07	0,0041	0,14	0,0072	0,47	0,0293	0,32	0,0136
	Wheat Smut	22	0,07	0,0045	0,14	0,0078	0,48	0,0151	0,33	0,0068
	Corn Smut	23	0,16	0,0082	0,28	0,0121	0,97	0,0907	0,49	0,0229
Fungi	neurospora intermedia	24	0,37	0,0161	0,55	0,0171	1,51	0,0640	0,60	0,0102
	Penicillium chrysogenum	25	0,26	0,0201	0,41	0,0254	0,95	0,0796	0,49	0,0212
grasses	Rye, Perennial	26	0,27	0,0264	0,42	0,0327	0,90	0,0944	0,47	0,0263
	Timothy	27	0,34	0,0251	0,50	0,0282	1,13	0,0914	0,53	0,0200
	ARD	28	0,28	0,0205	0,44	0,0248	1,10	0,0339	0,52	0,0077
	AFD	29	0,33	0,0311	0,49	0,0357	1,15	0,0617	0,54	0,0135

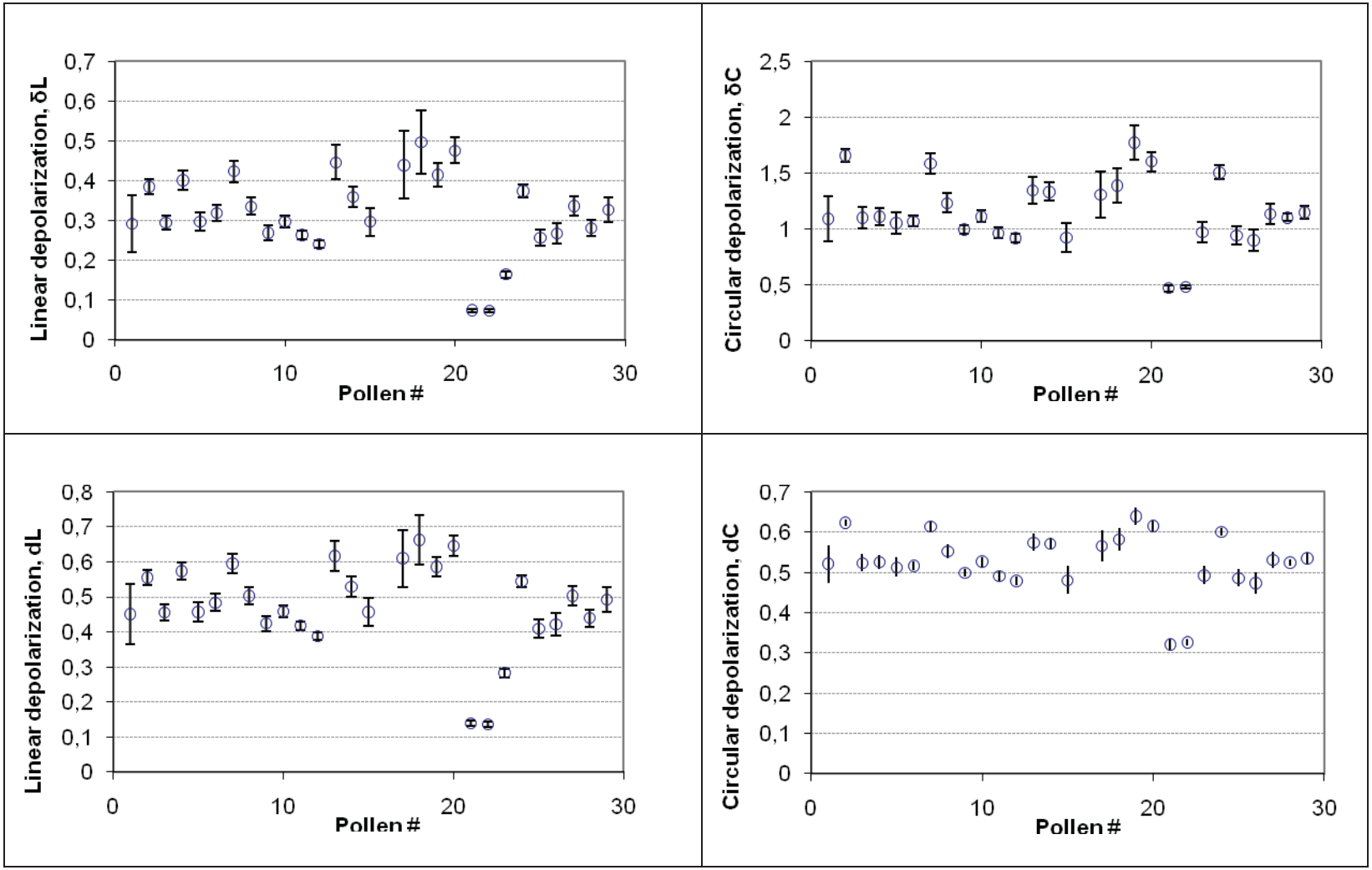

Figure 14: Graphs of depolarization ratios per pollen for 1064 nm

Table 7: Depolarization ratios per pollen for 1570 nm

	Wavelength	1570 nm Pollen#	δL	3*std_dev	dL	3*std_dev	δC	3*std_dev	dC	3*std_dev
trees and shrubs	Maple Sugar	1	0,32	0,22	0,49	0,2444	1,53	1,52	0,59	0,2229
	Mulberry, paper	2	0,49	0,03	0,66	0,0271	1,71	0,08	0,63	0,0115
	Aspen	3	0,52	0,03	0,69	0,0291	1,67	0,09	0,62	0,0126
	Birch, White	4	0,40	0,03	0,57	0,0332	1,45	0,08	0,59	0,0129
	Oak, White	5	0,34	0,03	0,51	0,0320	1,33	0,07	0,57	0,0133
	Elm, American	6	0,36	0,02	0,53	0,0204	1,13	0,06	0,53	0,0130
	Poplar, White	7	0,50	0,02	0,67	0,0213	1,67	0,08	0,62	0,0114
	Pine, Virginia	8	0,33	0,02	0,50	0,0229	1,32	0,10	0,57	0,0177
Weeds	ragweed, short	9	0,31	0,03	0,48	0,0318	1,24	0,05	0,55	0,0095
	Plantain, English	10	0,42	0,05	0,59	0,0447	1,46	0,11	0,59	0,0185
	Sagebrush, common	11	0,34	0,03	0,51	0,0296	1,42	0,08	0,59	0,0143
	Mugwort, Common	12	0,36	0,02	0,53	0,0256	1,39	0,06	0,58	0,0113
Flowers	sunflower	13	0,42	0,04	0,59	0,0361	1,50	0,10	0,60	0,0157
	Daisy, Ox-Eye	14	0,41	0,03	0,58	0,0252	1,51	0,08	0,60	0,0120
Cultivated Plants	Alfalfa	15	0,32	0,02	0,49	0,0268	1,33	0,06	0,57	0,0116
	Clover, Red	16								
	Mustard	17	0,34	0,05	0,51	0,0519	1,67	0,21	0,63	0,0287
Dusts	Barley Grain Dust	18	0,35	0,08	0,52	0,0888	1,92	0,50	0,66	0,0584
	Corn Grain Dust	19								
	Wheat Grain Dust	20	0,36	0,09	0,53	0,1026	1,93	0,63	0,66	0,0735
Smuts	Oat Smut	21	0,13	0,03	0,23	0,0460	1,02	0,07	0,51	0,0163
	Wheat Smut	22	0,15	0,02	0,27	0,0275	0,97	0,04	0,49	0,0098
	Corn Smut	23	0,34	0,02	0,51	0,0183	1,40	0,06	0,58	0,0098
Fungi	neurospora intermedia	24	0,40	0,05	0,57	0,0472	1,86	0,28	0,65	0,0337
	Penicillium chrysogenum	25	0,27	0,03	0,43	0,0426	1,39	0,14	0,58	0,0239
grasses	Rye, Perennial	26	0,38	0,04	0,55	0,0446	1,36	0,13	0,58	0,0233
	Timothy	27	0,39	0,03	0,56	0,0293	1,40	0,16	0,58	0,0285
	ARD	28	0,34	0,02	0,50	0,0200	1,39	0,08	0,58	0,0137
	AFD	29	0,36	0,03	0,53	0,0299	1,41	0,10	0,59	0,0170

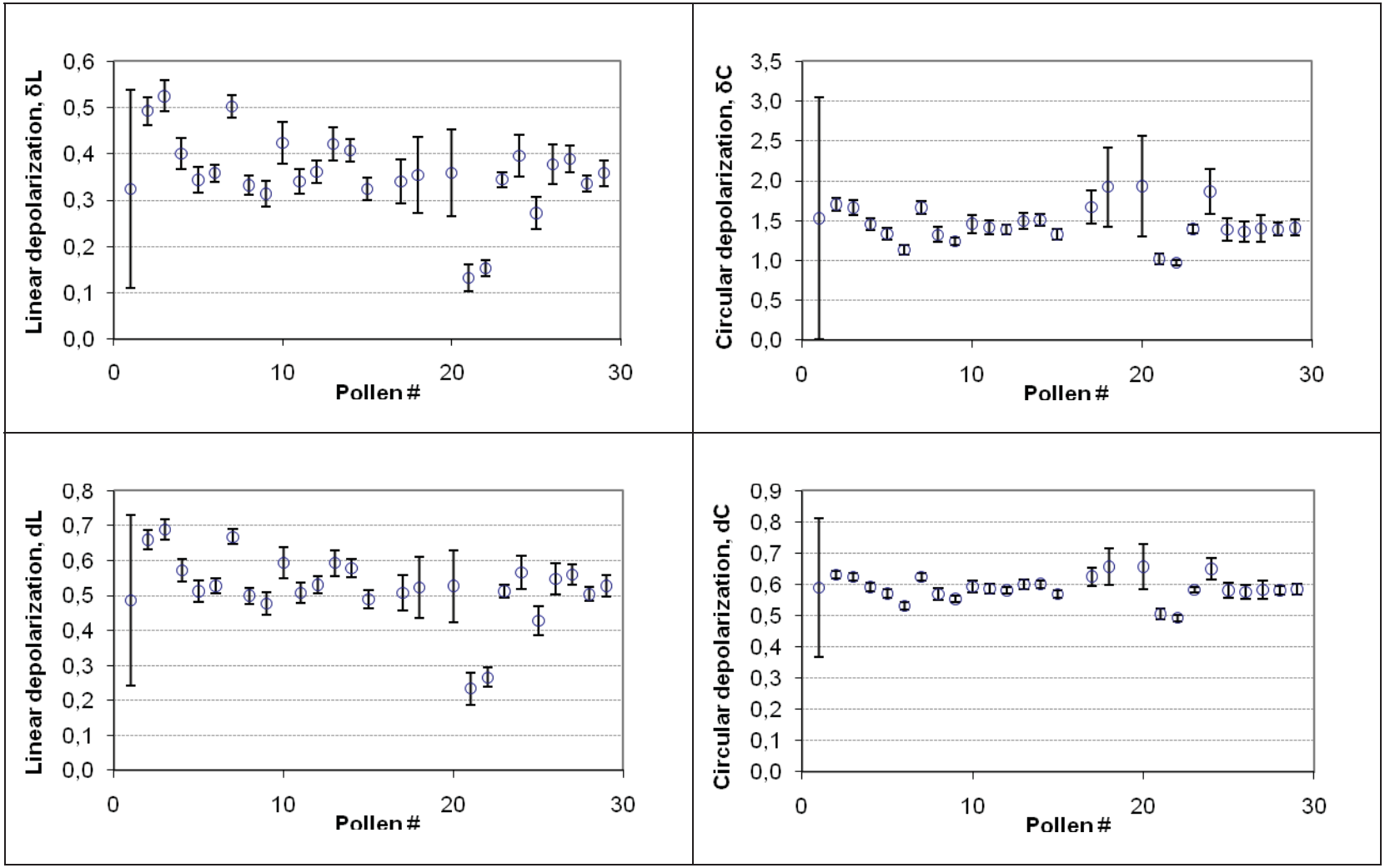

Figure 15: Graphs of depolarization ratios per pollen for 1570 nm

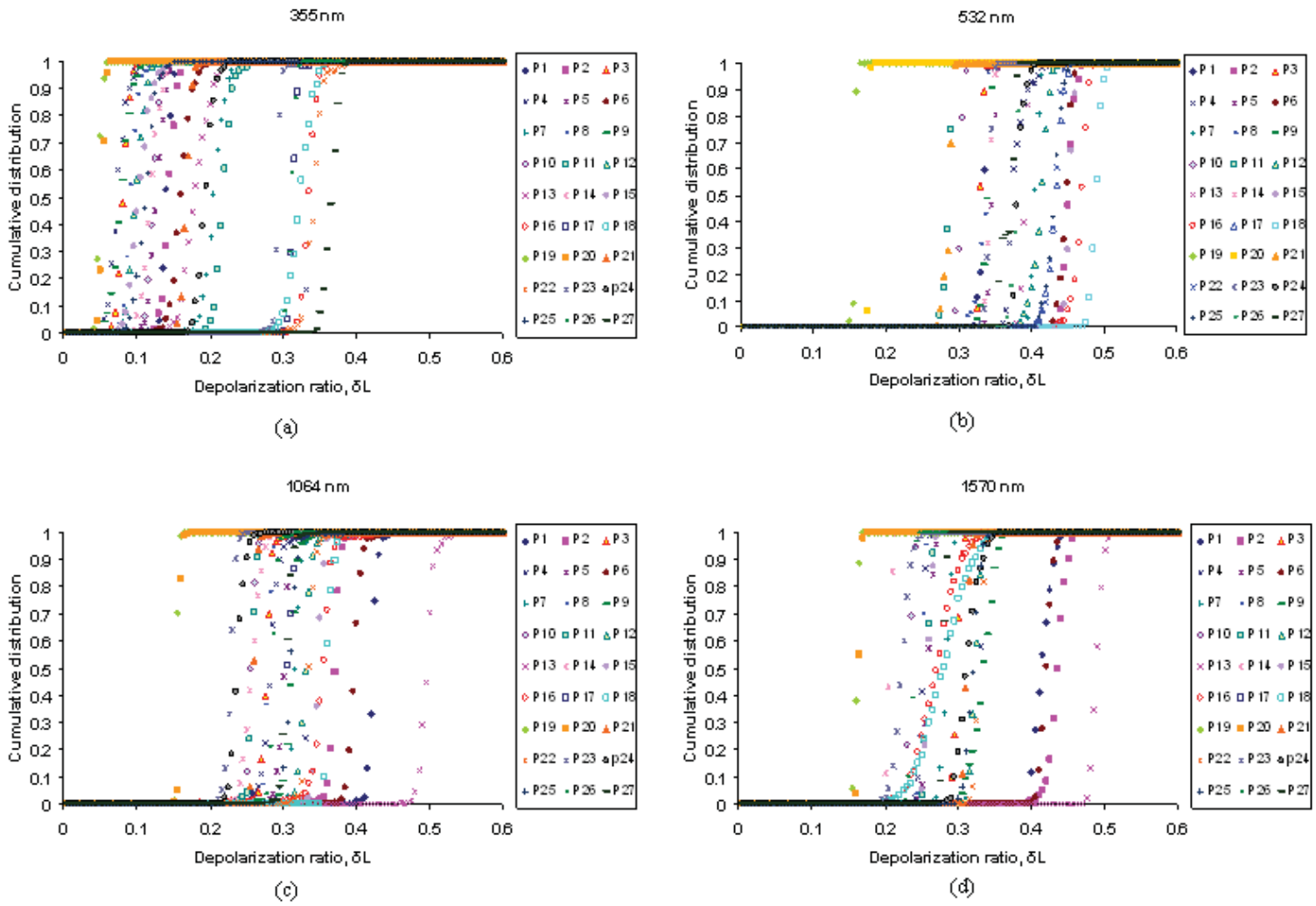

Figure 16: Cumulative distributions of depolarization ratios per pollens for wavelengths a) 355 nm, b) 532 nm, c) 1064 nm and d) 1570 nm

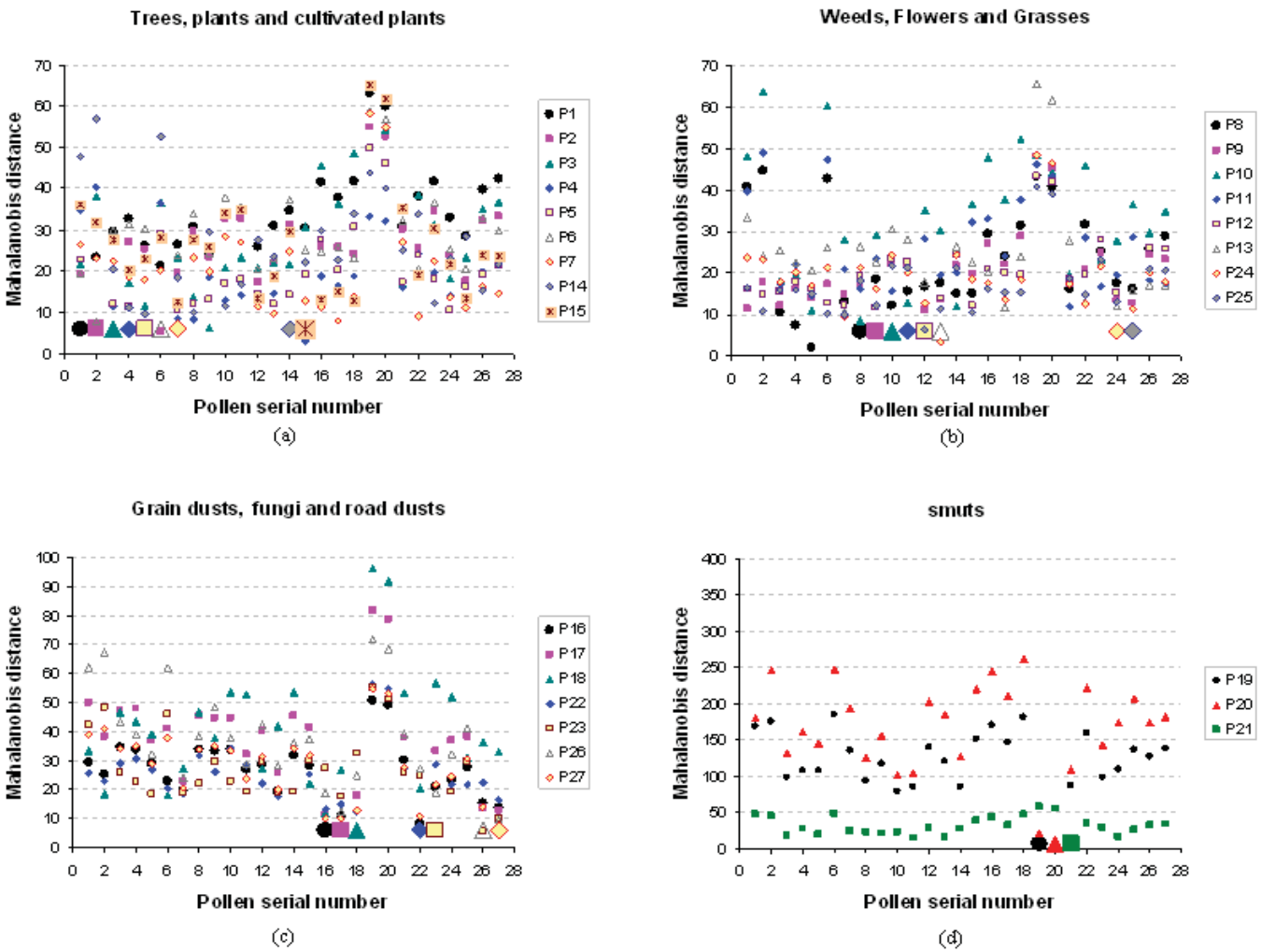

Figure 17: Mahalanobis-Distances for all pollens

Annex C TIME EVOLUTION OF POLARIZATION SIGNATURES OF DUSTS AS A FUNCTION OF TEMPERATURE AND HUMIDITY

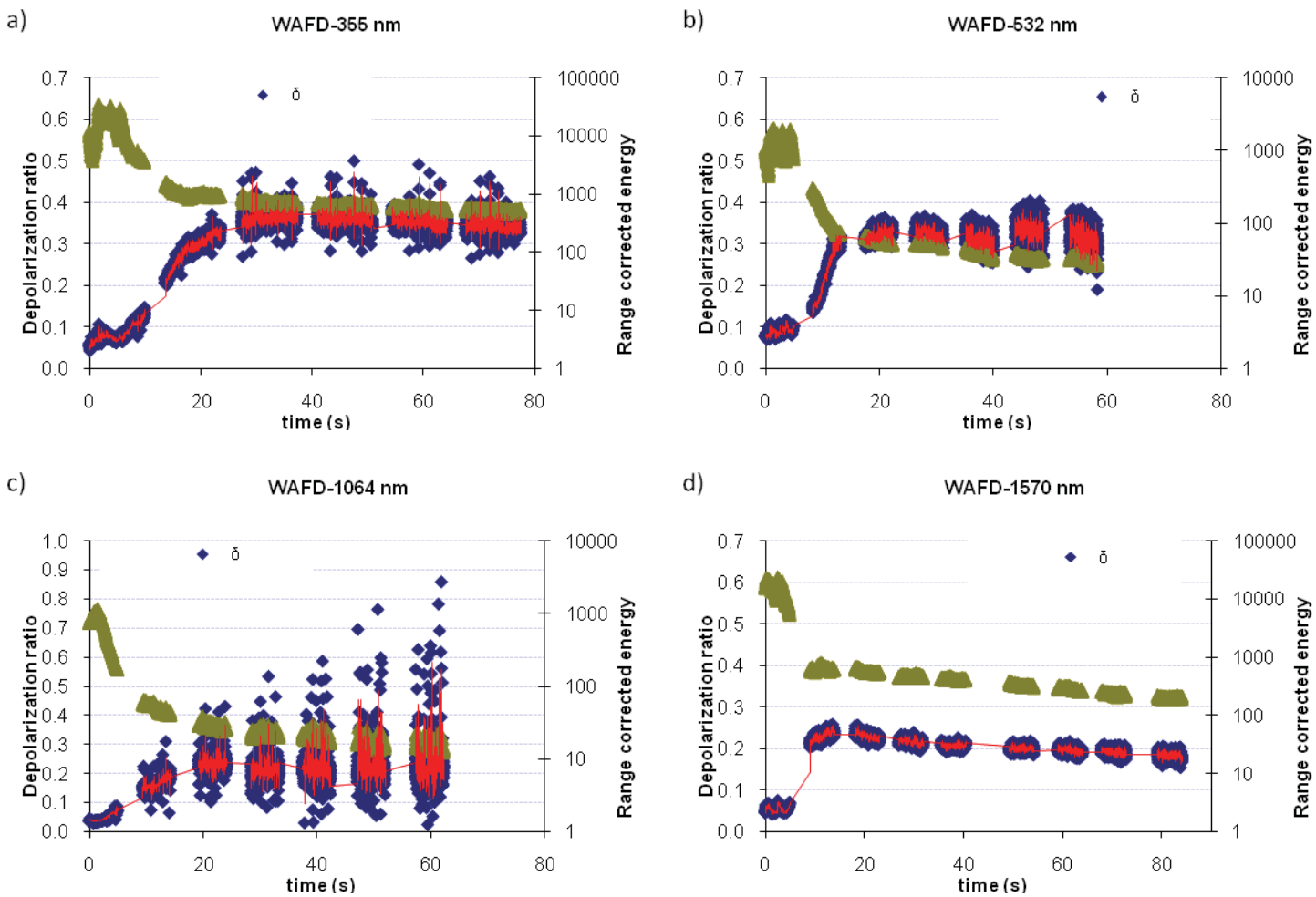

Figure 29: Time evolution of the depolarization ratio of wet AFD at a) 355 nm, b) 532 nm, c) 1064 nm and d) 1570 nm

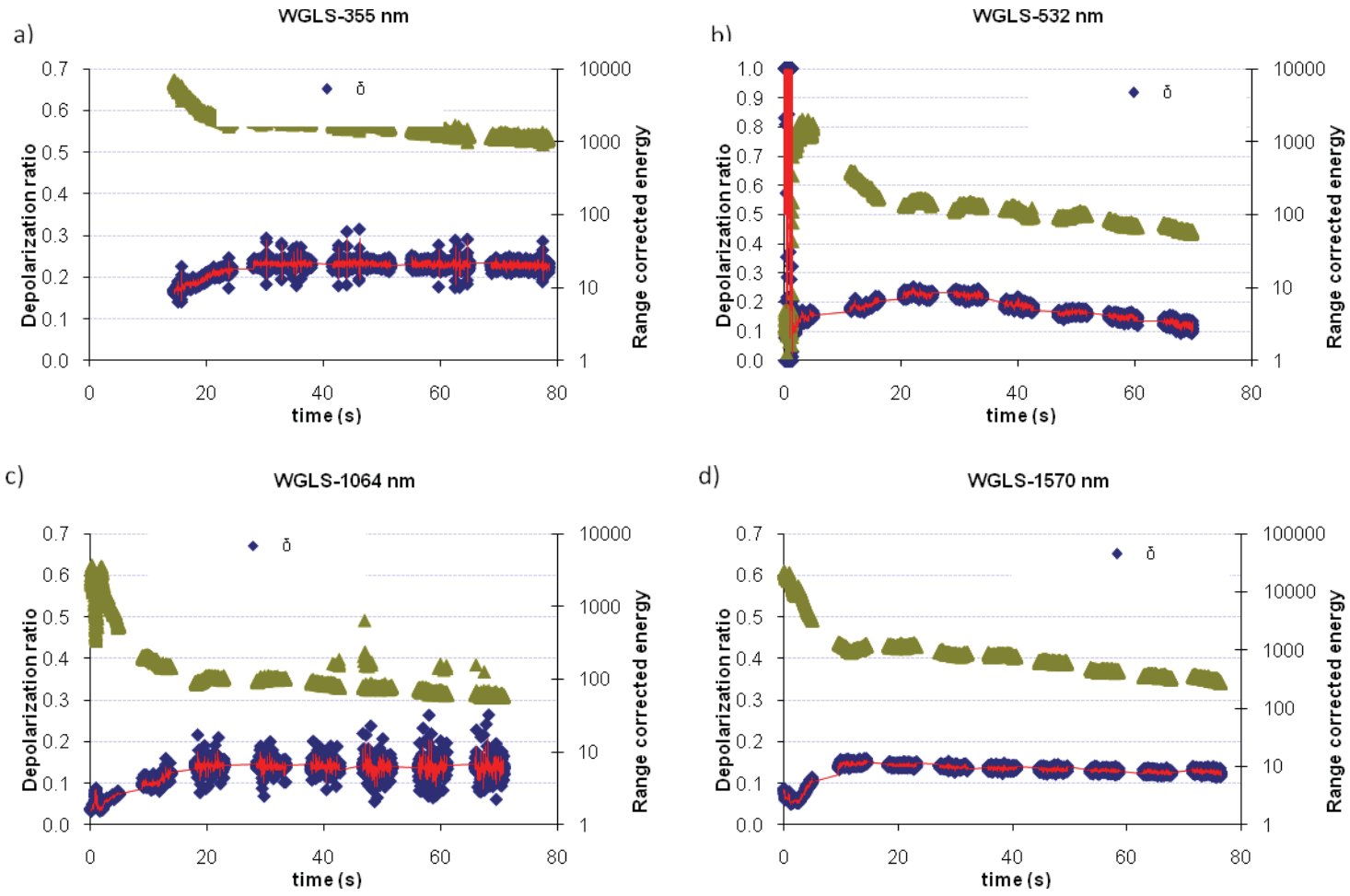

Figure 30: Time evolution of the depolarization ratio of wet GLS at a) 355 nm, b) 532 nm, c) 1064 nm and d) 1570 nm

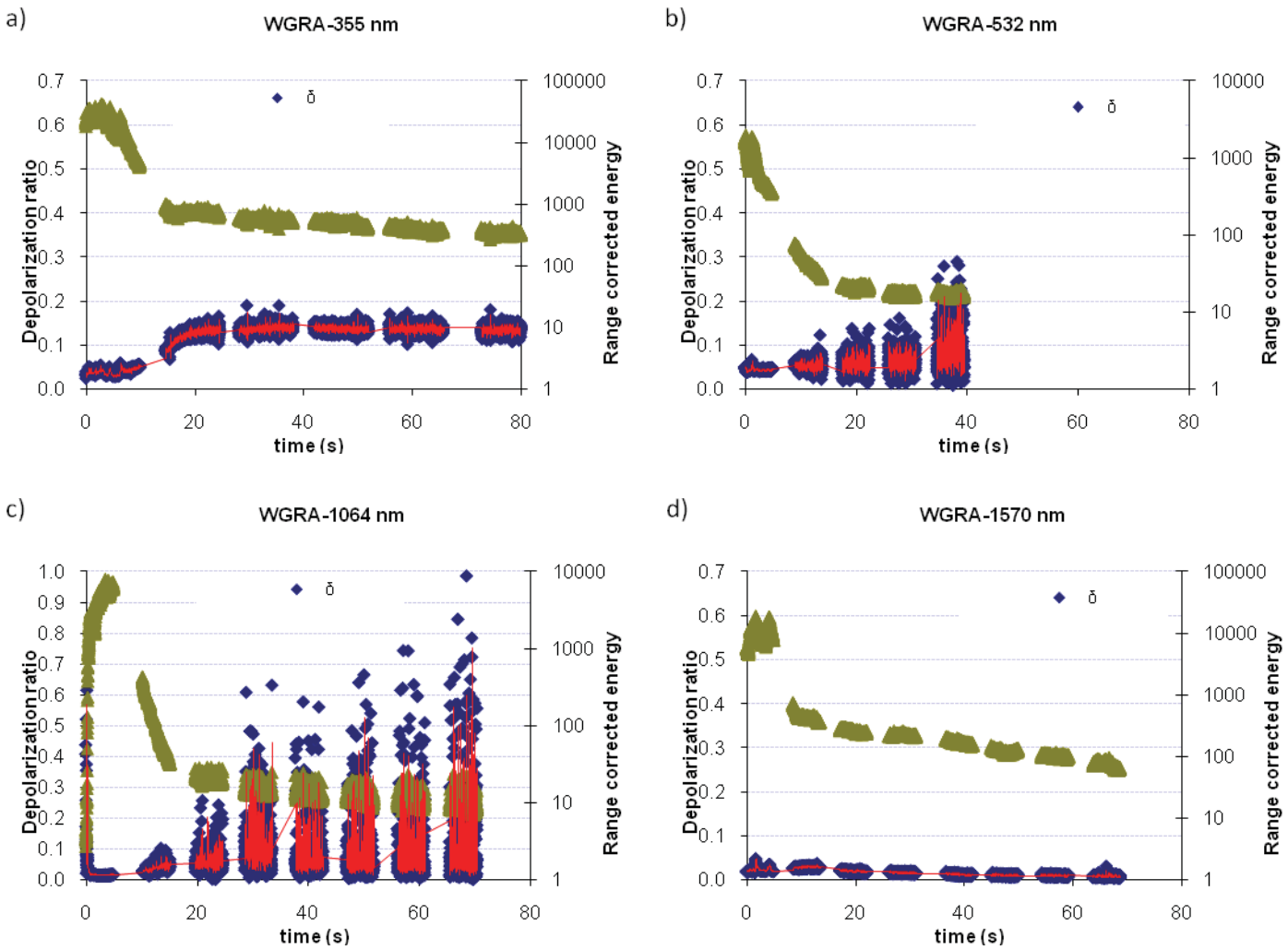

Figure 31: Time evolution of the depolarization ratio of wet GRA at a) 355 nm, b) 532 nm, c) 1064 nm and d) 1570 nm

References

[1] X. Cao, R Bernier., *Depolarization of light scattered by spherical and non-spherical particles*, Technical Report IOSL TR 2010-347, Oct. 2010, 84 pages

[2] X. Cao, G. Roy, N. Roy and R. Bernier. "Comparison of the relationships between lidar integrated backscattered light and accumulated depolarization ratios for linear and circular polarization for water droplets, fog-oil and dust.", Appl. Opt. 48, 4130-4141 (2009)

[3] Y. Hu, Z. Liu, D. Winker, M. Vaughan, V. Noel, L. Bissonnette, G. Roy and M. McGill "Simple relation between lidar multiple scattering and depolarization for water clouds", Optics Letters, Vol. 31, No. 12, pp. 1809-1811 (2006)

[4] G. Roy and N. Roy. "Relation between circular and linear depolarization ratios under multiple scattering conditions", Appl. Opt. 47, 6563-6579 (2008)

[5] G. G. Gimmestad, "Reexamination of depolarization in lidar measurements", Appl. Opt. 47, 3795-3802 (2008)

[6] C.J. Flynn, A. Mendoza, Y. Zheng and S.Mathur, "Novel polarization-sensitive micropulse lidar measurement technique*,"* Optics Express, 15(6), 2007, 2785-2790

[7] Schotland, R.M., Sassen, K. And Stone, R., Observations by lidar of linear depolarization ratios for hydrometeors, J. Appl. Meteorol. **10**, 1011-1017 (1971)

[8] Mishchenko, M.I., Hovenier, J.W., Depolarization of light backscattered by randomly oriented nonspherical particles, Opt. Lett., **20**, 1356-1358 (1995)

[9] E. Thrush, D. M. Brown, N. Salciccioli, J. Gomes, A. Brown, K. Siegrist, M. E. Thomas, N.T. Boggs and C.C. Carter, "Optical properties and cross-sections of biological aerosols," *Chemical, Biological, Radiological, Nuclear and Explosives (CBRNE) Sensing XI, Proc. Of SPIE* Vol. 7665 (2010)

[10] M. S. Quinby-Hunt, L. L. Erskine and A. J. Hunt, "Polarized light scattering by aerosols in the marine atmospheric boundary layer, " *Appl. Opt*. **36**, 5168-5184 (1997)

[11] T. Murayama, M. Furushima, A. Oda, N. Iwasaka and K. Kai, "Depolarization ratio measurements in the atmospheric boundary layer by lidar in Tokyo," *J. Meteorol. Soc. Japan.*, **74**, 571-578 (1996)

[12] X. Cao, G. Roy and R. Bernier, "Lidar polarization discrimination of bioaerosols," *Opt. Eng. 49(11) 116201-1-12* (2010)

[13] G. Roy, X. Cao and Robert Bernier (2011). "On linear and circular depolarization lidar signatures in remote sensing of bioaerosols - experimental validation of the Mueller matrix for randomly oriented particles," *Opt. Eng. 50(12) 116001-1-12* (2011)

DOCUMENT CONTROL DATA

(Security classification of title, body of abstract and indexing annotation must be entered when the overall document is classified.)

1. ORIGINATOR (Name and address of the organization preparing the document.)

Robert Bernier
Les instrument optique du St-Laurent
17500 Monté Gascon
Mirabel, Québec, J7J 2C5

2. SECURITY CLASSIFICATION (Overall security classification of the document, including special warning terms if applicable.)

UNCLASSIFIED
(NON-CONTROLLED GOODS)
DMC A
REVIEW: GCEC JUNE 2010

3. TITLE (The complete document title as indicated on the title page. Its classification should be indicated by the appropriate abbreviation (S, C or U) in parentheses after the title.)

Lidar Polarization discrimination of pollen

4. AUTHORS (Last name, followed by initials – ranks, titles, etc. not to be used.)

Xiaoying Cao and Robert Bernier

5. DATE OF PUBLICATION (month and year of publication of document.)

March2011

6. NO. OF PAGES (Including Annexes, Appendices and DCD sheet.)

88

7. DESCRIPTIVE NOTES (the category of the document, e.g. technical report, technical note or memorandum. If appropriate, enter the type of report, e.g. interim, progress, summary, annual or final. Give the inclusive dates when a specific reporting period is covered.)

Contractor Report

8a. PROJECT OR GRANT NO. (If appropriate, the applicable research and development project or grant number under which the document was written. Please specify whether project or grant)

8b. CONTRACT NO. (If appropriate, the applicable number under which the document was written)

W7701-071506

9a. ORIGINATOR'S DOCUMENT NUMBER (Official document number by which the document is identified by the originating activity. Number must be unique to this document.)

DRDC Valcartier CR 2011-237

9b. OTHER DOCUMENT NOS. (Any other numbers which may be assigned to this document either by the originator or the sponsor.)

10. DOCUMENT AVAILABILITY (Any limitation on further distribution of the document, other than those imposed by security classification.)

(x) Unlimited distribution
( ) Distribution limited to defence departments
( ) Distribution limited to defence contractors
( ) Distribution limited to government
( ) Distribution limited to Defence R&D Canada
( ) Controlled by Source

11. DOCUMENT ANNOUNCEMENT (Any limitation to the bibliographic announcement of this document. This will normally correspond to the Document Availability (10). However, where further distribution (beyond the audience specified in (10) is possible, a wider announcement audience may be selected.)

Unlimited

12. ABSTRACT (Brief and factual summary of the document. May also appear elsewhere in the body of the document itself. It is highly desirable that the abstract of classified documents be unclassified. Each paragraph of the abstract shall begin with an indication of the security classification of the information in the paragraph (unless the document itself is unclassified) represented as (S), (C), or (U). May be in English only).

Aerosols or solid targets m ay have an effect on the polarization of the light scattered by them. The depolarization, by such particles or objects, of the light transm itted by a lidar system may be used as a signature by which these objects can be identified and discrim inated against. This report is a bout the application of the RDDC-Valcartier polarization lidar system to the problem of discrim inating between various bi oaerosols, here namely pollens. For the first tim e to our knowledge, this technique has been applied to a great num ber of different bioaerosols, here 27. The developm ent and application to the experim ental data of the statistical t ool named Mahalanobis distance has allowed to dem onstrate that the polarization lidar technique renders possible the discrim ination between bioaerosols (pollens). The work reported herein also addresses the question of whether the use of onl y one kind of polarization (be it circular or linear) is sufficient or if both polarizations are required for a com plete discrimination among randomly distributed particles. This report concludes that only one polarization is sufficient.

13. KEYWORDS, DESCRIPTORS or IDENTIFIERS (Technically meaningful terms or short phrases characterizing a document and could be helpful in cataloguing it. Should be **Unclassified** text. If not , the classification of each term should be indicated as with the title. Equipment model designation, trade name, military project code name, and geographic location may be included. If possible, should be selected from a published thesaurus. e.g. Thesaurus of Engineering and Scientific Terms (TEST) and that thesaurus-identified.)

Lidar, polarization, discrimination, bioaerosols, mahalanobis distance

Defence R&D Canada

Canada's Leader in Defence
and National Security
Science and Technology

R & D pour la défense Canada

Chef de file au Canada en matière
De science et de technologie pour
la défense et la sécurité nationale

DEFENCE DÉFENSE

www.drdc-rddc.gc.ca